IVYSPRING INTERNATIONAL PUBLISHER

Theranostics

2026; 16(9): 4980-5015. doi: 10.7150/thno.128435

Review

Recent advances of metal-organic frameworks (MOFs) for drug delivery, cancer imaging and theranostics

Honglian Yu[1], Gan Lin[2], Peng Mi[1]✉

1. Department of Radiology and State Key Laboratory of Biotherapy, West China Hospital, and College of Polymer Science and Engineering, Sichuan University, No.17 South Renmin Road, Chengdu, Sichuan 610041, China.
2. Department of Biomedical Engineering, NanoSTAR Institute, University of Virginia School of Medicine, Charlottesville, VA 22908, USA.

✉ Corresponding author: Peng Mi (ORCID: 0000-0003-0123-4311), Email address: mi@scu.edu.cn.

Received: 2025.11.16; Accepted: 2026.01.23; Published: 2026.02.26

Abstract

Metal-organic frameworks (MOFs) are a unique class of porous materials constructed from metal-containing nodes, known as secondary building units (SBUs) and organic ligands. Their highly tunable structures enable the encapsulation of a broad range of therapeutic agents, spanning small-molecule chemotherapeutics to biomacromolecules such as proteins, DNA, and RNA. By rational selection of metal ions and organic linkers, diverse functionalities, including molecular imaging and phototherapeutic capabilities, can be included into MOFs, rendering them promising nanoscale platforms of nanomedicines. In this review, we summarize recent advances of MOFs for drug delivery, cancer imaging and theranostics. We discuss the progress in regulating the morphology and functions of MOFs through diverse synthetic strategies and surface modification approaches. We further systematically analyzed and discussed MOFs in the applications of drug delivery, molecular imaging, and cancer theranostics, with recent strategies. Finally, key limitations associated with the clinical translation of MOFs are discussed, along with the corresponding bottlenecks, future challenges, and emerging opportunities.

Keywords: metal-organic frameworks, nanocarriers, drug delivery, theranostics, molecular imaging.

Introduction

Cancer remains one of the leading causes of mortality worldwide. The development of effective therapeutic strategies is therefore critically needed [1]. However, conventional anticancer drugs often suffer from low bioavailability and significant side effects. To enable precise cancer therapy with enhanced therapeutic efficacy, a wide range of nanocarriers have been developed over recent decades, including organic systems such as dendrimers, micelles, and liposomes, as well as inorganic platforms such as magnetic nanoparticles, quantum dots, and metal nanoparticles [2,3]. Nanocarriers can be functionalized through interdisciplinary approaches for cancer molecular imaging, therapy, and theranostics [4,5]. Consequently, their biomedical applications have expanded rapidly, encompassing platforms such as liposomes, polymeric nanoparticles, MOFs, and covalent organic frameworks (COFs).

Recently, MOFs offer distinct advantages, including exceptionally high drug-loading capacity arising from their large surface area, as well as versatile functionalization via ligand modification or metal-node substitution. These features allow MOFs to function as integrated theranostic platforms. Since the seminal work by Hoskins and Robson elucidating the structures and anion-exchange properties of porous coordination polymers, this class of materials has rapidly evolved into a major research field [6,7]. The term of MOF was introduced by Yaghi and co-workers in 1995 [8], and subsequently established the standardized terminology by the International Union of Pure and Applied Chemistry (IUPAC) in 2013. Over the past decades, MOFs have been widely explored for applications in catalysis [9], gas storage [10], energy-related technologies [11], and drug delivery [12].

MOFs have demonstrated considerable promise across a broad range of biomedical applications, including molecular imaging, drug delivery, and theranostics. This potential arises from their intrinsic

physicochemical properties, such as tunable porosity, customizable architectures, high drug-loading capacity, partial biodegradability, and, in certain systems, acceptable biocompatibility. Owing to their highly porous architecture and large specific surface area, MOFs enable efficient encapsulation and controlled release of diverse therapeutic agents [13]. To data, MOFs have demonstrated efficient loading for a spectrum of cargos, including small-molecule anticancer drugs, nucleic acids, *e.g.*, short interfering RNA (siRNA) and DNA, contrast agents [14] for various applications including gene therapy [15], chemotherapy [16], immunotherapy [17,18], *etc.*

Beyond drug delivery, MOFs and their derivatives have been explored as molecular imaging probes or as carriers for imaging agents across multiple modalities, including fluorescence imaging (FL) [19], magnetic resonance imaging (MRI) [20], computed tomography (CT) imaging [21], positron emission tomography (PET) imaging [22], and photoacoustic imaging (PAI) [23]. Such versatility is achieved through rational selection of metal nodes and organic linkers or through the incorporation of dedicated imaging moieties. The integration of therapeutic agents within MOF-based carriers can further enhance cellular uptake, gene silencing, and overall therapeutic performance through rational structural and compositional design [24].

More recently, MOFs constructed by photosensitizer (PS) or radiosensitizer ligands have been reported to significantly enhance the efficacy of photodynamic therapy (PDT) and radiotherapy (RT) [25]. In addition, MOFs can act as versatile carriers for anticancer agents, enabling combinatorial and synergistic treatment strategies. Within the tumor microenvironment (TME), MOFs, typically with particle sizes in the range of 20-200 nm and favorable aqueous dispersibility, can preferentially accumulate at tumor sites via the enhanced permeability and retention (EPR) effect [26], thereby improving tumor targeting while mitigating off-target toxicity to healthy tissues [27]. Consequently, the multifunctional design of MOFs offers distinct advantages in the TME, facilitating precise delivery and controlled release of chemotherapeutics or imaging agents, ultimately enhancing both therapeutic efficacy and diagnostic accuracy.

Despite their promise, MOFs exhibit limitations compared with other nanocarriers, due to potential toxicity of heavy metal ions. Consequently, the choice of MOF nanocarrier must be guided by application-specific requirements—including drug characteristics, target tissues, administration routes—as well as safety and manufacturability considerations.

Herein, we provide a comprehensive overview of recent advances in synthetic methodologies and biomedical applications of MOFs for cancer treatment, with particular emphasis on drug delivery mechanisms, molecular imaging capabilities, and theranostic potentials (Figure 1). Additionally, we highlight key challenges and future perspectives in this rapidly evolving field, with the aim of guiding further research and innovation in MOF-based cancer nanomedicine.

Methods for preparing MOFs

The publication of a seminal 1989 study by Robson describing the self-assembly of MOFs through the coordination of metal ions or clusters with organic ligands stimulated broad interest in these materials within the scientific community [7]. In 1994, the first three-dimensional metal-porphyrin coordination polymer was synthesized using palladium-based tetrapyridine porphyrin ligands coordinated with Cd^{2+} ions [28]. In 1999, Yaghi and co-workers reported MOF-5, which was the first stable and porous MOF, and thereby established MOFs as an independent field of materials research [29]. Subsequently, Gérard Férey pioneered the development of large-pore and highly stable MIL frameworks, Kitagawa advanced the study of flexible and dynamic MOFs, and Joe established reticular chemistry as a unifying framework for predicting and classifying MOF structures [30,31]. In recent years, several representative MOF families, including MILs, ZIFs, HKUSTs, UiOs, *etc.* (Table 1), have been extensively investigated for biomedical applications. These MOFs are commonly synthesized via solvo/hydrothermal, microwave-heated, sonochemical, electrochemical, mechanochemical and reverse-phase microemulsions syntheses (Figure 2).

Classical method for synthesizing MOFs

Solvothermal/hydrothermal synthesis is one of the most widely used approaches for MOF fabrication, involving reactions between metal salts and ligands in sealed vessels under elevated temperature and pressure. Reaction parameters, including temperature, pressure, time, pH, precursor concentration, and filling degree, govern crystal size, yield, and morphology. Higher temperatures and pressures accelerate crystallization, while extended reaction times promote crystal growth from the nano- to microscale [45]. The introduction of modulators (*e.g.*, acetic, benzoic, or lauric acid) competes with organic ligands during nucleation, enabling precise control over particle size, morphology, and crystallization kinetics. pH optimization is highly system-dependent: acidic conditions weakened

diffraction intensity, whereas alkaline environments often led to the formation of phase impurities [46]. Recent optimization strategies have further incorporated controlled precursor hydrolysis and the use of polymer or surfactant additives to improve crystallinity and morphology regulation. The MOFs synthesized by solvothermal/hydrothermal approach usually exhibit good crystallinity and stable structure, with tunable pore sizes that enable effective drug loading and delivery. However, the high energy demand of this method limits its large-scale production, and post-synthetic treatments are usually required to obtain nanostructures.

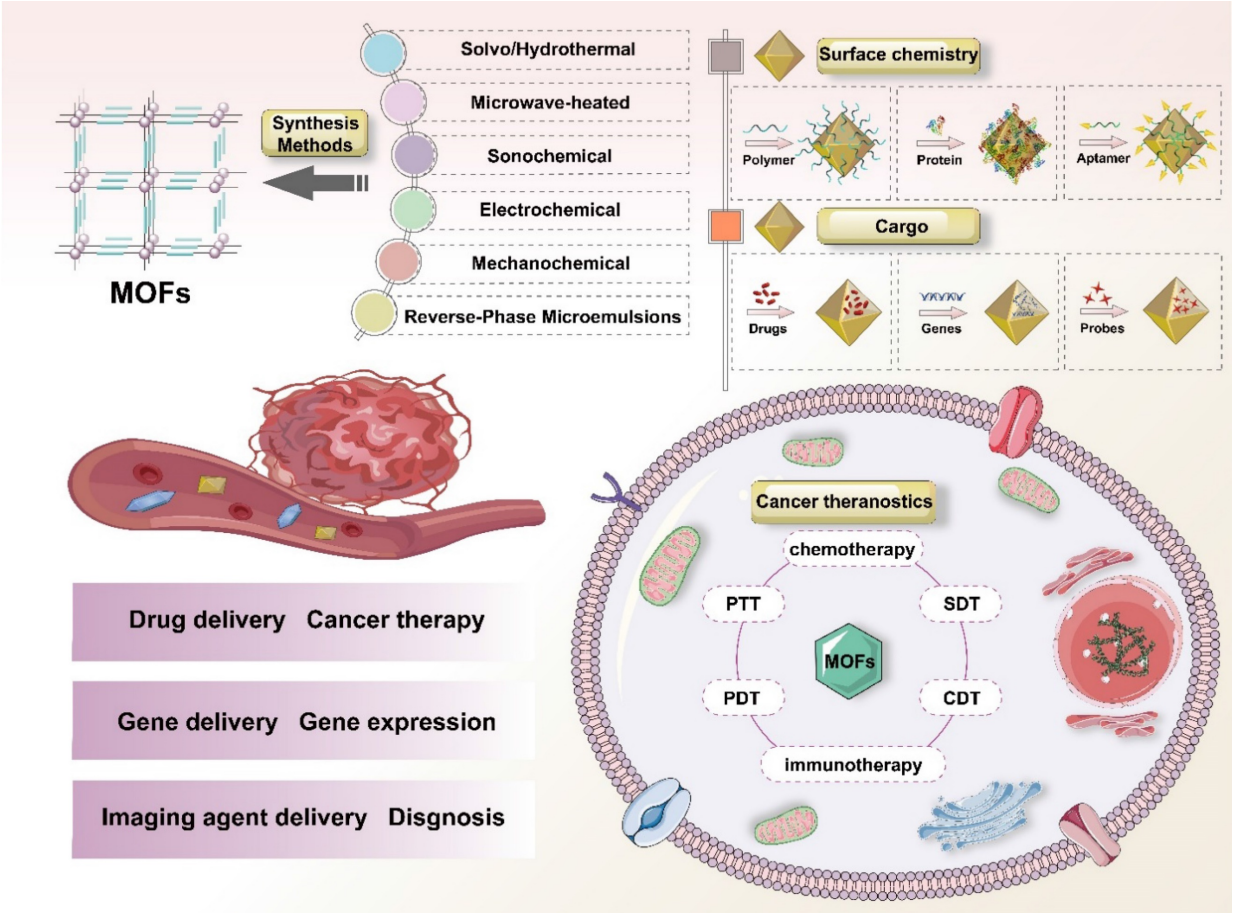

Figure 1. Schematic illustration of MOFs and their biomedical applications for drug delivery, cancer molecular imaging, and theranostics.

Table 1. Typical synthetic approaches of MOFs

Synthesis Methods	Energy source	MOFs	Approx. Reaction time	Approx. Temperature	Advantage	Disadvantage	Ref.
Solvo/ Hydrothermal	Thermal; Electric source	MIL-88A-Fe; MOF-5-Zn; ZIF-8-Zn	4-96 h	50-1000 °C	High yields; Good crystallinity; High porosity	Time-consuming; Toxic	[32-34]
Microwave-heated	Electromagnetic wave	MIL-100-Fe; MIL-101-Cr	5 min-4 h	30-150 °C	Shortening of reaction time; Narrow particle size distribution; High synthesis rate; Controllable particle size	Low productivity; High costs; Small synthesis scale	[35,36]
Sonochemical	Ultrasound	$[Gd_2(TATAB)_2]\cdot 6DMF$; MIL-88A (Fe)	5 min-2 h	25-50 °C	Small size; Green and efficient energy	Restricted temperature range	[37,38]
Electrochemical	Direct current power	HKUST-1 (Cu) ; [Zn(1,3-bdc)0.5(bzim)]	10 min-1 h	Room Temperature	Mild; Short reaction time; Continuous synthesis of controllable morphology	Requires special equipment	[39,40]
Mechanochemical	Mechanical force	HKUST-1-Cu; MOF-14-Cu	0.5 h-6 h	Room Temperature	Green; Low costs; High yields	Limited to specific MOFs; Might lead to the poor crystallinity	[41,42]
Reverse-Phase Microemulsions	-	DBP-UiO (Hf); $Mn_3(BTC)_2(H_2O)_6$	0.5 h-24 h	Room Temperature - 80 °C	Pure; Synthesis of controllable	Post-processing complex; High costs	[43,44]

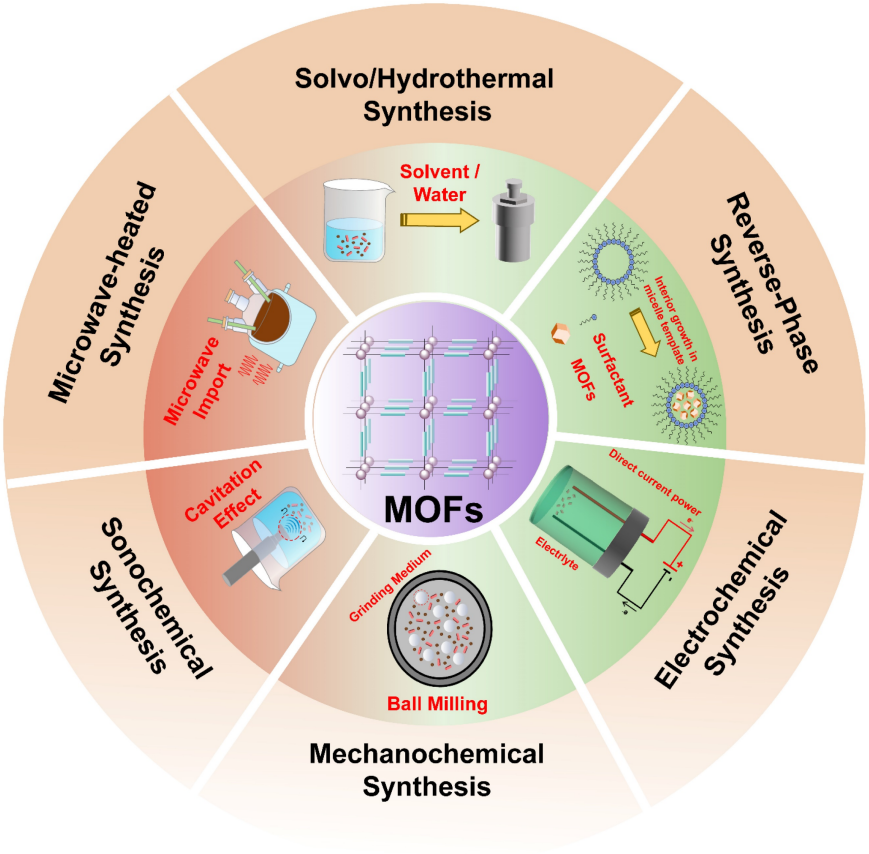

Figure 2. Schematic summary of classical methods for the synthesis of MOFs: Solvo/Hydrothermal synthesis, Microwave-heated synthesis, Electrochemical synthesis, Sonochemical synthesis, Mechanochemical synthesis, and Reverse-phase synthesis.

Microwave-assisted synthesis employs electromagnetic radiation (300 MHz-30 GHz) to directly couple with molecular dipoles, enabling rapid and heating that promotes MOF nucleation and crystallization in sealed high-pressure reactors. This volumetric heating mechanism markedly shortened reaction times and reduced particle sizes compared with conventional solvothermal methods, owing to uniform energy distribution and minimized local overheating [47]. For example, MIL-101(Cr) with a uniform particle size of approximately 20 nm can be synthesized within 5 min at 210 °C and 600 W without hydrofluoric acid, whereas traditional methods typically require about 8 h and with HF to yield heterogeneous microscale particles [48]. This approach enables the efficient production of small and monodisperse nanoparticles with readily tunable synthesis parameters, rendering it well suited for intravenous administration. However, the presence of thermal gradients under certain conditions may induce structural defects, potentially compromising framework integrity and drug-loading efficiency.

Sonochemical synthesis represents an efficient unconventional method for MOF fabrication. Under ultrasonic irradiation (20 kHz to 10 MHz), acoustic cavitation generates localized extreme conditions (> 5000 K, ~1000 atm) with rapid heating/cooling rates (> 10^{10}K s^{-1}), which promote homogeneous nucleation and accelerated crystallization [49]. Compared with conventional thermal heating, ultrasound delivers energy more uniformly throughout the reaction medium, thereby significantly enhancing MOF crystallization. The first MOF synthesized via the sonochemical route was $Zn_3(BTC)_2$ [50], which was obtained within 5 min with an average particle size of ~90 nm and a high yield of 75.3%. In contrast, the conventional hydrothermal method requires 24 h at 140 °C to produce the same compound [51]. Although this method enables relatively rapid synthesis of small-sized MOFs, it often suffers from reduced crystallinity, high sensitivity to ultrasonic parameters, and potential formation of amorphous or defective structures, which may compromise drug-loading stability.

Electrochemical synthesis encompasses multiple strategies, including cathodic/anodic synthesis, bipolar electrodeposition, potential shift, and electrophoretic deposition. These approaches rely on electrode-electrolyte interfacial reactions under precisely controlled current or potential conditions. Among them, cathodic reduction and anodic oxidation are widely employed due to their mild

operation conditions, accurate potential control, and minimal by-product formation [52]. Electrochemical synthesis was first applied to fabricate HKUST-1 ($Cu_3(BTC)_2$) films on copper substrates [53]. This technique offers several advantages, including short reaction times, benign reaction conditions, high product purity (owing to the absence of metal salts or anionic residues), and tunable morphology, rendering it well suited for continuous synthesis. Using this technique, MOFs such as ZIF-8(Zn), NH_2-MIL-53, HKUST-1, MIL-53(Al), and MIL-100(Al) have been successfully prepared. Moreover, electrochemical synthesis is typically conducted in a solvent-free or aqueous system, providing favorable biocompatibility. Precise control of electrochemical parameters enables the formation of MOFs with stable pore architectures and high drug-loading capacities. However, the resulting MOFs are predominantly as thin films, which limits their applicability to specific drug delivery formats, such as implantable device coatings or wound dressings.

Mechanochemical synthesis employs mechanical forces, such as shear, friction, or compression to induce reactions between metal salts and organic ligands, leading to MOF formation without the need for bulk solvents. This solvent-free or solvent-minimized approach enables scalable powder production with reduced environmental impact and lower cost compared with conventional solvent-based methods. Typically, synthesis is conducted in in grinding jars containing balls, metal ions precursors, organic ligands, and additives. The first mechanochemically synthesized MOF was obtained by manually grinding metal oxides with imidazole ligands [54]. Subsequent methodological advances led to the development of liquid-assisted grinding (LAG) and ion- and liquid-assisted grinding (ILAG). In LAG, small amounts of solvent are introduced to accelerate reaction kinetics and improve crystallinity, whereas ILAG further incorporates inorganic salts to enhance precursor dissolution, reaction homogeneity, and grinding efficiency [55]. Overall, mechanochemical synthesis offers a green and scalable route for MOF production, with simplified post-synthetic processing that facilitates drug loading and delivery. However, MOFs produced via this method often exhibit lower porosity than those synthesized by alternative routes, which could limit their drug-loading capacity.

Microemulsions are thermodynamically stable dispersions formed by emulsifying immiscible liquids into dispersed droplets (typically 5-100 nm), resulting in transparent or translucent systems composed of oil, water, surfactants, and cosurfactants. In reverse-phase microemulsion synthesis, surfactants self-assemble into micelles, microemulsions, or liquid-crystals phases that act as organic templates, providing confined nanoscale reactors for MOF formation. Metal ions and ligands react at the droplet interface, yielding MOFs nanoparticles with controlled dimensions. By tuning the surfactants-to-water ratio, the size and morphology of the resulting MOFs could be precisely regulated [56]. The approach has been successfully extended to widely applied to MOFs, such as zinc-based frameworks [57]. Precise control over the "water-core" size enables the synthesis of small, highly monodisperse MOF nanoparticles and allows *in situ* loading of either hydrophobic or hydrophilic drugs according to their physicochemical properties. The confinement effect promotes uniform drug distribution within MOF pores and high encapsulation efficiency. Nevertheless, complete removal of surfactants and solvents, which may induce toxicity, remains a major challenge.

Advances in micro- and nanotechnology have provided more synthetic strategies of MOFs, including microfluidics-assisted and ionthermal methods [58,59]. For example, Fe-TCPP MOFs fabricated via droplet-based microfluidics and subsequently functionalized with oxaliplatin prodrugs through ligand exchange exhibited precise size and morphology control, improved batch-to-batch reproducibility, and enhanced encapsulation efficiency. Ionthermal synthesis, which employs ionic liquids as both solvents and structure-directing agents, facilitates the preparation of highly stable MOFs, such as NH_2-MIL-53-Al, offering high porosity and proton conductivity, while benefiting from intrinsic conductivity and green characteristics of ionic liquids. These techniques have also been extended to the synthesis of spherical porous carbon nanoparticles (SPCNs) and other porous carbon materials derived from MOF templates [60].

In addition, MOF-derived single-atom catalysts (SACs), characterized by atomically dispersed metal active centers, have attracted increasing attention. The low-coordination environments of exposed unsaturated metal atoms maximize catalytic activity; however, suitable substrates are usually required to prevent atom aggregation and maintain the uniform dispersion and long-term stability [61]. Among the available strategies, high-temperature pyrolysis remains the most widely used approach, involving thermal decomposition of MOFs under controlled gas atmospheres to generate isolated metal atoms embedded within carbonaceous matrices. For instance, Pd nanoparticles can be transformed into Zn-MOF-based Pd single-atom catalysts by pyrolysis at 900 °C for 3 h under an inert atmosphere using ZIF-8 as a template [62].

Despite the wide range of synthesis routes

explored, no single method is universally optimal. Each approach presents distinct advantages and limitations in terms of reaction conditions, particle morphology, size control, uniformity, scalability, and environmental impact. Therefore, the selection of an appropriate synthesis technique depends on the specific requirements of the intended MOF application. As summarized in Table 1, the choice of synthesis method critically influences MOF structure, functionality, and performance. In practice, integrating complementary techniques to offset the limitations of individual approaches has emerged as an effective strategy for producing high-quality MOF materials with tailored properties.

Although various synthetic methods for MOFs have been developed, the key factors governing MOF synthesis are highly interconnected. These factors include both compositional parameters, such as solvents, reactants, and solution pH, and process parameters, including reaction temperature, pressure, and duration. By rationally modulating these variables, the structures and properties of MOFs could be effectively tailored for biomedical applications. Therefore, careful optimization of relevant parameters and selection of appropriate synthetic methods are essential to meet application-specific requirements.

With the exception of mechanochemical synthesis, most MOF preparation routes begin with dissolving metal precursors and organic ligands in suitable solvents. The influence of the solvent on MOF formation is primarily reflected in reactant solubility, solvent polarity and coordination ability, as well as potential templating effect. These factors need to be considered collectively to identify solvents that facilitate controlled crystal nucleation and growth. Variations in the chemical structures of metal precursors and ligands, together with adjustments in their concentration ratios, can significantly alter the resulting MOF topology. In general, decreasing precursor concentration reduces particle size; however, excessive dilution may lead to particle aggregation and morphological heterogeneity. Because reactant selection varies across synthesis methods, careful control of the precursors is particularly critical for achieving particle sizes suitable for biological applications. For example, mechanochemical synthesis commonly employs metal oxides as precursors. The solution pH strongly influences MOF synthesis by modulating organic ligand solubility, impurity activity, and the degree of ligand deprotonation, thereby indirectly affecting the metal-ligand coordination and crystal growth [63].

Process parameters, including temperature, pressure, and their respective ramping profiles, further influence crystallization kinetics and functional group coordination. Among these available approaches, hydrothermal synthesis offers a distinct advantage by enabling reactions under elevated temperature and pressure, thereby overcoming the poor solubility of certain reactants under ambient conditions and promoting crystallization. Reaction duration also plays a critical role in determining particle size and may lead to aggregation. Accordingly, the choice of synthesis method should be guided by the desired MOF characteristics and reasonable reaction time, with solvothermal methods generally requiring longer synthesis durations.

Ultimately, the biological fate and therapeutic efficacy of MOFs in drug delivery applications are fundamentally dictated by their intrinsic chemical composition, including the nature of metal nodes, organic linkers, pore architecture, and structural defects. These features collectively determine their stability, biocompatibility, targeting ability, drug loading and release kinetics, and clearance behavior *in vivo*. The selection of metal nodes is essential: endogenous or therapeutic ions relevant ions (*e.g.*, Zn^{2+} and Fe^{3+}) offer improved biosafety and stimuli-responsive degradation, whereas more inert metals (*e.g.*, Zr^{4+}), despite their high structural stability, raise concerns regarding long-term accumulation. Organic linkers further modulate surface chemistry, hydrophilicity, and functionality potential. Pore geometry, including size, shape, and surface chemistry, directly governs drug loading capacity and release behavior. Moreover, the deliberate introduction of structural defects can enhance drug loading, facilitate diffusion, and fine-tune degradation kinetics while preserving overall framework integrity. Collectively, the coordinated interplay of MOF chemical components dictates critical biological outcomes: including colloidal stability in circulation, immune evasion, cellular uptake, endosomal escape, stimuli-triggered drug release, and biodegradable clearance.

AI-assisted prediction of MOF synthesis

Artificial intelligence (AI) has advanced rapidly in recent years, driven by the proliferation of big data and increasing computational power. With continuously improvement, AI has emerged as a powerful tool for addressing complex challenges across multiple aspects of materials science. Accordingly, the design and synthesis of MOFs are increasingly positioned to benefit from AI-assisted approaches [64,65].

AI-enabled MOF development begins with the construction of high-quality databases. Several well-established MOF databases, such as CoRE MOF,

SynMOF, and the Cambridge Structural Database (CSD), are now available and can serve as training and validation datasets for machine learning models. These datasets support model development across four major learning paradigms: supervised, unsupervised, semi-supervised, and reinforcement learning, depending on the availability of labeled data. By integrating traditional computational methods with machine learning algorithms, researchers can rapidly screen large numbers of candidate materials, thereby prioritizing the most promising systems for experimental validation and significantly reducing trial-and-error efforts [66,67]. The structures and functions of MOFs can be systematically optimized through modulation of metal nodes, organic linkers, and reaction conditions. AI offers a powerful means to accelerate this optimization by identifying structure–property–performance relationships. For instance, AI-guided screening of microwave-assisted synthesis parameters has been shown to enhance MOF crystallinity, leading to improved material performance [68].

Looking forward, MOF design and synthesis are expected to become increasingly dynamic and impactful through deeper integration with AI and computational technologies. AI-driven strategies are anticipated to accelerate the development of stimuli-responsive MOFs for drug delivery, while also enabling more sustainable and environmentally friendly synthesis pathways. Such advances may yield MOF systems with improved *in vivo* safety, higher drug loading capacity, and enhanced targeting responsiveness, ultimately facilitating their clinical translation.

Surface modification of MOFs for biomedical applications

The surface chemistry of MOFs plays a critical role in determining their application, as it governs key processes including targeting and uptake. Furthermore, numerous MOFs are susceptible to hydrolysis, framework dissociation, or ligand exchange under physiological conditions. Moreover, unmodified MOF surfaces are prone to nonspecific adsorption of plasma proteins, leading to the formation of a "protein corona". This corona accelerates clearance and compromises targeting ability. Hence, surface functionalization has been widely employed to augment structural stability in physiological conditions and to enable the conjugation of therapeutic agents for site-specific delivery. In biomedical applications, surface functionalization strategies generally adhere to three fundamental principles: establishing stable interactions between hydrophilic components and the MOF surface, minimizing nonspecific protein adsorption, and enabling controlled and robust attachment for biological functional moieties [69].

Physical interaction

The first strategy involves physical adsorption of biomaterials, such as polymers or macromolecules on the MOF surface. These interactions are often mediated by electrostatic forces and can enhance MOF properties including structural stability. For instance, electrostatic assembly between negatively charged glucose oxidase and positively charged PCN-222-Fe markedly improves the stability and reusability, thereby yields a new class of chemical and biological catalysts that can be used for biomedical applications [70].

Beyond simple adsorption, additional physical surface modifications include entrapment, self-assembly, and layer-by-layer (LbL) deposition. Entrapment typically involves dissolving target molecules in a solvent together with the host material, followed by controlled expansion and subsequent non-solvent-induced shrinkage of the matrix, thereby physically trapping the molecules. For instance, encapsulating lipase within ZIF-8 via biomineralization preserves enzymatic activity while imparting excellent thermal stability at 50-70 °C [71]. Self-assembly refers to the spontaneous organization of discrete building blocks, from individual molecules to structural units, into ordered superstructures. In MOFs, surfactants such as Cetyltrimethylammonium bromide (CTAB) can act as a cationic surfactants and capping agents to produce highly monodisperse, submicron truncated rhombic dodecahedral ZIF-8 colloidal particles, which are suitable for sensing, storage, catalysis, and photonics applications [72]. LbL deposition entails the sequential adsorption of molecules or atoms on a substrate, enabling directional, ordered, and controllable MOF surface modification. Although inherently time-consuming, this approach affords precise control over MOF structure and composition while maintaining high crystallinity and structural integrity. For example, *in situ* growth of CuBTC on carboxymethylated cotton via LbL maintains the MOF's crystallinity and microporosity, while simultaneously enhancing water stability and mechanical toughness, thereby broadening its potential applications in self-cleaning textiles and UV shielding [73].

Chemical modification

Chemical surface modification entails the selective grafting or covalent functionalization of MOFs to tailor their surface chemistry, producing robust coatings suitable for biological applications.

Compared with physical interaction, chemical modification offers greater stability and durability, making it particularly advantageous for biomedical use, such as preventing MOF aggregation during circulation and enhancing targeted drug delivery. Common chemical functionalization strategies introduce various surface functional groups (*e.g.*, -OH, -COOH, $-NH_2$, $-SO_4^{2-}$), which regulate hydrophilicity, surface charge, and interactions with protein/cell [74]. Surface oxidation introduces oxygen-containing groups, such as carboxyl and carbonyl on MOF surfaces, through the incorporation of peroxide groups. Surface hydrolysis cleaves ester bonds under acidic or alkaline conditions, generating hydroxyl and carboxyl groups. Aminolysis incorporates reactive amino groups, often increasing surface roughness and wettability, thereby modulating interactions with proteins and cells. In addition, plasma treatment generates charged particles by exciting gaseous precursors, which bombard the material surface and induce physicochemical modifications.

MOF surfaces can be functionalized with three main types of biomolecular or synthetic modifiers: polymers, proteins, and aptamer, yielding MOF-polymers, MOF-proteins, and MOF-aptamers systems. Polymers can be further categorized based on their functional roles, including targeting polymers [*e.g.*, folic acid (FA), hyaluronic acid (HA)], polymers with imaging agents (*e.g.*, fluorescent dyes), and polymers-drug conjugates. The incorporation of polymeric coatings substantially enhances MOF stability in biological environments. Notably, polyethylene glycol (PEG) modification usually prolongs blood circulation, increases tumor accumulation via the EPR effect, while markedly reducing protein adsorption and immune clearance. Furthermore, polydopamine-modified MOFs (including HKUST-1-Cu, ZIF-67-Co, ZIF-8-Zn, UiO-66-Zr, Cu-TDPAT, MOF-74-Mg, and MIL-100-Fe), prepared via Michael addition reactions under oxygen (O_2), exhibit improved structural stability across diverse environments [75]. These modifications are crucial for therapeutic applications, such as cancer therapy, by protecting MOFs from premature degradation and maintaining the functional integrity.

MOF-protein conjugates primarily leverage the innate biological functions of proteins to enable active targeting, immune evasion, or catalytic therapy. Proteins are typically attached to MOF surfaces via amide bonds or click chemistry. Alternatively, MOFs could be synthesized on protein templates, or proteins could be incorporated directly as part of the ligand during MOF construction. For instance, covalent conjugation of transferrin to MOF surface enabled specific recognition of the transferrin receptor, which is overexpressed on many tumor cells, thereby facilitating active targeting and significantly enhancing MOF uptake [76]. In addition, coating MOFs with intact cell membranes (*e.g.*, via extrusion or sonication) could achieve homologous targeting; for example, cancer cell membranes camouflaged MOFs preferentially accumulate in tumors of the same cellular origin [77].

MOF-aptamer systems utilize single-stranded DNA or RNA aptamers with their high affinity and specificity for selected targets, such as cell surface proteins, small molecules, enabling highly precise cell-level targeting. For example, thiolated AS1411 aptamers have been conjugated to surface-modified, drug-loaded MOFs, allowing selective delivery to cancer cells and promoting their endocytosis [78]. In practical applications, combinatorial strategies often yield superior outcomes. For instance, integrating polymer coatings with aptamer functionalization could simultaneously achieve prolonged circulation and precise tumor targeting, representing a promising direction for future MOF surface engineering. Surface modification also plays a pivotal role in enhancing MOF biocompatibility. Phospholipid bilayer-coated Zr-MOFs, formed via Zr-O-P coordination, exhibited enhanced stability, cell uptake, and biocompatibility [79].

Similarly, covalent PEGylation of Zr-MOFs improved their hydrophilicity, aqueous dispersibility, and biological biocompatibility. Surface-modified MOFs demonstrate exceptional performance in targeted drug delivery applications. Among them, the ZIF family, particularly ZIF-8, is widely employed for TME-responsive therapy due to its acid-sensitive degradation. FA-PEG-modified ZIF-8, leverages the overexpression of folate receptors on cancer cells to promotes selective uptake and enables multi-stimuli-responsive drug release [80]. Such strategies selectively target cancer cells while minimize off-target toxicity. In addition to drug delivery, MOFs can be functionalized with imaging agents to facilitate real-time monitoring of distribution and therapeutic response. Certain MOFs function directly as contrast agents; for example, Gd-doped polydopamine (PDA) MOFs loaded with PS chlorin e6 (Ce6), enable integrated diagnosis and therapy applications [81]. Overall, surface modification strategies endow MOFs with enhanced stability, biocompatibility, targeting precision, and multifunctionality, underscoring their considerable potential in advanced biomedical applications.

MOFs for drug delivery

Traditional free-form drugs often exhibit

unsatisfactory efficacy due to nonspecific biodistribution. Drug delivery systems (DDS) have emerged as a multidimensional strategy designed to enhance drug transport to specific pathological sites (*e.g.*, tumors), thereby improving therapeutic outcomes while minimizing systemic toxicity. The introduction of the first DDS, Spansule®, in 1952, marked the advent of modern controlled-release technologies [86]. Over subsequent decades, DDS have successfully addressed many inherent limitations of free drugs, although they have also introduced new challenges related to biocompatibility, stability, and drug-loading efficiency.

As discussed above, DDS research extends beyond the therapeutic agents themselves. Ideal carriers should provide high specificity, robust stability and efficient drug-loading capacity, thereby expanding the clinical applicability of therapeutic agents. MOFs enable drug loading through two principal mechanisms. In the first approach, some drugs themselves can be applied as materials for synthesizing MOFs via strong host-guest or coordination interactions, affording drug protection and enabling controlled release [87]. In the second approach, drugs are incorporated into MOF pores through diffusion or adsorption, allowing drug release while maintaining carrier integrity [88]. Compared with liposomes and hydrogels, whose drug release depends on carrier degradation or disassembly and often suffers from limited loading efficiency, MOFs offer superior capacity due to their high porosity.

In general, drug release from carriers depends on carrier stability, degradability, and biodistribution. Owing to their large surface area and tunable size, MOFs are particularly well suited for use as drug carriers. Therapeutics can be incorporated into MOFs through diverse mechanisms, including surface adsorption (*e.g.*, electrostatic interactions, coordination bonding, or π-π stacking), pore loading (*e.g.*, PSs, gases, or nanoparticles), and covalent or confinement-based encapsulation of biomacromolecules such as proteins and nucleic acids [89]. Extensive studies have explored the controlled drug release, biodegradation behavior, and stimulus responsiveness of MOFs, including their sensitivity to both endogenous (*e.g.*, tumor microenvironment) and exogenous (*e.g.*, physical stimuli) triggers [90].

This section summarizes recent advances in the application of MOFs as multifunctional carriers for the precise delivery of diverse therapeutic and diagnostic agents, including chemotherapeutics, genes and imaging probes to tumor tissues (Figure 3).

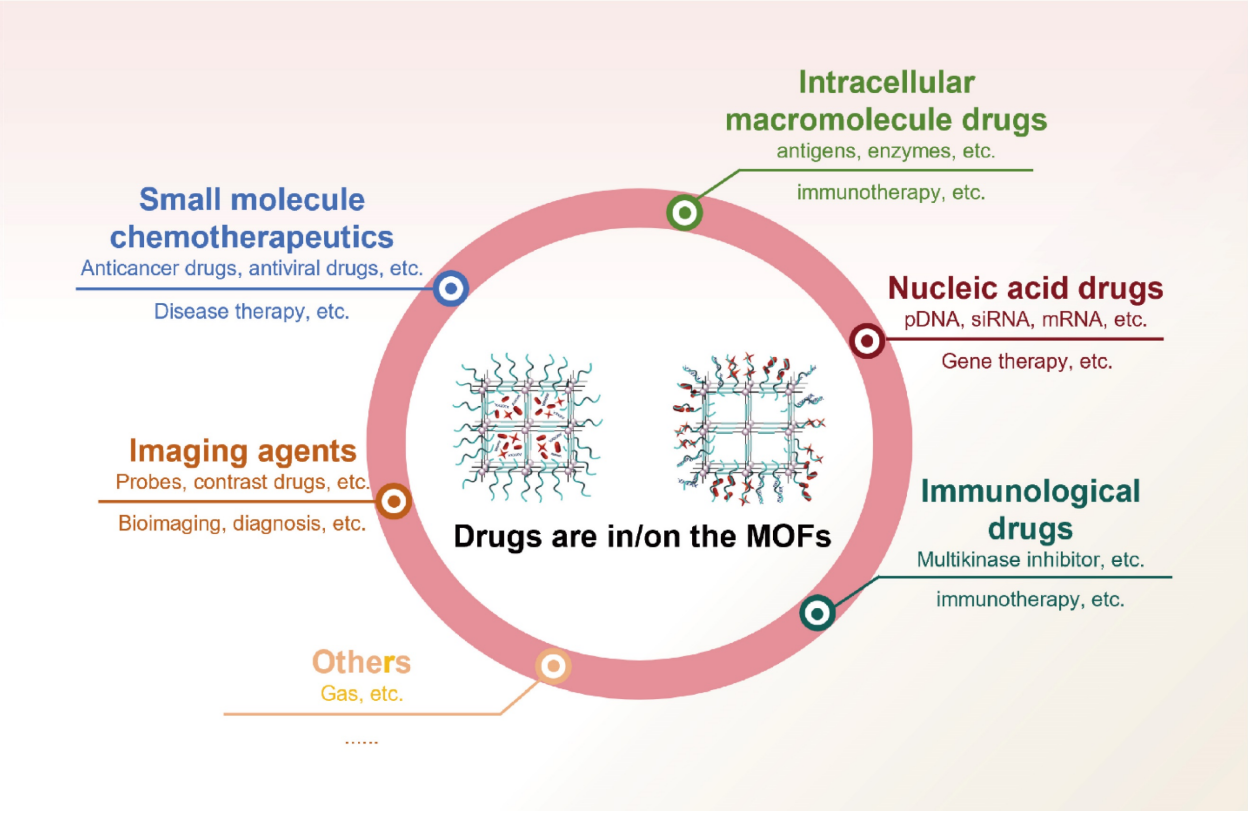

Figure 3. Applications of MOFs for drug delivery, including small molecule chemotherapeutics, macromolecules, nucleic acid drugs, immunological drugs, and imaging agents.

Table 2. Summary of MOFs-based drug delivery systems for chemotherapy.

MOFs	Drug	Loading percentage (wt%)	Release	Ref.
MIL-53-Cr	ibuprofen	22.0	18 days (SBF)	[92]
MIL-53-Fe	ibuprofen	21.0	20 days (SBF)	
	caffeine	29.2	6 h (SBF)	[93]
	busulfan	18.0	8 h (phosphate-buffered saline, PBS)	[94]
MIL-100-Cr/MIL-101-Cr	ibuprofen	25.8/58.0	3/6 days (SBF)	[96]
AuNR@ZIF-8-Zn	DOX	26.3	12 h (PBS, 95%)	[100]
AuNR@ZIF-8-Zn Janus	DOX	30.0	24 h (PBS, > 80%)	[101]
CAD@ZIF-8-FA (Zn)	DOX	34.75	96 h (PBS)	[102]
ZIF-8-Zn	5-FU	45.4	7 days (PBS)	[98]
	DOX	4.7	30 days (66%, DI Water)	[99]
	rapamycin	9.4	96 h (about 86%, PBS)	[103]
	camptothecin	26.3	15 h (76.3%, PBS)	[104]
	caffeine	28.0	27 days (SBF)	[105]
Fe-Zn-ZIF-8	5-FU	15.7	24 h (about 76%, PBS)	[106]
NiCo-Tb-PEGMA-AS1411	DOX	60.3	48 h (52.8%, PBS)	[107]

MOFs for chemotherapeutic compounds delivery

In conventional chemotherapy, many chemotherapeutic agents face significant barriers to clinical application, including poor solubility, chemical instability, low bioavailability, short circulation half-life, nonspecific tissue distribution and systemic toxicity. A fundamental limitation of traditional chemotherapy is the reliance on high drug doses to compensate for inefficient biodistribution, which frequently results in dose-dependent adverse effects. The development of DDS has alleviated several of these challenges by enabling improved targeting and controlled release of chemotherapeutic agents. Among diverse developed DDS platforms, MOFs have emerged as particularly promising carriers owing to their tunable pore architectures, high surface areas, high drug-loading capacities, and controllable multifunctionality. Iron-based MOFs, in particular, have demonstrated favorable biocompatibility and therapeutic efficacy as nanocarriers for the controlled delivery of antitumor and antiviral agents [32]. For instance, MIL-100(Fe) has been shown to efficiently encapsulate and deliver bisulfan (25.5%), azidothymidine triphosphate (21.2%), doxorubicin (DOX, 9.1%), and cidofovir (16.1%), enabling effective treatment of both cancer and Acquired Immune Deficiency Syndrome (AIDS). Remarkably, MOFs with diverse architectures have achieved maximum drug-loading efficiencies of up to 81.6 ± 0.6% [91]. A summary of representative MOF-based nanocarriers, along with their corresponding cargo types and drug-loading efficiencies (wt%) is presented in Table 2.

In 2008, Horcajada et al. [92] reported two representative MOFs (*i.e.*, MIL-53-Fe, MIL-53-Cr), capable of efficiently loading ibuprofen (IBU). Chemical analyses revealed that both MIL-53(Fe) and MIL-53(Cr) could adsorb approximately 20 wt% of IBU, with sustained release over a three-week period in simulated body fluid (SBF). Owing to its favorable physicochemical properties, MIL-53(Fe) exhibited a higher loading capacity and broader applicability, as further demonstrated with additional cargos such as caffeine (29.2 wt%) [93] and busulfan (18.0 wt%) [94].

Among the first-generation MOFs investigated for drug delivery, the Cr-based MIL-100 and MIL-101 have been extensively studied as classical DDS platforms (Figure 4A) [95]. These frameworks exhibited high loading efficiencies for a wide range therapeutics, including azidothymidine triphosphate, cidofovir, DOX, IBU, and caffeine. Notably, IBU, a representative nonsteroidal anti-inflammatory drug, exhibited loading capacities of 0.347 g g^{-1} in MIL-100(Cr) and 1.376 g g^{-1} in MIL-101(Cr) (Figure 4B) [96]. The markedly enhanced loading and prolonged release of IBU observed in MIL-101(Cr) were attributed to strong interactions between IBU and Lewis acid metal sites within the framework (Figure 4C, D). Despite these advantages, Cr-based MOFs present notable cytotoxicity, which limits their direct biomedical translation.

Zinc-based MOFs, particularly the ZIF series, have emerged as a major focus in DDS research since their initial report in 2006 [97]. Among them, ZIF-8 has attracted considerable attention due to its high stability under neutral and alkaline conditions, coupled with rapid degradation in acidic environments, which are particularly advantageous for tumor-targeted drug release. For instance, 5-fluorouracil (5-FU), a thymidylate synthase inhibitor widely used in cancer therapy, was successfully encapsulated within ZIF-8 with a loading capacity of 45.4%. This formulation exhibited markedly accelerated drug release at pH 5.0 compared with at pH 7.4, achieving 90% release within 12 h under acidic conditions [98]. The first

report of DOX loading into ZIF-8 in 2012 demonstrated a loading efficiency of 4.67% [99]. Subsequent studies employing chemical surface modifications substantially improved DOX loading efficiencies and enhanced both tumor-targeting capability and pH-responsive release (Figure 5A) [102].

Further optimization was achieved through the incorporation of pH-sensitive linkers, namely cis-aconitic anhydride (CAA) conjugated to DOX, in combination with FA functionalization. This strategy enhanced drug-loading efficiency and cellular targeting, while the tuning of particle size offered additional control over release behavior (Figure 5B, C). Beyond DOX and 5-FU, ZIF-8 has also been widely utilized to encapsulate a variety of therapeutic agents, such as rapamycin [103], camptothecin [104] and caffeine [105], underscoring its versatility as a robust platform for pH-responsive drug delivery.

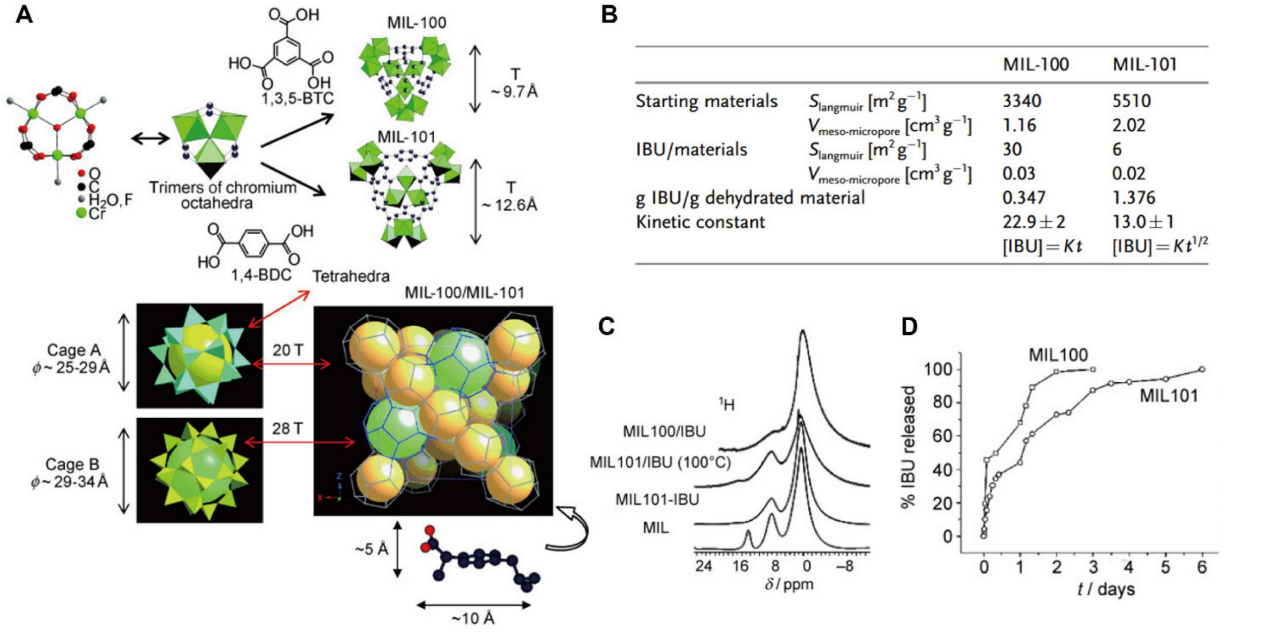

		MIL-100	MIL-101
Starting materials	$S_{langmuir}$ [$m^2 g^{-1}$]	3340	5510
	$V_{meso\text{-}micropore}$ [$cm^3 g^{-1}$]	1.16	2.02
IBU/materials	$S_{langmuir}$ [$m^2 g^{-1}$]	30	6
	$V_{meso\text{-}micropore}$ [$cm^3 g^{-1}$]	0.03	0.02
g IBU/g dehydrated material		0.347	1.376
Kinetic constant		22.9 ± 2	13.0 ± 1
		$[IBU] = Kt$	$[IBU] = Kt^{1/2}$

Figure 4. (A) 3D schematic of a tetrahedron (T) consisting of a chromium octahedron and 1,4-benzenedicarboxylate moieties or 1,3,5-benzenetricarboxylate groups in MIL-100/MIL-101, respectively; **(B)** Nitrogen adsorption data and the IBU content of MIL-100/MIL-101 investigate; **(C)** ^{1}H NMR spectra of MIL-100/IBU and MIL-101/IBU; **(D)** IBU delivery from MIL-100/MIL-101. Adapted with permission from [96], copyright 2006 WILEY-VCH.

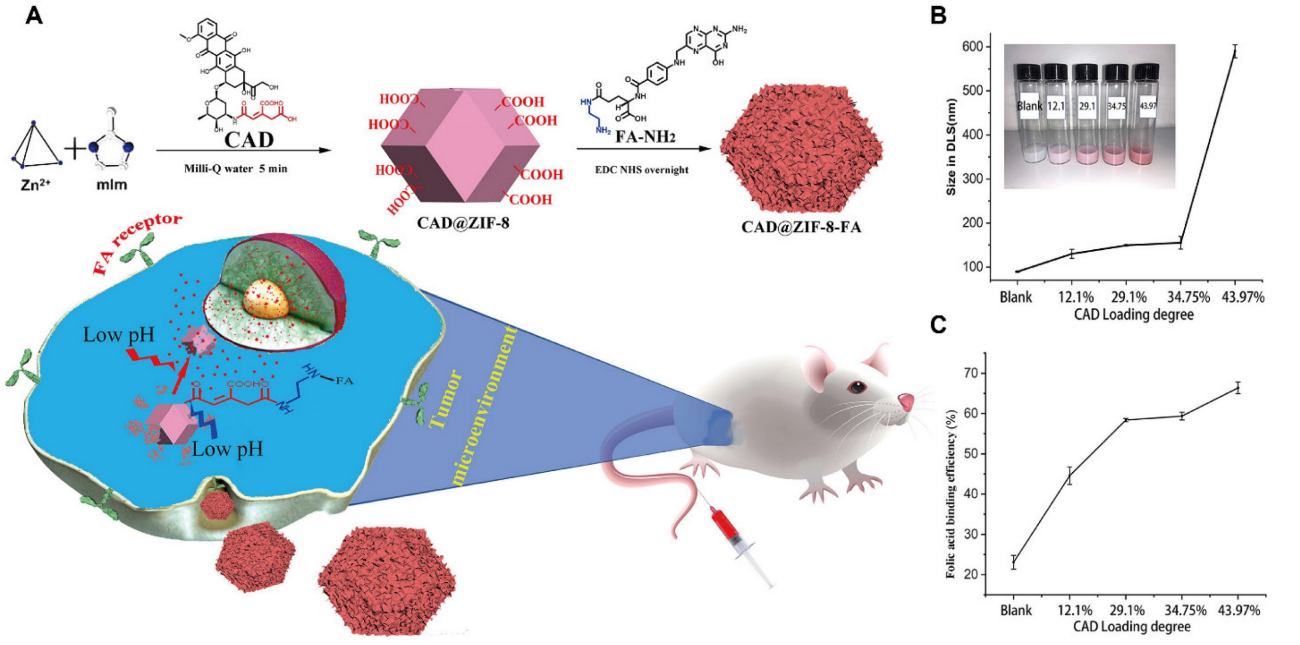

Figure 5. Zn-MOFs for delivery CAD toward TME. (A) Scheme of CAD@ZIF-8-FA NPs as a versatile nanocarrier for cancer treatment; **(B)** The size results of carriers with different drug loading rates in DLS; **(C)** The results of FA binding efficiency with different drug loading rates. Adapted with permission from [102], copyright 2020 American Chemical Society.

Polymetallic MOFs often exhibit enhanced drug delivery performance due to synergistic interactions among distinct metal centers. For example, Fe-Zn-ZIF-8 magnetic nanocarriers integrated the high drug-loading capacity of Fe-based MOFs with the pH-responsive behavior of Zn-MOFs, thereby achieving dual responsiveness to the TME [106]. Similarly, bimetallic NiCo-MOFs doped with Tb^{3+} demonstrated high drug-loading efficiency, pH sensitivity, strong fluorescence emission, and imaging capability [107]. Distinct metal centers impart unique physicochemical properties to MOFs: Fe-MOFs generally possess high porosity, Zn-MOFs offer great pH responsiveness, and Gd- and Mn-based MOFs offer superior imaging functionalities. Despite their compositional diversity, several consistent trends have emerged across MOF-based DDS research. First, MOFs generally exhibit substantial drug-loading capacities, often comparable to or exceeding those of conventional delivery platforms. Second, the internal pore structure of MOFs plays a critical role in determining drug encapsulation efficiency. Third, the hydrophilic-hydrophobic balance of organic linkers strongly influences drug-release kinetics, with more hydrophobic frameworks typically affording prolonged release profiles. Finally, the nature of the incorporated metal ions significantly affects biocompatibility; Fe-based MOFs generally exhibit lower toxicity than the Cr- or Zn-based analogues.

MOFs for gene delivery

Over the past two decades, RNA- and DNA-based cancer therapies have attracted considerable attention as promising strategies for cancer treatment. However, as large biological macromolecules, nucleic acid therapeutics face substantial barriers to effective delivery, including high susceptibility to nuclease-mediated degradation in bloodstream, limited accumulation in tumor tissues, poor cellular uptake and poor endosomal escape. Gene delivery largely relies on nanocarriers, including cationic nanomaterials such as liposomes, polymeric vectors, and inorganic nanoparticles. Nonetheless, conventional nanocarriers often suffer from low transfection efficiency and may induce adverse effects, including hemolysis.

Gene therapy was initially conceived to correct diseases caused by defective or aberrant genes through the introduction of functional genes into target cells. More broadly, it now encompasses DNA- and RNA-based therapeutic approaches for treating diverse diseases, including ocular, cardiovascular, and oncological disorders. For cancer gene therapy, the delivery of naked nucleic acids is particularly challenging, as effective *in vivo* delivery must overcome multiple biological barriers to reach specific tissues. Moreover, therapeutic efficacy depends on intracellular delivery, which is hindered by electrostatic repulsion between negatively charged nucleic acids and cell membranes [108], as well as susceptibility to hydrolysis and enzymatic degradation. Therefore, the development of tailored delivery systems is essential to achieve targeted and efficient gene delivery.

MOFs for DNA delivery

MOFs have emerged as promising platforms for gene delivery. To protect DNA from degradation and facilitate intracellular delivery, MOFs can be synthesized and loaded with DNA. For example, UiO-66-N_3 ($Zr_6O_4OH_4(C_8H_3O_4\text{-}N_3)_6$) was surface-functionalized with oligonucleotides via a strain-promoted click reaction, representing the first MOF -nucleic acid conjugate [109]. In this system, dibenzylcyclooctyne-modified DNA was conjugated to azide-functionalized UiO-66-N_3. MOFs can also be surface-modified with DNA to create nano-composites, such as ZIF-67-based constructs, which exhibit favorable biocompatibility and sustained drug release. Although DNA-loaded MOFs effectively protect nucleic acids during transport, achieving tumor-specific delivery remains a significant challenge. To cope with this limitation, disulfide bonds have been incorporated into the loop region of DNA hairpins, enabling electrostatic and coordination interactions with MOFs and allowing cancer cell-specific release triggered by elevated endogenous glutathione (GSH) at tumor tissues. In addition, plasmid DNA (pDNA), including sequences encoding green fluorescent protein, has been loaded into ZIF-8 [110]. In this system, MOFs not only shielded DNA but also enhanced cellular uptake and promoted endosomal escape, resulting in efficient intracellular gene expression across multiple cell types (Figure 6A).

MOFs for RNA delivery

RNA interference (RNAi) has been widely employed to selectively silence target messenger RNA (mRNA), thereby reducing gene and protein expression in gene therapy. Among RNAi therapeutics, synthetic siRNA and microRNA (miRNA) are the most extensively studied. Zeolitic imidazolate framework-8 (ZIF-8), a representative zinc-based MOF, exemplifies the potential of MOFs for RNA delivery (Figure 6B) [111]. For instance, a light-responsive nanoswitch based on ZIF-8 enabled intracellular and lysosomal disruption-triggered gene release. When co-loaded with indocyanine green (ICG) and siRNA, ZIF-8 generated heat upon laser irradiation, promoting siRNA release into the

cytoplasm and facilitating RNAi for cancer therapy. MOFs for siRNA delivery can also be fabricated via biomimetic synthesis strategies (Figure 6C). Cell membrane-coated MOFs have been developed to improve biocompatibility, immune evasion, and tumor targeting, thereby enhancing the translational potential of nucleic acid–based therapies. Similarly, ZIF-8 has been shown to protect miR-34a-m from *in vivo* degradation [112], allowing it to bind to complementary mRNA, suppress translation, and induce apoptosis. Compared with siRNA and miRNA, mRNA therapeutics face additional challenges due to their larger size and increased instability. To overcome these limitations, Zr-based MOFs chemically modified with polycationic ethanolamine-conjugated poly(glycidyl methacrylate) [PGMA(EA)] have been developed, these modified MOFs enhanced mRNA stability, cellular uptake and intracellular gene expression [113].

Overall, gene therapy has demonstrated broad potential for cancer therapy that are not fully addressable by traditional treatments. Nevertheless, several obstacles remain, including optimal target selection, formulation optimization, and carrier-cargo stability. Ideally, gene therapy should enable precise delivery, effectively suppress tumor growth, and minimize off-target effects. Recent advances in MOF-based gene delivery systems indicate substantial progress toward these goals (Table 3).

MOFs for imaging agents

Molecular imaging enables *in vivo* visualization and analysis of cellular, molecular, and genetic processes, facilitating early, sensitive, and quantitative disease diagnosis. Molecular imaging has become an indispensable tool across a broad range of biomedical research applications by integrating principles from biology, physics, chemistry, and medicine. However, traditional small-molecule imaging agents often suffer from limited specificity and suboptimal signal sensitivity. Nanomaterials with precisely engineered sizes, shapes, and compositions offer enhanced imaging sensitivity and targeting specificity, prompting the development of advanced imaging vectors over the past decade to improve diagnostic accuracy [117,118].

MOFs have emerged as promising nanoplatforms for molecular imaging due to their intrinsic luminescence, tunable size and morphology, and selective adsorption properties. The high porosity, periodic framework structure, and abundant functional groups of MOFs provide numerous active sites for the conjugation of imaging agents, resulting in high loading capacity. MOFs can serve either as standalone imaging probes or as versatile carriers for integrating multiple imaging agents, enabling multimodal imaging and improving diagnostic precision. Moreover, MOFs constructed from intrinsically fluorescent metal nodes or organic

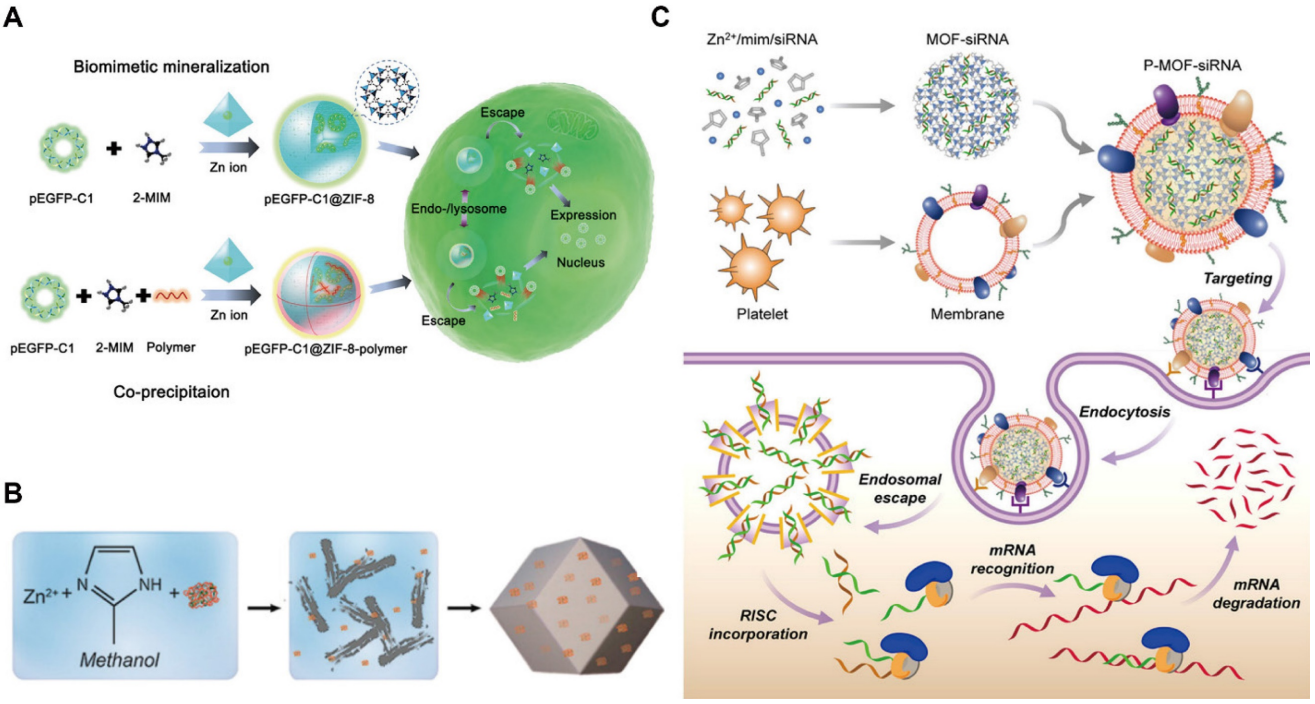

Figure 6. (A) Schematic representation of synthesis of pEGFP-C1@ZIF-8/pEGFP-C1@ZIF-8-polymer. Adapted with permission from [110], copyright 2019 WILEY-VCH; **(B)** The schematic shows the preparation of ZIF-8-based gene DDS [111], copyright 2014 American Chemical Society; **(C)** P-MOF-siRNAs (Platelet membrane-coated siRNA-loaded MOFs) for gene silencing. Adapted with permission from [112], copyright 2019 AAAS.

ligands can function as autonomous imaging reagents. As summarized in Table 4, this section highlights recent advances in applications of MOFs for cancer imaging and theranostics, including infrared-photothermal (IP), FL, MRI, CT, PET, and PA imaging.

MOFs for fluorescence imaging

Fluorescence imaging employs photo-luminescent probes to selectively target cancer cells, enabling direct *in vivo* visualization of the dynamic behavior of therapeutic agents. Over the past decades, fluorescent dyes, particularly ICG, have been widely used as imaging agents and approved by the Food and Drug Administration (FDA) for clinical applications. However, their use in cancer diagnostics is limited by poor aqueous solubility and low tumor specificity. MOFs offer an effective strategy to overcome these limitations. For instance, ICG-loaded MIL-100-Fe MOF nanoprobes were synthesized via HA surface modification (Figure 7A), exhibiting a uniform spherical morphology by transmission electron microscope (TEM). These nanoprobes achieved an ICG loading efficiency of up to 40%, leading to enhanced active tumor targeting and imaging intensity. The HA coating enabled active tumor targeting through specific recognition of CD44 receptors overexpressed on cancer cells.

Compared with free ICG, MOF@HA@ICG exhibited markedly higher fluorescence intensity at tumor sites, reduced degradation, and prolonged retention *in vivo*, with detectable signals persisting for up to 72 h post-administration (Figure 7B-D). These results highlight the excellent biocompatibility and biodegradability of the MOF-based system. Beyond cargo loading, MOFs can also serve as intrinsic fluorescent probes through the incorporation of emissive organic ligands. Porphyrins, characterized by favorable photostability, high fluorescence quantum yield, large Stokes shifts, and long excitation/emission wavelengths (λ_{ex}=420 nm, λ_{em}=660 nm), are particularly suitable for fluorescence imaging applications. For example, porphyrin-based MOFs coordinated with Fe^{3+} centers were loaded with dihydroartemisinin (DHA) to suppress premature drug release and subsequently coated with $CaCO_3$ to yield NMOF@DHA@$CaCO_3$. These MOF-based nanostructures functioned simultaneously as PSs and fluorescent probes [120].

Table 3. Summary of MOFs-based gene drug delivery systems (cargo, loading rate, MOFs materials, MOFs diameter, and application).

Cargo	MOFs	Materials	Loading rate (wt%)	Diameter (nm)	Application	Ref.
DNA	DNA@UiO-66-N3	UiO-66 (Zr)	12.3/13.0 pmol cm^{-2}	14/19	synthesis	[109]
DOX-SOR-DNA	ZIF-67@DS@ext-DNA	ZIF-67 (Co)	59.7/60.2	100-1000	therapy for MCF-7 cells	[114]
HP-SS-BT (DNA)	HP-SS-BT@UiO66-NH_2	UiO-66 (Zr)	72.3	115	nanoprobe	[115]
pDNA	pEGFP-C1@ZIF-8	ZIF-8 (Zn)	3.4	275.7	therapy for MCF-7 cells	[110]
siRNA	ICG@ZIF-8@siRNA	ZIF-8 (Zn)	8.15	166	therapy for A549 cells	[111]
siRNA	P-MOF-siRNA(Zn)	ZIF-8 (Zn)	/	175	therapy for SK-BR-3 cells	[112]
miRNA	miR-34a-m@ZIF-8	ZIF-8 (Zn)	3.6	255	therapy for MDA-MB-231 cells	[113]
mRNA	MOF-PGMA(EA)	UiO-66 (Zr)	/	26.4/41.7	drug delivery	[116]

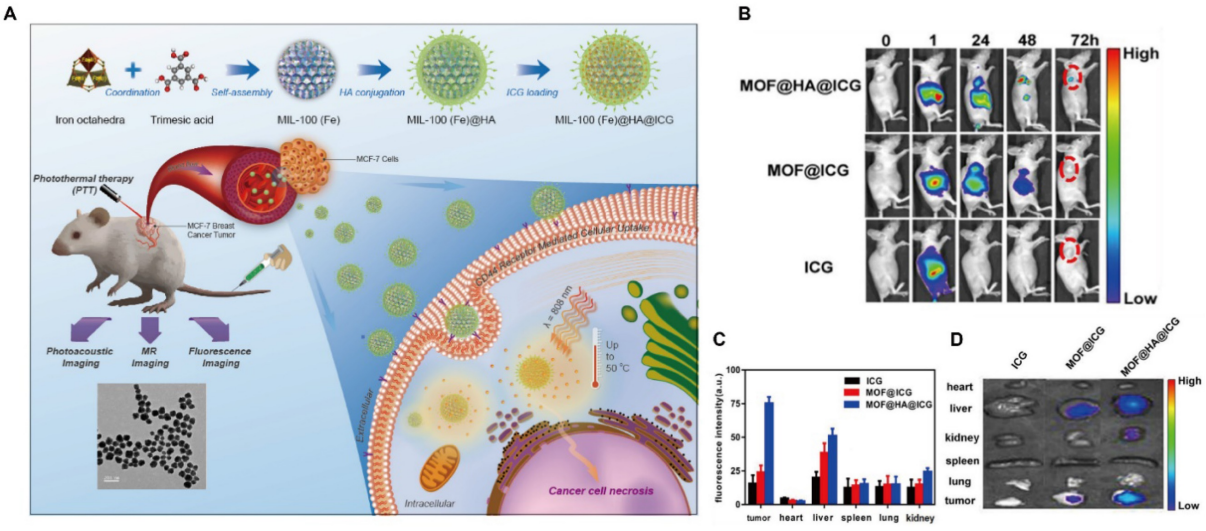

Figure 7. Fluorescence imaging of MIL-100-Fe@HA@ICG. (A) Schematic diagram of Fe-MOF synthesis and theranostics; **(B)** FL images of MCF-7 tumor-bearing mice injected with different treatments; **(C)** and **(D)** FL images and intensity of major organs and tumors. Adapted with permission from [119]. copyright 2017 American Chemical Society.

Table 4. The applications of MOFs for molecular imaging (imaging modality, MOFs, cargo, cell line, and application).

Imaging Modality	MOFs	Cargos	Cell line	Applications	Ref.
FL/MRI/PAI	MIL-100-Fe	ICG (40%)	MCF-7	Imaging (r_2: 54 $mM^{-1}s^{-1}$), PDT	[119]
FL/MRI	Fe-TCPP	DHA (75%)	4T1	Imaging, PDT, Chemotherapy	[120]
MRI	Gd/MPC	aPD-1 (28.23%)	SCC7	Imaging, Immunotherapy (Tumor inhibition rate: 84.6%)	[122]
MRI/FL	UiO-66(Zr)-$(COOH)_2$	DOX	4T1	Imaging (r_1: 18.77 $mM^{-1}s^{-1}$), Chemotherapy	[123]
MRI/FL	Mn-TCPP	-	4T1	Imaging (r_1: 6.08 $mM^{-1}s^{-1}$), PDT	[124]
MRI	Zr-MOF@MnO_2@Tm	Apatinib (32.9%)	4T1	Imaging, PDT, Chemotherapy	[125]
MRI	MnO_x/UiO-66-F/PPEG	-	4T1	Imaging (r_1: 11.16 $mM^{-1}s^{-1}$)	[126]
MRI	Fe_3O_4@UiO-66-Zr@WP6	5-FU (0.83 μmol mg^{-1})	Hela	Imaging (r_2: 72.23 $mM^{-1}s^{-1}$), Chemotherapy	[127]
IP/MRI	PPy@MIL-53-Fe/DOX	DOX (90%)	4T1	Imaging, PTT, Chemotherapy	[128]
MRI/FL	$Mn_3[Co(CN)_6]_2$@MIL-100@AS	Artesunate (53%)	Hela	Imaging (r_1: 6.61 $mM^{-1}s^{-1}$, r_2: 76.24 $mM^{-1}s^{-1}$), Chemotherapy (Tumor inhibition rate: 82.8%)	[129]
MRI	UCNP@Fe-MIL-101_NH_2	-	KB	Imaging (r_2: 67.32 $mM^{-1}s^{-1}$)	[130]
CT	Cu(I_4-BDC)/Zn(I_4-BDC)	-	-	-	[131]
CT	UiO(Zr)-PDT	BODIPYs	Walker-256	Imaging (CT value: 92 HU), PDT	[132]
CT	DOX@LA-AuNR/ZIF-8	DOX (30%)	H-22	Imaging, PTT, Chemotherapy (Tumor inhibition rate: 93%)	[101]
CT/MRI/PA	GNR-MSNs-MA-Fe	-	4T1	Imaging, PTT, Chemotherapy	[133]
PET	DOX@^{64}Cu-MOF-Au-PEG	DOX	U87MG	Imaging, RT, Chemotherapy (Tumor inhibition rate: 89%)	[135]
PET/FL	DOX@^{89}Zr-UiO-66/Py-PGA-PEG-F3	DOX (50%)	MDA-MB-231	Imaging, Chemotherapy	[136]
PET	Zr-MOF-PAC	DOX (25.1 μmol g^{-1})	U87MG	Imaging	[137]
PAI	Au@ZIF-8	-	4T1	Imaging, PTT (Tumor apoptosis: 77.48%)	[139]
PAI/MRI/CT	Au@MIL-88(A)	-	U87MG	Imaging	[140]
PAI/IR	Au@MOF-DOX	DOX (29%)	H22	Imaging, PTT, Chemotherapy	[141]

MOFs for magnetic resonance imaging

MRI is a non-invasive diagnostic technique based on the energy transitions of atomic nuclei possessing magnetic moments in an external magnetic field, with signal detection primarily arising from hydrogen nuclei in biological tissues. The acquired MRI signals are reconstructed into images; however, intrinsic tissue contrast is often limited because many tissues exhibit similar signal intensities, necessitating the use of contrast agents. These agents can be broadly categorized as T_1 (positive) or T_2 (negative) agents. T_1 agents, such as paramagnetic Gd^{3+} or Mn^{2+} ions, shorten longitudinal relaxation times and enhance anatomical contrast, whereas T_2 agents, typically superparamagnetic iron oxide nanoparticles, reduce transverse relaxation time to enhance image contrast, making areas of tissue damage or pathology more conspicuous. The rational selection of metal ions and organic ligands is critical, as coordination within complexes enhances thermodynamic stability and reduces toxicity compared to free ions [121]. MOFs emerged as effective nanoplatforms in delivering paramagnetic ions for MRI. For instance, Gd^{3+}-based MOFs synthesized via reverse microemulsion methods have demonstrated dual T_1 and T_2 contrast capabilities. Gd-MOFs loaded with anti-Programmed Death-1 (aPD-1) antibodies can integrate microwave hyperthermia, immunotherapy, and MRI, with tumor targeting enhanced by SCC7 membrane vesicle modification [122].

Mn^{2+}-based MOFs have attracted increasing attention due to their lower toxicity relative to Gd^{3+}. Mn^{2+} and DOX co-loaded Zr-MOFs with PEGylation showed improved stability and evaded the reticuloendothelial system, and enabled T_1-weighted MRI for cancer detection [123]. Recent advances have also focused on Mn^{3+}-centered MOFs, such as porphyrin-based Mn-MOFs, which exhibit enhanced stability relative to Mn^{2+} complexes. These GSH-activated nanosystems enable T_1-weighted imaging by consuming tumor-site GSH and releasing Mn^{2+} contrast agents upon intracellular reduction (Figure 8A) [124]. Mn-based MOFs commonly incorporate Mn^{3+} centers, electron-donating substituents on the porphyrin backbone further enhance the stability of Mn^{3+}-MOFs. Upon cellular internalization, Mn^{3+}-sealed MOF nanosystem deplete intracellular GSH, triggering the reduction of Mn–TCPP and subsequent Mn^{2+} release, thereby activating MRI contrast. *In vivo* fluorescence imaging and *ex vivo* organ analysis confirmed efficient tumor accumulation of the MOF probe (Figure 8B, C). Manganese oxides can also act as effective GSH scavengers. MnO_2 shells coating drug-loaded Zr-MOFs imparted acid responsiveness and eliminated excess intratumoral GSH, while modification with 4T1 cell membranes further enhanced tumor targeting efficiency [125]. In addition, doping MnO_x into the Zr-MOF shell via redox reactions combined with polymer modification yielded multifunctional, stimuli-responsive MOFs with MRI capability [126].

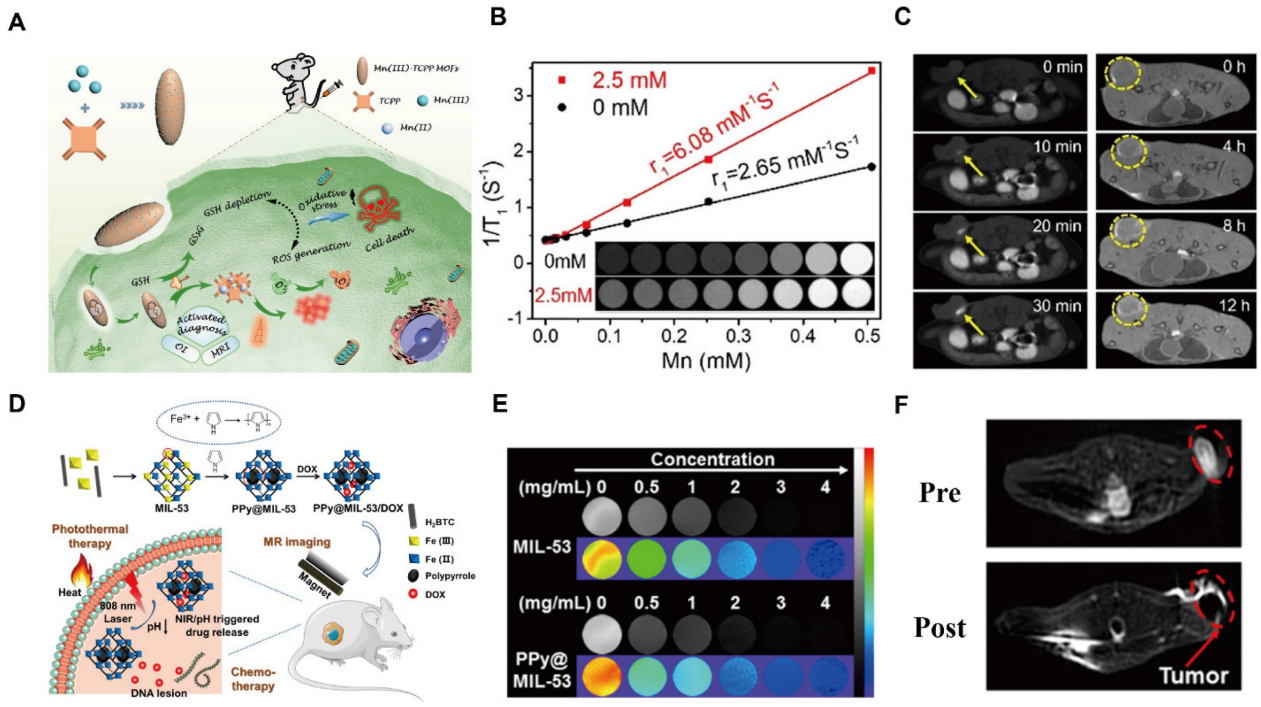

Figure 8. Mn-MOF/Fe-MOF as T_1/T_2 contrast agents for MR imaging. (A) Schematic illustration of a Mn(III)-MOF for imaging and therapy; **(B)** T_1 imaging of MOFs with or without GSH; **(C)** T_1 contrast signals after intratumoral injection (left) or intravenous injection (right). Adapted with permission from [124], copyright 2019 American Chemical Society; **(D)** Illustration of Fe-MOF synthesis for theranostics; **(E)** T_2-weighted MRI images and pseudo-color imaging of MIL-53 and PPy@MIL-53; **(F)** T_2-weighted MRI of PPy@MIL-53 (4T1 tumor lesion delineated by red lines). Adapted with permission from [128], copyright 2018 American Chemical Society.

As representative T_2-type contrast agents, superparamagnetic iron oxide nanoparticles (SPIONs) have been extensively investigated. Although Fe-MOF-based MRI contrast agents exhibit improved biocompatibility, their relatively moderate relaxation rates limit imaging sensitivity and impede clinical translation. To overcome this challenge, integrating magnetic nanoparticles within MOF frameworks offers a promising strategy. For instance, a multifunctional core-shell nanoplatform, Fe_3O_4@UiO-66@WP6, was developed by incorporating Fe_3O_4@MOF with pillar[6]arene nanovalves [127]. This system enables controlled multi-stimuli-responsive drug release and achieves MRI-guided cancer therapy. Release is accelerated under acidic conditions, while abnormal Zn^{2+} or Ca^{2+} levels associated with pathological states further modulate release behavior, effectively integrating intelligent drug delivery, MRI imaging, and chemotherapy within a single nanoplatform.

The MIL family, including MIL-53, MIL-100, and MIL-101, is well recognized for its high drug-loading capacity, controlled release behavior, T_2-weighted MRI capability, and low toxicity. MIL-53, featuring mixed-valence iron centers, can function as a microreactor that provides unsaturated iron sites essential for pyrrole (Py) oxidation to polypyrrole (PPy), enabling *in situ* synthesis of a photothermal–chemotherapeutic MOF [128]. Owing to its iron content, MIL-53 also serves as a T_2-weighted MRI contrast agent (Figure 8D), allowing visualization of nanocomposite distribution and synergistic photothermal and chemotherapeutic effects. Its MRI performance was validated through *in vitro* T_2-weighted and pseudocolor imaging at various concentrations of MIL-53 and PPy@MIL-53, as well as *in vivo* MRI evaluation (Figure 8E, F). MIL-100 has likewise been employed to construct a core-shell MOF nanoplatforms with high drug-loading efficiency, primarily driven by hydrophobic interactions [129].

The system serves as a dual-mode MRI contrast agent for T_1 (Mn)-T_2 (Fe) imaging, exhibiting enhanced performance compared with single-mode agents. The enhanced r_1 relaxivity likely arose from amplified T_1 effects induced by the external T_2 component, while integrating T_1 and T_2 contrast agents mitigates spin coupling among T_2 agents, reducing local magnetic field attenuation. Multimodal imaging strategies have been pursued via integrating different imaging modalities. A core-shell nanostructure, UCNP@Fe-MIL-101-NH_2, was constructed using MIL-101 as the substrate [130]. Subsequent surface modification with PEG and FA improved tumor targeting through FA receptor recognition. Both *in vitro* and *in vivo* studies demonstrated strong upconversion luminescence (UCL) and progressively enhanced T_2-weighted MRI contrast in tumor regions. Overall, MOF-based

multifunctional contrast agents, characterized by low toxicity, structural tunability, and integrated imaging capabilities, represent a promising nanoplatform for biomedical imaging and theranostic applications.

MOFs for CT imaging

CT serves as an important complementary diagnostic modality that utilizes X-ray radiation to generate high-resolution three-dimensional images based on the differential attenuation of X-ray by tissues and organs. Conventional CT contrast agents are typically composed of high atomic number (Z) elements, such as iodine, barium, and bismuth, which effectively absorb X-rays. Representative clinical agents include iodixanol, barium sulfate, and gadopentetate dimeglumine.

MOFs incorporating high-Z elements have demonstrated intrinsic CT imaging capability and have offered a promising nanoplatform as CT contrast agents. In 2009, a class of MOFs with CT contrast potential was synthesized using Cu^{2+} and Zn^{2+} as metal centers in combination with an iodide-based organic ligand (Z_I = 53) [131]. The theoretical iodine loadings of these MOFs reached 63.2% and 55.3%, respectively, both exceeding that of iodixanol (49%)—highlighting their potential for enhanced CT contrast. Moreover, a highly crystalline and monodisperse UiO-PDT nanocrystal was fabricated by incorporating a photoactive iodine-BODIPY dye ligand into UiO-type MOFs (Figure 9A) [132]. *In vivo* studies at a dose of 100 mg kg^{-1} demonstrated negligible acute and subacute toxicity, with no significant adverse effects observed. UiO-PDT exhibited excellent CT imaging capacities, achieving optimal contrast enhancement at 24 h post intravenous administration (Figure 9B).

Gold (Au) possesses superior X-ray attenuation properties owing to its high atomic number (Z_{Au} = 79) and K-edge energy (k_{Au} = 81), providing stronger contrast than iodine-based CT agents. Gold nanorods (GNRs) encapsulated within ZIF-8 have been developed as dual-functional CT contrast and photothermal agents, with DOX further loaded following lactobionic acid (LA) modification to enable liver cancer targeting [161]. The resultant near-infrared (NIR)/pH-responsive MOF system allows for CT-guided chemotherapy and photothermal therapy (PTT) combinational therapy.

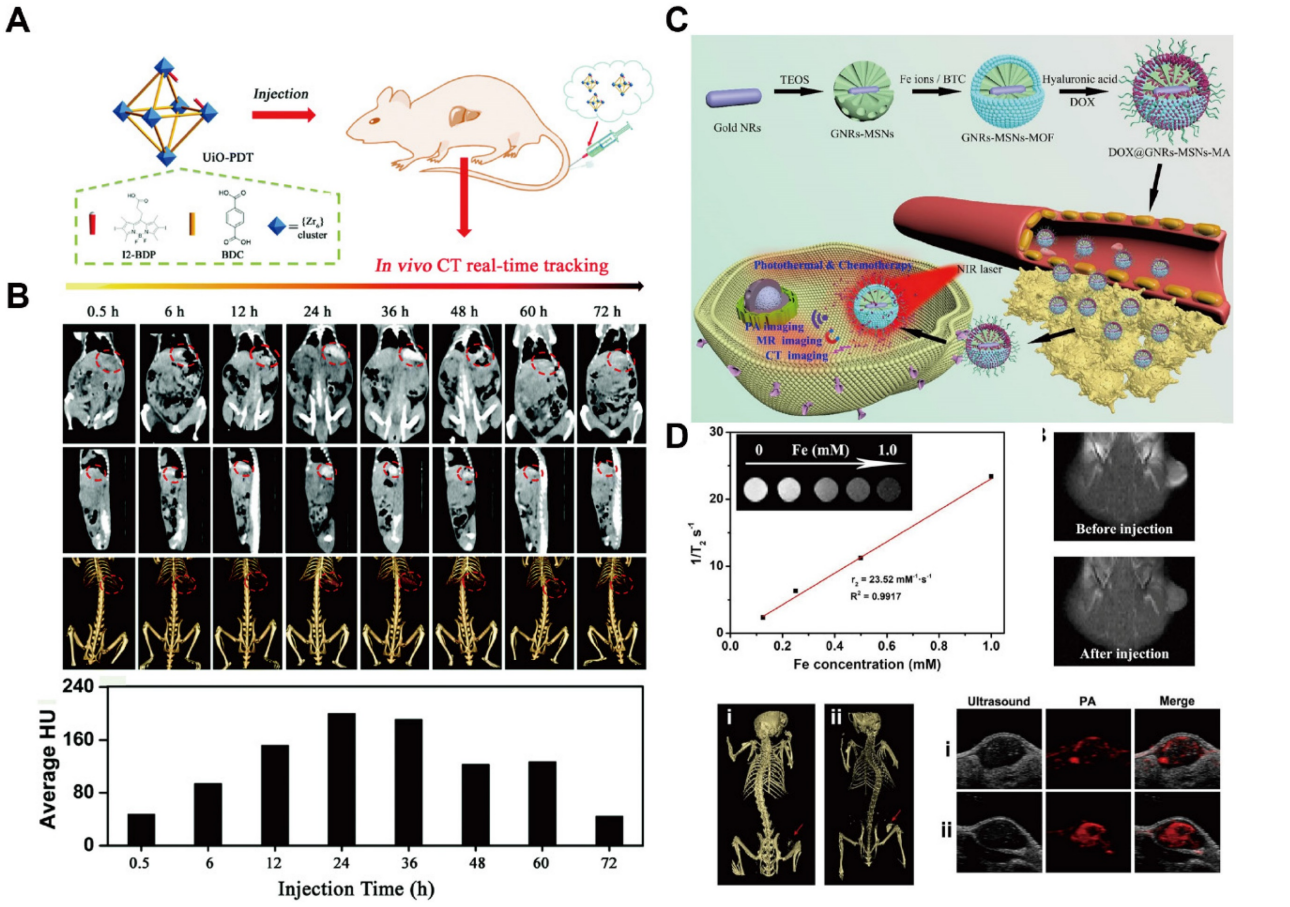

Figure 9. MOFs for tumor imaging by CT. (A) Synthesis of UiO-PDT MOF for CT imaging; (B) CT images of Walker-256 tumors in a rat by UiO-PDT MOFs. Adapted with permission from [132], copyright © 2020 Royal Society of Chemistry; (C) Diagrammatic representation of the synthesis, imaging, and therapy of the GNRs-MSNs-MA; (D) MRI/CT/PA images of 4T1 tumors in mice with (i) GNRs-MSNs-MOF and (ii) GNRs-MSNs-MA. Adapted with permission from [133], copyright © 2021 Elsevier.

Owing to their high drug-loading capacity, MOFs can also be integrated with other nanoparticles to enhance CT contrast and enable multimodal imaging. For example, GNRs encapsulated within MOFs have demonstrated effective CT imaging capability (Figure 9C) [133]. In this design, an iron-based MOF was synthesized *in situ* on dendritic mesoporous silica-coated GNRs (GNRs-MSN) to form a core-shell nanostructure, followed by HA modification to improve tumor targeting. The strong X-ray attenuation of GNRs embedded within the MOF confirmed their CT contrast performance. Moreover, the resultant nanoplatform exhibited tri-modal imaging capability (MRI/CT/PA) and enhanced tumor accumulation after HA modification (Figure 9D). Nevertheless, the complexity of the synthesis process remains a major challenge, limiting large-scale production and clinical translation. Current research efforts are therefore focused on simplifying MOF fabrication while further improving their multimodal imaging performance.

MOFs for PET imaging

PET is a widely used nuclear imaging modality that provides tissue-, cellular-, and molecular-level information by detecting positrons emitted from short-lived radioisotopes such as ^{11}C, ^{13}N, ^{15}O, ^{18}F, ^{64}Cu, ^{68}Ga, ^{89}Zr, and ^{124}I. Despite its high sensitivity, excellent quantitative capability and deep tissue penetration, PET imaging faces several challenges, notably the short half-lives of radionuclides and limited diagnostic specificity [134]. MOFs, owing to their high drug-loading capacities and multiple metal-ion nodes, have emerged as promising platforms for PET imaging. For example, a Zr-TCPP MOF integrated with gold NPs, loaded with DOX, and further modified with PEG-SH was developed as an oxygen-regulating nanoplatform (Figure 10A) [135]. Following intravenous injection of ^{64}Cu-labeled MOF-Au-PEG in tumor-bearing mice, whole-body and organ-specific PET imaging revealed pronounced tumor accumulation at multiple time points (Figure 10B, C).

Beyond surface radiolabeling, the intrinsic structural versatility of MOFs allows direct incorporation of positron-emitting isotopes into their frameworks. For example, ^{89}Zr was directly introduced into UiO-66 to construct a DOX-loaded radioactive MOF [136]. Subsequent surface functionalization with pyrene-polyethylene glycol (Py-PGA-PEG) and an F3 peptide ligand endowed the system with enhanced targeting toward triple-negative breast cancer (Figure 10D). PET imaging demonstrated that tumor accumulation of the modified MOF was approximately three- to fourfold higher than that of the unmodified counterpart (Figure 10E). Comprehensive toxicity studies confirmed the absence of both acute and chronic toxicity. However, the susceptibility of Zr-based MOFs to degradation in phosphate-rich environments remains a limitation. To address this, bis[2-(methacryloxy)ethyl] phosphate (BMAP) ligands were grafted on the surface of ^{64}Cu-Zr-MOFs, effectively preventing acid and phosphate-induced decomposition, prolonging circulation time, and enhancing targeted delivery [137]. Upon reaching TME, intracellular GSH triggered polymer degradation, exposing the MOF core to phosphate ions and promoting the release of encapsulated therapeutics. Overall, the integration of stimuli-responsive designs with intrinsically radioactive MOFs represents a promising strategy to improve drug utilization efficiency and PET imaging performance (Figure 10F).

MOFs for PA imaging

PA imaging is a rapidly advancing, non-invasive, and non-ionizing imaging modality that utilizes pulsed laser irradiation to generate US waves in light-absorbing regions of biological tissues. The resultant acoustic signals are detected by an external ultrasound transducer and reconstructed into high-contrast images of internal structures. By combining the advantages of optical excitation and ultrasonic detection, PA imaging offers high spatial resolution and relatively deep tissue penetration, making it highly promising for early cancer diagnosis and treatment monitoring [138].

Despite these advantages, PA imaging often suffers from weak intrinsic signal intensity in biological tissues, necessitating a high amount of exogenous contrast agents at the target site. However, the limited targeting ability of many conventional agents reduces their effective utilization. To address these challenges, MOFs have been explored as versatile PA contrast platforms capable of enhancing imaging sensitivity and therapeutic efficacy. For instance, embedding Au nanoparticles within Zn-MOFs enabled pH- and GSH-responsive release, inducing strong plasmonic NIR absorption and thereby enhancing PA signal intensity [139]. Similarly, core-shell Au@MIL-88(A) nanostructures (89 nm) with star-like morphology exhibit high crystallinity and multimodal PAI/MRI/CT imaging capabilities (Figure 11A) [140]. Moreover, the integration of MOFs with chemotherapeutics enables synergistic imaging and therapy. A yolk-shell nanostructure was fabricated by depositing ZIF-8 on Au nanostars, followed by tannic acid etching and DOX loading, resulting in a multifunctional platform that combines

enhanced PA imaging with chemotherapy (Figure 11B) [141]. In addition, chemical surface modification can endow MOFs with active targeting functionality, further improving PA imaging performance.

Although most MOFs lack intrinsic PA activity, their tunable composition, favorable biocompatibility, and high porous structure render them promising scaffolds for the development of next-generation PA contrast agents. Enhancing the sensitivity and selectivity of MOF-based agents remains a highly, and continued advances in rational design are expected to significantly broaden their applications in theranostics.

MOFs for delivering other bioactive compounds

While immunotherapy has attracted considerable interest as a promising cancer treatment, its clinical efficacy remains limited by challenges such as low response rates, limited tumor specificity, and systemic toxicity. MOFs, owing to their high loading capacity and large surface area, have emerged as versatile platforms for enhancing antitumor immunotherapy. MOFs can potentiate cancer immunotherapy through multiple mechanisms, including targeted delivery of antigens and immunostimulatory agents, modulation of immune dysfunction within the TME, and synergistic therapeutic effects. For instance, ovalbumin (OVA) encapsulated in ZIF-8, with surface modification by unmethylated cytosine-phosphate-guanine oligodeoxynucleotides (CpG ODNs), enables precise targeted immunotherapy, effectively promoting antigen presentation while enhancing the overall biocompatibility and immunogenicity [142]. Similarly, incorporating the Toll-like receptor 7/8 (TLR7/8) agonist R848 into bimetallic FeMn-MOFs allows HA-mediated targeted delivery, where the released metal ions and R848 within the TME induce ICD and potentiate immunotherapy [143].

Given their catalytic versatility, enzymes have been explored for metabolic modulation in cancer therapy; however, their poor stability limits standalone application. MOFs provide a protective and stabilizing matrix for enzyme delivery. For example, lactate oxidase loaded into Fe-MOFs, in combination with siRNA, can deplete lactic acid and reverse the immunosuppressive TME [144]. DNAzyme-MOFs systems further function as multifunctional nanocarriers capable of accommodating nucleic acids (*e.g.*, DNAzymes and CpG) through electrostatic and coordination interactions [145]. The acidic TME facilitates ZIF-8 degradation, enabling controlled release of DNAzymes and photosensitizer Ce6 for combinational therapy. Moreover, MOFs possess intrinsic diagnostic and therapeutic potential, supporting their development as nanotheranostic agents that integrate tumor detection and treatment. The following section summarizes recent advances in MOF-based strategies across diverse cancer therapies.

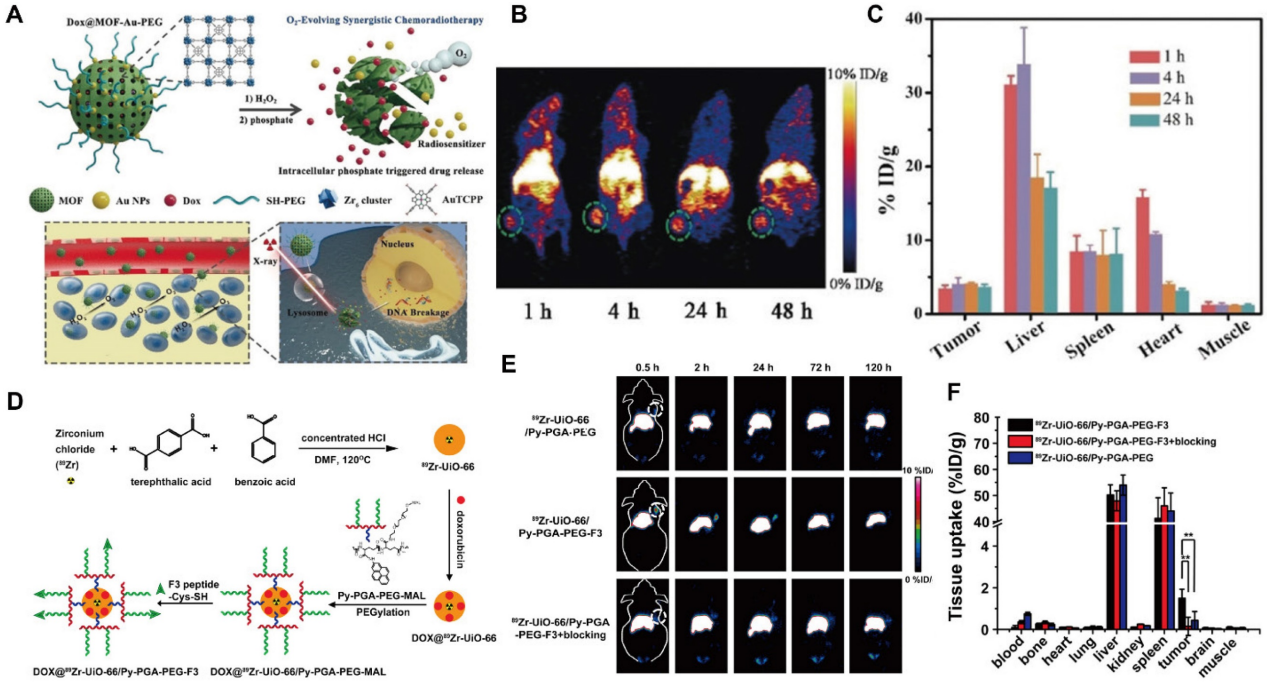

Figure 10. MOFs for tumor imaging by PET. (A) Schematic representation of DOX@MOF-Au-PEG synergistic chemoradiotherapy; **(B)** PET imaging of ^{64}Cu-MOF-Au-PEG; **(C)** Quantitative ROI assay of major tissues. Adapted with permission from [135], copyright 2019 WILEY-VCH; **(D)** Schematic of the synthesis of ^{89}Zr-UiO-66/Py-PGA-PEG-F3 Conjugates; **(E)** PET images of MDA-MB-231 tumors in mice by ^{89}Zr-MOFs; **(F)** Organ distribution of ^{89}Zr-MOFs at 120 h. Adapted with permission from [136], copyright 2017 American Chemical Society.

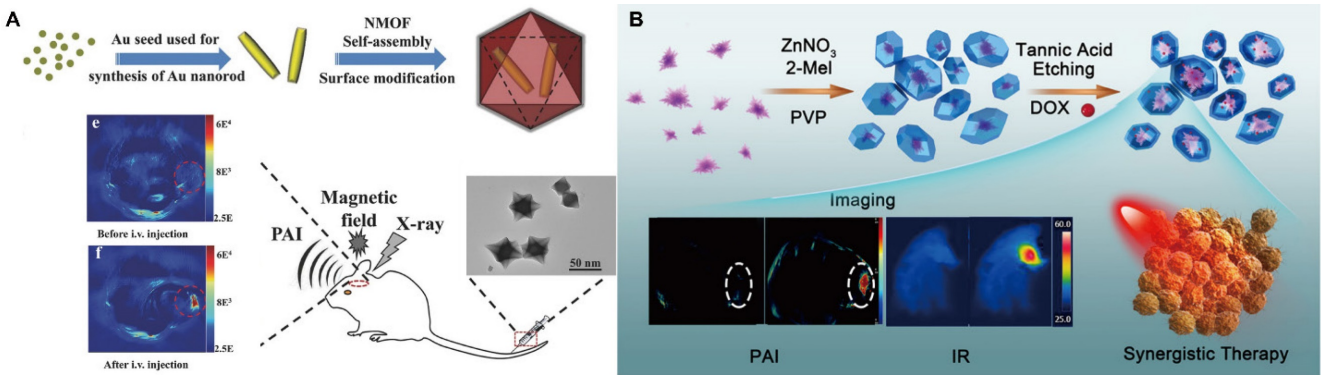

Figure 11. MOFs for tumor imaging by PAI. (A) Schematic illustration of the synthesis of core-shell Au@MIL-88(Fe) nanostars and one of the PAI images in triple-modal. Reproduced with permission. Adapted with permission from [140], copyright 2017 WILEY-VCH. **(B)** Schematic illustration of the fabrication of Au@MOF-DOX, PAI imaging effects. Adapted with permission from [141], copyright 2019 American Chemical Society.

MOFs for cancer theranostics

Conventional cancer treatments, including surgery, chemotherapy, and RT, remain the mainstay of clinical oncology. However, chemotherapy is often limited by non-specific drug distribution, multidrug resistance, and severe side effects. To address these challenges, the integration of traditional therapeutics with nanomedicine has emerged as a promising strategy. Compared with conventional materials, MOFs offer distinct advantages for drug delivery. As discussed earlier, MOFs possess high drug-loading capacities and can be readily engineered for targeted and stimuli-responsive release. Consequently, multifunctional MOF-based nanoplatforms have demonstrated considerable potential and have been extensively explored for cancer therapy. MOFs can act as efficient carriers for therapeutic agents or imaging contrast agents, thereby enabling simultaneous treatment and diagnosis of tumors. Moreover, MOF-based systems have advanced conventional therapies and facilitated the development of emerging treatment modalities such as radiotherapy, PTT, PDT, chemodynamic therapy (CDT), sonodynamic therapy (SDT), and immunotherapy. As summarized in Table 5, this section focuses on multifunctional MOF-based nanoplatforms designed for integrated cancer therapy.

MOFs for RT based theranostics

RT, a clinically available approach for cancer treatment, exerts its therapeutic purpose by utilizing ionizing radiation to inhibit cancer cells within the irradiated region. However, the intrinsic radio-resistance of certain tumor types, together with unavoidable radiation-induced toxicity to surrounding normal tissues, often limits the efficacy of RT as a standalone treatment. These challenges have motivated the development of radiosensitizers—agents with low intrinsic toxicity that can enhance tumor sensitivity to radiation. MOFs have been investigated as promising radiosensitizers for cancer radiotherapy.

Hf-MOF and Zr-MOF, constructed from high-atomic-number metal centers within the UiO framework, have been shown to act as efficient X-ray absorbers, thereby enhancing RT therapeutic efficiency to some extent. Subsequently, metal elements with even higher atomic numbers (such as bismuth) were introduced into porphyrin-based MOFs (Figure 12A, B). Compared to Hf, these elements exhibit superior X-ray absorption and energy transfer efficiencies, resulting in more pronounced radiosensitization effect [146].

Beyond single-modality enhancement, current research increasingly focuses on RT-based multi-modal therapy strategies. For instance, leveraging the high drug-loading capability of MOFs, the stimulator of interferon genes (STING) agonist 4-(5,6-dimethoxybenzo[b]thiophen-2-yl)-4-oxobutanoic acid (MSA-2) has been encapsulated into a MOF based on Hf6 SBUs and hexakis(4′-carboxy[1,1′-biphenyl]-4-yl)benzene (HCBB) bridging ligands for robust cancer radio-immunotherapy (Figure 12C) [147]. Alternatively, RT can be combined with radiodynamic therapy (RDT), in which scintillators convert X-ray radiation energy into visible light to activate photosensitizers. This process promoted the interactions between photosensitizers and oxygen to generate singlet oxygen ($^1O_2$), thereby inducing extensive tumor cell apoptosis. As an illustrative example, hemoglobin (Hb) was loaded on Hf-TCPP to provide a substantial oxygen supply, alleviating tumor hypoxia and significantly enhancing the therapeutic efficacy of the combined RT-RDT strategy (Figure 12D) [148].

Table 5. The application of MOFs for theranostics (cargo, modifier, imaging, properties, and applications).

MOFs	Cargo (wt %)	Modifier	Imaging	Properties and Applications	Ref.
Hf-DBP/Bi-DBP	-	-	-	RT/RDT for TRAMP-C2/Panc02 tumor	[146]
Hf-HCBB/MSA-2	MSA-2 (29.2%)	-	-	RT for CT26 tumor	[147]
Oxy-HB@HP (Hf)	Oxygen	Hemoglobin(48.9%)	-	RT/RDT for CT26 tumor	[148]
ICG@ZIF-8	ICG (10.2%)	-	FL	PTT for SMMC-7721 tumor	[149]
pDA/MTX@ZIF-8	MTX (16.5%)	pDA	-	IC50: 8.27 μg mL^{-1}, PTT/chemotherapy for MG63 tumor	[150]
HMPB (Fe)@PEI/ICG/DOX	ICG/DOX (32.12%/40.46%)	PEI	FL/IR	Photothermal conversion efficiency: 45.51%, Tumor inhibition rate: 95.5%, PTT/PDT/chemotherapy for 4T1 tumor	[151]
PS@MIL-100-Fe-F127	Ce6/TPEDC/TPETCF (42%/49%58%)	F127	-	PDT for 4T1 tumor	[152]
DBP-UiO (Hf)	-	-	-	PDT for SQ20B tumor	[153]
HA-DOX-PCN	DOX (51.9%)	HA	-	PDT for Hek-297T/SCC7/MDA-MB-231 cells	[154]
Fe-TCPP@BSA/SDs@MnO_2	MnO_2	BSA/SDs	MRI (r_1: 6.09 $mM^{-1}s^{-1}$)	PDT for 4T1 tumor	[155]
CM-MMNPs (Zr)	MnO_2 nanosheet	Cancer cell membrane	MRI	PDT for 3T3 tumor	[156]
$MnFe_2O_4$@MOF (Zr)	-	PVP	MRI	PDT for 4T1 tumor	[157]
MOFs (Fe)@SF@TPZ	TPZ (7.7%)	silk fibroin	FL	Tumor inhibition rate: 99.6%, PDT/CDT/chemotherapy for 4T1 tumor	[158]
Mn-MOF (Zr)	-	-	-	Tumor inhibition rate: 89.2%, pulmonary nodules inhibition rate: 96.9%, SDT/immunotherapy for H22 tumor	[160]
D-Ti-MOF	-	-	-	SDT/CDT for 4T1 tumor	[161]
Zn-N_3-ZIF-8	-	-	-	Tumor inhibition rate: 84.6%, SDT for 4T1 tumor	[162]
ABTS@Fe-PVP	ABTS (22.0%)	PVP (25.3%)	PA/IP	CDT/PTT for 4T1 tumor	[164]
JMIL-101-Fe@CM	Juglone (10.2%)	Cell membrane (80.3±5.1 μg mg^{-1})	-	Tumor inhibition rate: 77.0%, CDT/chemotherapy for PC-3 tumor	[165]
Co-Fc (Fe)@GOx	GOx (1%)	PVP	-	CDT/starvation therapy for 4T1 tumor	[166]
ZIF-8 (Zn)@ICG@DOX@PVP	ICG/DOX (16.84%)	PVP	FL/PA/IP	PTT/PDT/chemotherapy/immunotherapy for 4T1 tumor	[168]
cMn-MOF@CM	CpG (20%)	B16-OVA membrane	-	SDT/immunotherapy for B16-OVA tumor	[169]
LYS-NPs (Zn)	Perforin/ Granzyme B (71.36%)	CD63-Aptamer	FL	Tumor inhibition rate: 70.9%, Immunotherapy for A549 tumor	[170]
P/M@CasMTH1 (Zr)	Cas9/sgMTH1	Thioglycolald-ehyde/PEI	FL	ROS level: 83.0%, Tumor inhibition rate: 60%, SDT/immunotherapy for A549 tumor	[172]
FdMI (Mn/Zr)	-	PDA/fucoidan	FL	Tumor inhibition rate: 78.7%, MT/MDT for 4T1 tumor	[173]
POM@ZIF-8 (Zn)	-	POM	-	EDT for Hela tumor	[175]
Nic-MOF@HA (Zr)	Nic (24.12%)	HA	FL	Tumor inhibition rate: 95.66%, Target therapy for 4T1 tumor	[176]

MOFs for PTT based theranostics

PTT, which eradicates tumors through localized thermal ablation, has been extensively investigated owing to its minimal side effects. Temperature elevation at the tumor site arises from the conversion of light energy into heat by photothermal agents, leading to direct hyperthermia in cancer cells. Upon accumulation at the lesion site, these agents are irradiated with NIR light to achieve effective tumor ablation. ICG, an FDA-approved NIR dye, is widely recognized as an efficient photothermal agent. For example, ZIF-8 loaded with ICG enabled fluorescence imaging-guided PTT, integrating diagnosis and therapy within a single platform [149]. In addition, the incorporation of surface-modified polymers as photothermal agents, together with strategies to enhance the stability and biocompatibility of MOFs, represents effective approaches. PDA can be coated on the surface of ZIF-8 to function as a photothermal agent, while the MOF interior serves as a reservoir for the chemotherapeutic drug Methotrexate (MTX), enabling combinational photothermal and chemotherapy treatment [150].

Beyond serving as drug carriers, certain MOFs also exhibit intrinsic photothermal properties and can be applied to enhance the effect of conventional PTT agents. For example, a MOF can be etched to form hollow mesoporous nanoparticles (HMPB NPs) with improved drug-loading capacity [151]. These nanoparticles can be co-loaded with ICG and DOX to generate HPID NPs (Figure 13A). The HPID NPs exhibit enhanced photothermal performance, while the MOF framework mediates temperature-responsive drug release (Figure 13B, C). Furthermore, the MOF-based system enabled the monitoring of drug accumulation and distribution via fluorescence and infrared imaging (Figure 13D, E), thereby integrating tumor diagnosis with PTT-based triple combination therapy (Figure 13F).

MOFs for PDT based theranostics

As outlined earlier, PDT represents one of the three therapeutic modalities within the HPID nanomedical platform. PDT is a light-activated anticancer strategy that requires the concurrent presence of three components: a PS, light of a specific wavelength, and endogenous O_2. The treatment

process generally consists of two stages: targeted delivery of the PS, followed by controlled light irradiation. Upon activation by light, the PS transfers energy to surrounding O_2 molecules, generating reactive oxygen species (ROS) that ultimately induce cancer cell death. PSs, such as hematoporphyrin derivatives, were first introduced in cancer PDT in the 1970s. However, the intrinsic hydrophobicity of many PSs has limited their clinical application. To address this limitation, various strategies have been developed to load PSs into MOFs. For instance, Ce6, 2-((4′-(2,2-bis(4-methoxyphenyl)-1-phenylvinyl)-[1,1′-biphenyl]-4-yl)(phenyl)methylene)malononitrile (TPEDC), and (E)-2-(4-(4-(2,2-bis(4-methoxyphenyl)-1-phenylvinyl)styryl)-3-cyano-5,5-dimethylfuran-2(5H)-ylidene)malononitrile (TPETCF) have been encapsulated in MIL-100-Fe and further modified with F127 to enhance tumor targeting, resulting in effective PDT [152]. Encapsulation within MOFs prevents PS aggregation and premature leakage while minimizing undesired interaction with O_2 prior to reaching the lesion site. Porphyrins can also serve as organic ligands for MOFs, giving rise to intrinsic photodynamic MOFs that inherently function as PSs. For example, 5,15-bis(p-benzoic acid) porphyrin (H2DBP) has been coordinated with Hf^{4+} SBUs to construct porphyrin-based MOFs for cancer PDT [44]. This design strategy suppressed porphyrin self-quenching associated with aggregation and significantly enhanced PDT efficacy. Subsequently, numerous studies have reported the development of intrinsic photodynamic MOFs [153]. Among these, Zr^{4+}-based MOFs incorporating tetrakis(4-carboxyphenyl)porphyrin (TCPP) as the organic ligand have attracted particular attention due to their high ROS generation, excellent structural stability, and favorable biodegradability [154].

The therapeutic efficacy of PDT can be further enhanced by optimizing ROS generation efficiency within TME. The most direct strategy involves increasing endogenous O_2 levels and/or reducing ROS scavenging in the TME. One established approach is to load MnO_2 into MOFs, where MnO_2 decomposes the elevated hydrogen peroxide (H_2O_2)

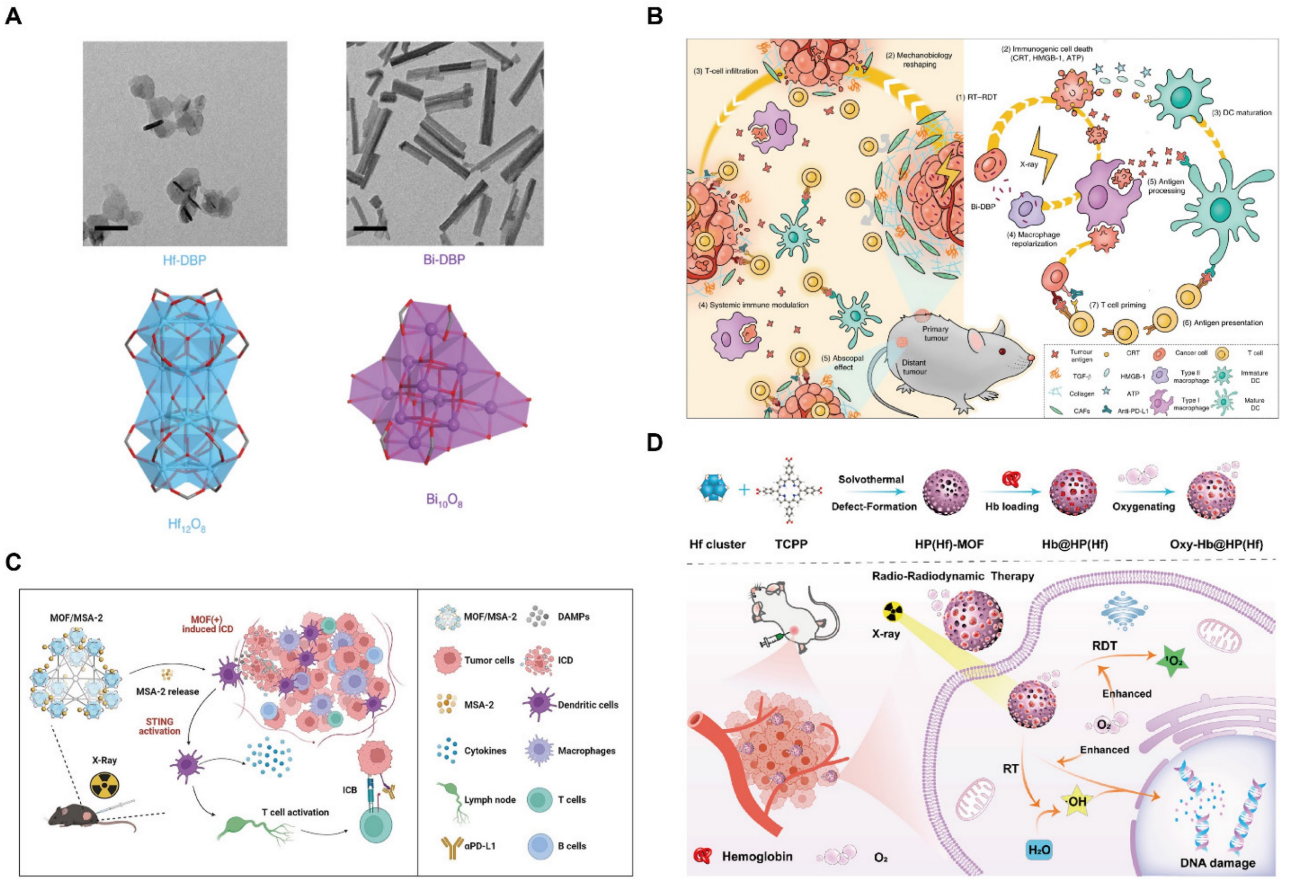

Figure 12. (A) Transmission electron microscopy images of Hf-DBP/Bi-DBP and structures of $Hf_{12}O_8$ SBUs in Hf-DBP and Bi10O8 SBUs in Bi-DBP (Scale bars: 100 nm); **(B)** Scheme of Bi-DBP-mediated RT–RDT for modulating biomechanics to promote T-cell infiltration. Adapted with permission from [146], copyright 2022 Springer Nature; **(C)** Synergistic mechanism of MOF/MSA-2 for radio-sensitization and immune activation. Adapted with permission from [147], copyright 2024 WILEY-VCH; **(D)** Schematic illustration of the oxygen-enriched Hb@HP(Hf) nanosensitizer for RT-RDT cancer therapy: synthesis and mechanism of action. Adapted with permission from [148], copyright 2023 American Chemical Society.

in the TME to generate O_2, thereby alleviating local O_2 concentration. Concurrently, MnO_2 degrades into Mn^{2+} within the TME, enabling MRI-guided tumor diagnosis [155,156]. Moreover, core-shell MOF nanostructures have been engineered to simultaneously convert H_2O_2 into O_2 and deplete GSH, thereby minimizing ROS scavenging and achieving enhanced PDT efficacy (Figure 14A) [157]. The release of Mn^{2+} enabled MRI-guided, precision cancer treatment (Figure 14B, C).The localized O_2 depletion induced during PDT can also potentiate the efficacy of hypoxia-activated chemotherapeutic agents, providing a foundation for PDT-based combination therapy. Tirapazamine (TPZ), a hypoxia-activated prodrug (HAP), exhibits preferential cytotoxicity under hypoxic conditions. Silk fibroin–modified Fe-TCPP MOFs loaded with TPZ (denoted as NST) enabled simultaneous PDT and hypoxia-activated chemotherapy. Within the TME, MOF degradation and the Fe^{3+}/Fe^{2+} redox cycle reduce ROS consumption by reacting with GSH, while further depleting endogenous O_2 to enhance PDT efficacy and amplify HAP therapeutic effects (Figure 14D, E) [158]. Fluorescence imaging confirmed tumor accumulation of NST. Both *in vitro* (Figure 14F, G) and *in vivo* studies (Figure 14H) demonstrating that the combinational treatment significantly outperformed single-modality therapies.

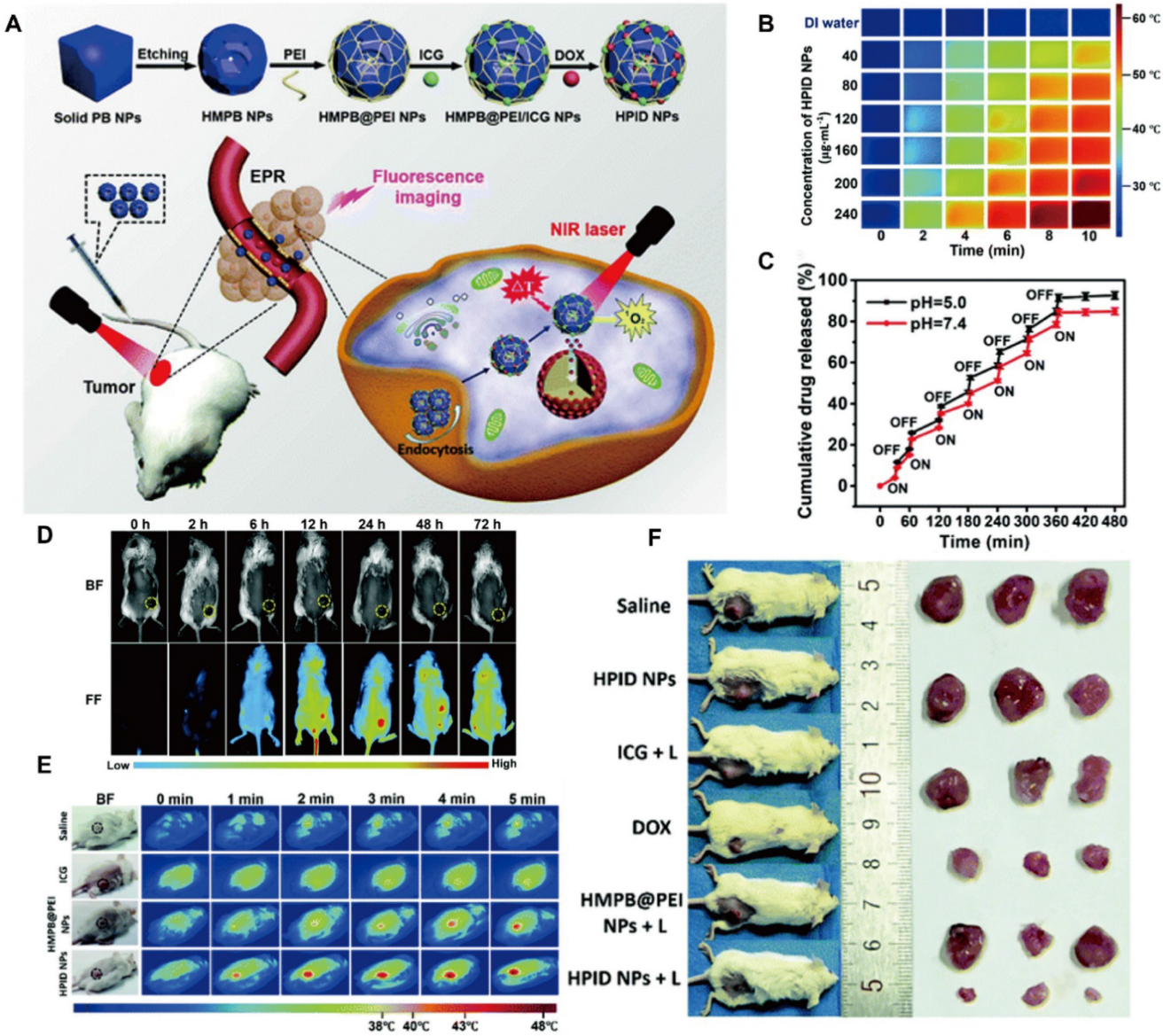

Figure 13. (A) Schematic diagram of the synthesis process of HPID NPs; **(B)** Infrared thermal images with HPID NPs (808 nm, 2 W cm^{-2}); **(C)** DOX release kinetics of HPID NPs; **(D)** Bright-field and fluorescence images after *i.v.* of HPID NPs; **(E)** Thermal imaging of tumor site irradiated by NIR laser at different times. Adapted with permission from [151], copyright 2019 Royal Society of Chemistry.

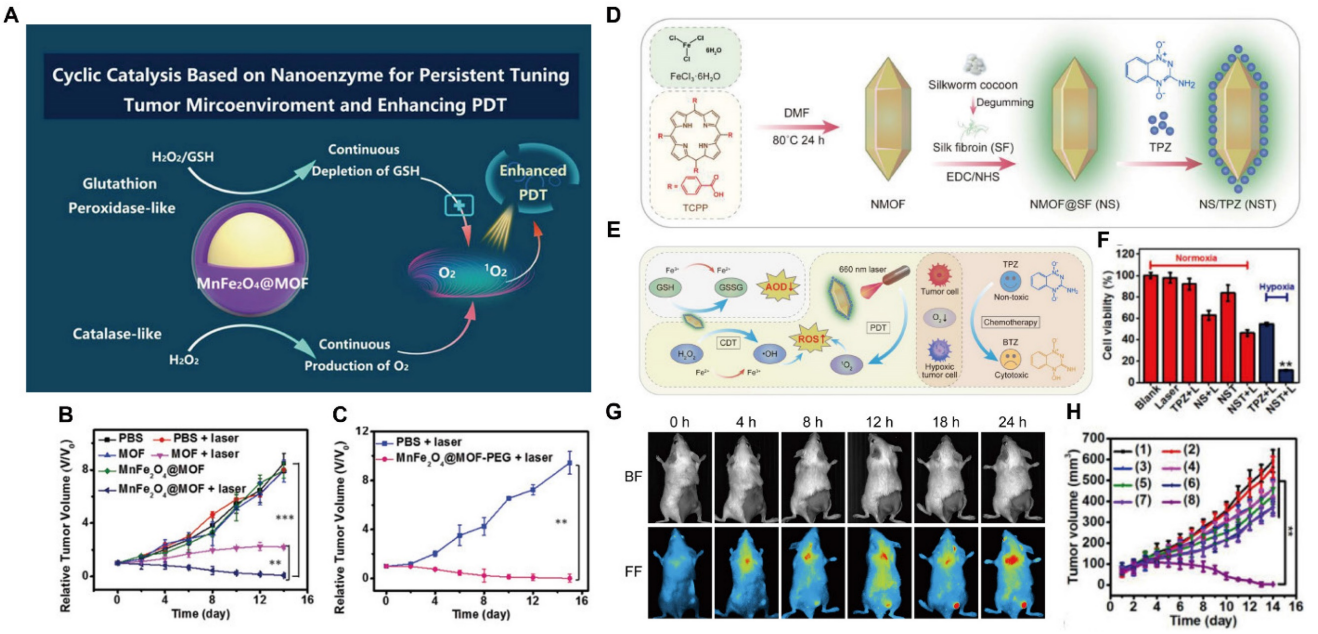

Figure 14. (A) The core-shell structure and mechanism of $MnFe_2O_4$@MOF for continuous depletion of GSH and production of O_2 to enhance PDT; **(B)** Tumor growth curve after Intratumoral injection; **(C)** Intravenous injection. Adapted with permission from [157], copyright 2019 WILEY-VCH. **(D)** and **(E)** The structure and mechanism of treatment of NST; **(F)** Viability of tumor cells after various treatments under normoxic/hypoxic conditions; **(G)** Bright-field and fluorescence images after *i.v.* of NST NPs; **(H)** Changes in tumor volume. Adapted with permission from [158], copyright 2022 Elsevier.

MOFs for SDT based theranostics

Despite the development of diverse combination treatment strategies that have significantly enhanced PDT efficacy, its therapeutic potential remains fundamentally constrained by the limited penetration depth of light in biological tissues. Consequently, PDT exhibits reduced efficacy in the treatment of deep-seated solid tumors. To overcome this limitation, SDT has emerged as a promising non-invasive treatment modality. SDT employs a sonosensitizer and O_2 to generate ROS, gas bubbles, and cavitation effects under low-intensity or dose-graded short-term repeated ultrasound irradiation. Due to its relatively higher tissue penetration, spatial selectivity and minimal off-target damage to surrounding healthy tissues, SDT exhibits an excellent safety profile and considerable potential. However, SDT faces two critical challenges. First, the bioavailability of sonosensitizers, particularly organic sonosensitizers, is often limited, and they typically lack effective tumor-targeting capabilities. Second, similar to PDT, the hypoxic tumor microenvironment restricts ROS generation and compromises SDT efficacy. Addressing these limitations by improving sonosensitizer bioavailability and endogenous O_2 concentration is essential for fully realizing the therapeutic potential of SDT [159].

MOFs have attracted considerable attention in SDT due to their exceptional sonodynamic properties. Inspired by the development of MOFs for PDT, early SDT-oriented MOFs primarily focused on their intrinsic SDT properties rather than merely passive carriers for free sonosensitizers, while simultaneously enabling efficient drug loading of additional chemotherapeutics. For example, a manganese porphyrin-based MOF (Mn-MOF) was engineered to facilitate synergistic SDT and ferroptosis-mediated cancer therapy [160]. In this system, Zr^{4+} ions served as coordination nodes and were bridged by manganese 5,10,15,20-tetrakis(4-benzoic acid) porphyrin (Mn-TCPP), which functioned as sonosensitizers. Notably, Mn^{2+} catalyzed the decomposition of H_2O_2 to generate O_2, while Zr^{4+} depleted GSH, collectively promoting ROS accumulation and enhancing SDT efficacy (Figure 15A). Furthermore, US irradiation suppressed GPX4 activity and exacerbated ROS mediated ferroptosis (Figure 15B). Mn-MOF also exhibited potent anticancer effects by increasing the infiltration of activated CD8+ T cells and mature dendritic cells (DCs) while reducing myeloid-derived suppressor cells (MDSCs) within TME, thereby enabling a combined SDT-immunotherapy. TiO_2 is a classical inorganic sonosensitizer; however, its ROS generation is severely limited by rapid electron-hole (e^-/h^+) recombination (50 ± 30 ns). In contrast, MOFs exploiting linker-to-metal-cluster charge transfer can significantly enhance charge transport and catalytic activity. A defective NH_2-MIL-125 (Ti) (D-Ti-MOF), composed of Ti^{4+} clusters and 2-aminoterephthalic acid linker, was synthesized as one of the earliest highly effective a photocatalytic MOF [161].

Subsequent hydrogen reduction generated Ti^{3+} (Figure 15C), resulting in bandgap narrowing, improved charge transfer, and enhanced e^-/h^+ separation, thereby markedly increasing SDT efficiency (Figure 15D). Moreover, the unique valence band (VB) and conduction band (CB) configuration enabled generation of $^1O_2$ and hydroxyl radicals (•OH) via water catalysis, as confirmed by EPR spectra (Figure 15E).

In conventional sonosensitizers, metal-nitrogen moieties often serve as key active sites for sonoocatalysis. Inspired by this, a novel MOF featuring atomically dispersed transition-metal-nitrogen-coordinated Zn-Nx sites within the microporous carbon framework derived from ZIF-8 was developed [162]. The unsaturated Zn-N active sites exposed on the (110) crystal facet enhanced electron transfer under US irradiation, effectively mimicking the functions of conventional sonosensitizers. These studies highlight that a critical future direction for SDT lies in the rational engineering of MOF structures to develop novel sonosensitizers with superior catalytic activity and therapeutic performance.

MOFs for CDT based theranostics

CDT is an emerging anticancer modality that induces tumor cell apoptosis and necrosis by catalytically converting endogenous H_2O_2 into highly reactive •OH via the Fenton or Fenton-like reaction mediated by metal-based nanomaterials (*e.g.*, Fe, Cu, Mn, Cr). Compared with normal tissues, the TME exhibits is characterized by aberrant metabolism, resulting in a mildly acidic pH and elevated levels of H_2O_2—conditions that are particularly favorable for CDT [163]. As a therapeutic strategy driven by endogenous stimuli, CDT exhibits high tumor selectivity and rational activation, highlighting its strong potential for clinical translation. Owing to their tunable architectures and intrinsic catalytic metal centers, MOFs are especially well suited for CDT applications.

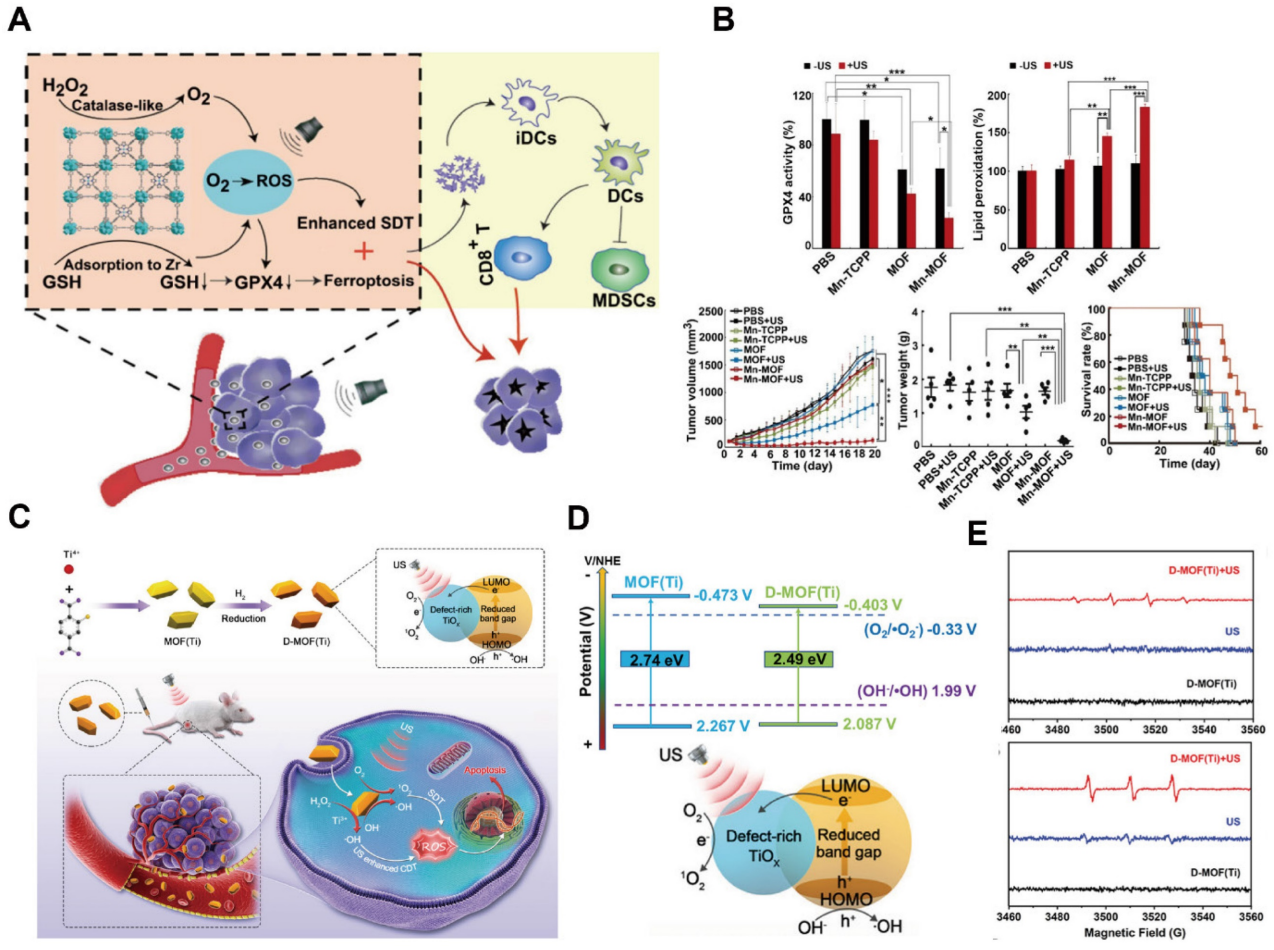

Figure 15. (A) Schematic diagram of Mn-MOF enhancing combination in cancer treatment (SDT and ferroptosis); **(B)** GPX4 activity and lipid peroxidation treated in different groups, with or without US irradiation; Tumor volume/weight changes and survival rate after different treatments. Adapted with permission from [160], copyright 2021 PubMed Central; **(C)** Schematic illustration of structure, mechanism and treatment style of D-MOF(Ti); **(D)** The charge transfer of MOF(Ti) and D-MOF(Ti) enhances the mechanism diagram and corresponding energy band diagram of SDT; **(E)** Determination of ROS by EPR spectrum (up: ·OH , down: $^1O_2$). Adapted with permission from [161], copyright © 2021 WILEY-VCH.

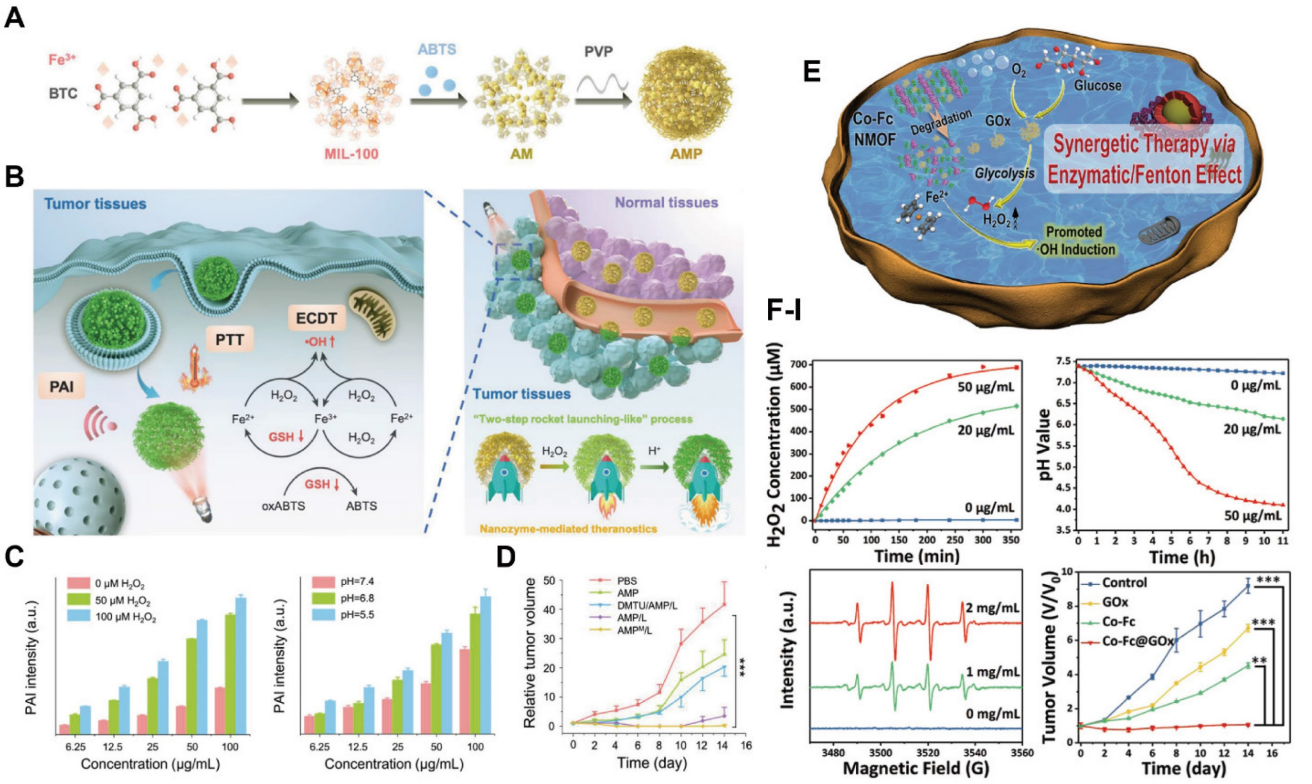

Figure 16. (A) Schematic diagram of AMP NPs preparation; **(B)** AMP as a dual-mode image-guided diagnostic reagent combination mechanism diagram (PTT-CDT); **(C)** PAI signal intensity under varying concentrations of H_2O_2 or at different pH levels; **(D)** The tumor volume changes. Adapted with permission from [164], copyright 2019 WILEY-VCH; **(E)** Schematic diagram of Co-Fc@GOx in synergetic therapy; **(F)** Changes in pH value of Co-Fc@GOx under different concentrations of glucose solution; **(G)** Changes in H_2O_2 concentration of Co-Fc@GOx under different concentrations of glucose solution; (H) EPR spectroscopy was used to detect the ability of Co-Fc@GOx to produce ·OH at different concentrations of glucose solutions; **(I)** The tumor volume changes in mice after treatments. Adapted with permission from [166], copyright 2020 WILEY-VCH.

For example, a MIL-100-based MOF loaded with 2,2′-azino-bis(3-ethylbenzothiazoline-6-sulfonic acid) (ABTS) and surface-modified with polyvinylpyrrolidone (PVP) was developed as a diagnostic and therapeutic nanoplatform for PA imaging-guided PTT and CDT combinational therapy (Figure 16A, B) [164]. This system not only enabled efficient PAI but also promoted H_2O_2 activation under acidic conditions, amplifying the PAI signal (Figure 16C). Notably, the PAI intensity was detectable even in small tumors (~20 mm^3), highlighting its promise for early tumor diagnosis. *In vivo* studies further validated the synergistic antitumor efficacy of the combined CDT-PTT therapy (Figure 16D).

Enhancing CDT efficacy generally relies on increasing endogenous H_2O_2 concentrations and further acidifying the TME. For instance, MIL-101(Fe)-based MOF incorporating juglone, a redox-active compound, significantly improved CDT performance by elevating intracellular H_2O_2 levels through an electron-transfer cascade, thereby enhancing Fenton reaction efficiency and tumor eradication [165]. Similarly, a cobalt–iron bimetallic MOF (Co-Fe-MOF) with strong Fenton catalytic activity was developed and further functionalized with glucose oxidase (GOx) to construct a cascade nanoplatform (Figure 16E) [166]. GOx catalyzes glucose oxidation within the TME, generating H_2O_2 and gluconic acid, which simultaneously increases H_2O_2 concentration and lowers pH. This synergistic coupling of enzymatic and Fenton reactions markedly enhanced CDT efficacy, as demonstrated by comprehensive *in vitro* and *in vivo* experiments (Figure 16F-I).

MOFs for immunotherapy based theranostics

Cancer immunotherapy harnesses the immune system to selectively recognize and eradicate malignant cells, thereby inducing durable antitumor immunity and preventing metastasis and tumor recurrence. Currently, the major immunotherapeutic strategies include adoptive cell therapy, cancer vaccines, and immune checkpoint blockade therapy. Representative examples of adoptive cell therapy encompass chimeric antigen receptor (CAR) T-cell therapy, T-cell receptor-engineered (TCR) therapy and chimeric antigen receptor-natural killer cell (CAR-NK) therapy. Immune checkpoint blockade therapy functions by inhibiting immunosuppressive checkpoints, whereas cancer vaccines aim to elicit an immune response against tumor-associated antigens

(TAAs) [167]. In recent years, MOFs have attracted considerable attention as platforms for enhancing cancer immunotherapy, particularly when combined with external stimuli such as light, ultrasound, X-rays, or magnetic fields. Beyond direct tumor ablation, these externally activated MOF systems can induce immunogenic cell death (ICD), leading to the release of damage-associated molecular patterns (DAMPs) and TAAs. This process promotes DC maturation and T-cell activation, ultimately eliciting systemic antitumor immune responses. For example, an intracellular acid-responsive polymer-MOF hybrid (DIMP) was designed to co-deliver the chemotherapeutic agent DOX and the photo-therapeutic agent ICG for breast cancer therapy [168]. This nanoplatform enabled precise and targeted drug delivery while effectively inducing ICD, enhancing DC maturation, and improving therapeutic efficacy, thereby achieving synergistic therapy. Such strategies also mitigated systemic toxicity and adverse effects associated with conventional pharmacological agents.

In addition to ROS-induced ICD, the direct incorporation of immune adjuvants into MOFs represents another promising approach for combination immunotherapy. For instance, a manganese-based MOF (Mn-MOF) electrostatically bound CpG oligonucleotides, which are Toll-like receptor 9 (TLR9) agonists functioning as potent immune adjuvants [169]. Subsequently, a cancer cell membrane derived from B16 melanoma cells expressing the OVA antigen was coated on this complex to form cMn-MOF@CM. This biomimetic construct prolonged systemic circulation and enhanced tumor targeting. The synergistic effects of CpG-mediated immune stimulation and efficient SDT promoted ICD, DC maturation, and T-cell activation, ultimately generating robust antitumor immunity.

In addition, MOFs have demonstrated considerable potential in facilitating adoptive T-cell therapies. A lysosome-responsive MOF nanoplatform (LYS-NP) was developed, which functioned as a TCR-based therapeutic strategy [170]. These MOFs selectively targeted lysosomes within adoptive T cells, which subsequently functioned as intracellular carriers—termed adoptive T-cell vectors (ATVs)—for the controlled delivery of cytotoxic proteins. During fabrication, ZIF-8 frameworks were loaded with perforin and granzyme B, both of which are capable of inducing apoptosis in tumor cells. The MOF surface was further mineralized with calcium carbonate ($CaCO_3$) and functionalized with a CD63 aptamer (CD63-Apt), enhancing biocompatibility and lysosomal targeting (Figure 17A). When the TCR was inactive, ATVs were retained within lysosomes in a quiescent state. Upon major histocompatibility complex (MHC)-mediated activation, lysosomal exocytosis was triggered, resulting in the localized release of perforin, granzyme B, and Ca^{2+} at the immunological synapse and effectively initiating localized tumor cell killing (Figure 17B, C). The CRISPR-Cas9 system is a versatile gene-editing platform that enables precise genomic modification, including knockout, knock-in, inhibition, and activation for cancer therapy. Stimuli-responsive and controlled release of the CRISPR-Cas9 complex is highly desirable to enhance therapeutic precision while minimizing genotoxicity [171]. In this context, nanoscale MOFs have been utilized as efficient sonosensitizers to amplify SDT efficacy while simultaneously enabling ultrasound-triggered release of CRISPR-Cas9 ribonucleoproteins (RNPs) [172]. Specifically, the CasMTH1 RNP complex was covalently conjugated to a porphyrin-integrated nMOF via ROS-responsive thioether linkages and subsequently coated with polyethyleneimine (PEI) to facilitate lysosomal escape (Figure 17D). Upon ultrasound irradiation, ROS generation cleaved the thioether bonds, triggering RNP release and disruption of the MutT Homolog 1 (MTH1) gene, a key enzyme responsible for detoxifying oxidized nucleotides and protecting tumor cells from oxidative stress. The synergistic combination of SDT-induced ROS production and CRISPR-mediated MTH1 gene disruption effectively undermined tumor cell defenses, leading to substantial inhibition of tumor progression both *in vitro* and *in vivo*.

MOFs for other therapy-based theranostics

In addition to the mainstream therapeutic strategies discussed above, MOFs have also been explored in several emerging cancer treatment modalities. Microwave thermotherapy (MT), a clinically established localized tumor ablation technique, induces tumor cell necrosis by exploiting the heat generated from the rapid rotation and friction of dipolar molecules under microwave irradiation [173]. Compared with conventional surgical resection, MT offers several advantages, including reduced invasiveness, lower cost, and real-time intraoperative monitoring enabled by imaging guidance. To further improve the precision and efficacy of MT, tumor-targeted MOFs have been developed as microwave sensitizers capable of amplifying localized thermal effects within tumor sites. For instance, an Mn- and ionic liquid-doped MOF, following surface modification, was engineered as a highly efficient microwave sensitizer that effectively eradicated tumor cells via combined MT and microwave-dynamic therapy (MDT). Notably, microwave irradiation was found to stimulate antitumor immune

responses, thereby enabling multimodal therapeutic synergy [173]. Given the intrinsic metal content of MOFs, their *in vivo* metabolism and clearance were systematically evaluated to ensure biosafety (Figure 18A, B). Quantitative analysis of Zr and Mn in feces and urine within seven days after intravenous administration revealed a rapid decline over time, indicating efficient hepatic, biliary, and renal clearance, underscoring the favorable biocompatibility and safety profile of these MOFs (Figure 18C).

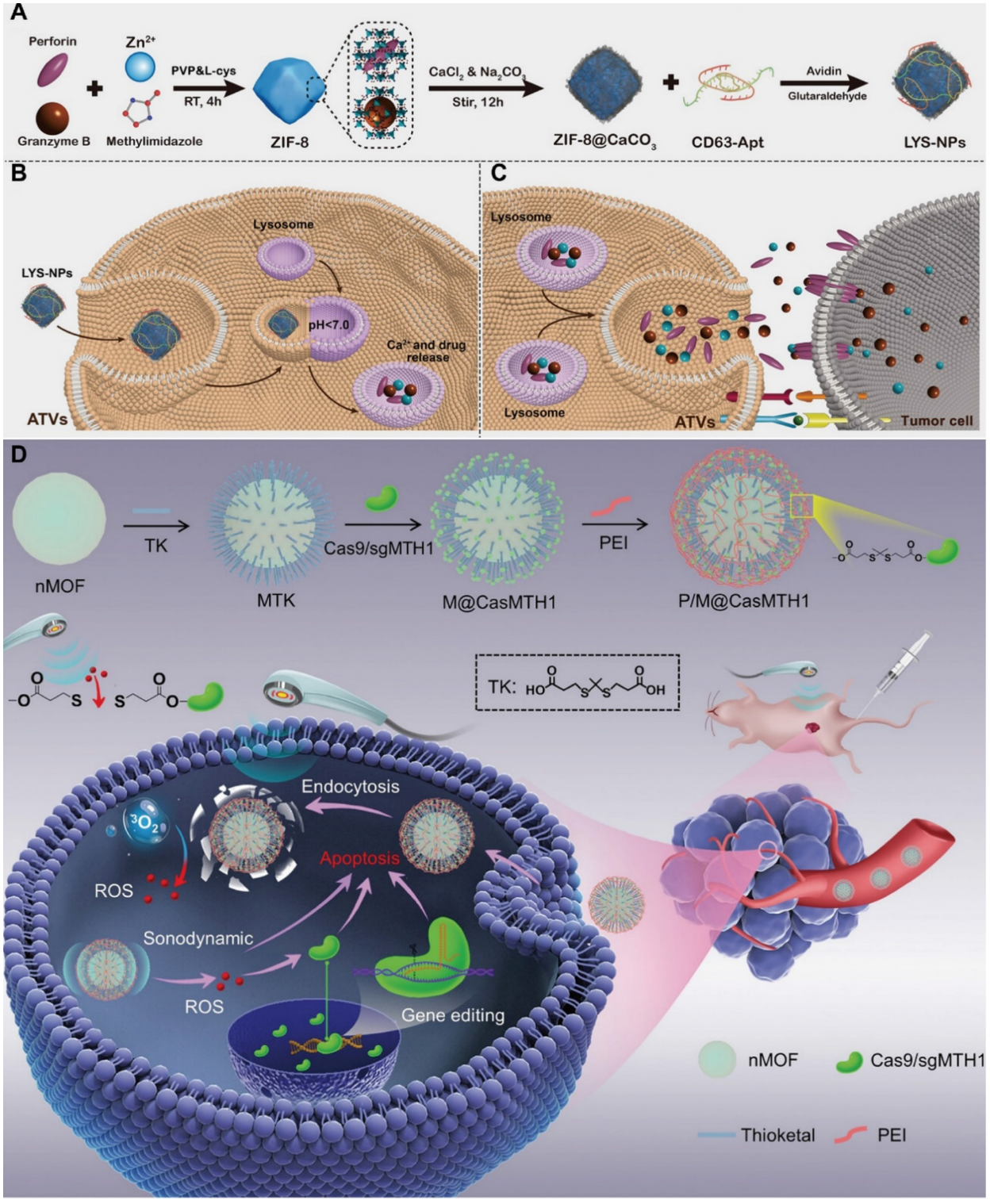

Figure 17. (A) Schematic illustration of LYS-NPs; **(B)** Lysosomal targeting and degradation of ATVs via CD63+ aptamer recognition; **(C)** ATVs releasing cytotoxic proteins and calcium ions in reconstructed lysosomes for tumor destruction. Adapted with permission from [170], copyright 2021 WILEY-VCH; **(D)** Schematic illustration of P/M@CasMTH1 for tumor treatment. Adapted with permission from [172], copyright 2021 WILEY-VCH.

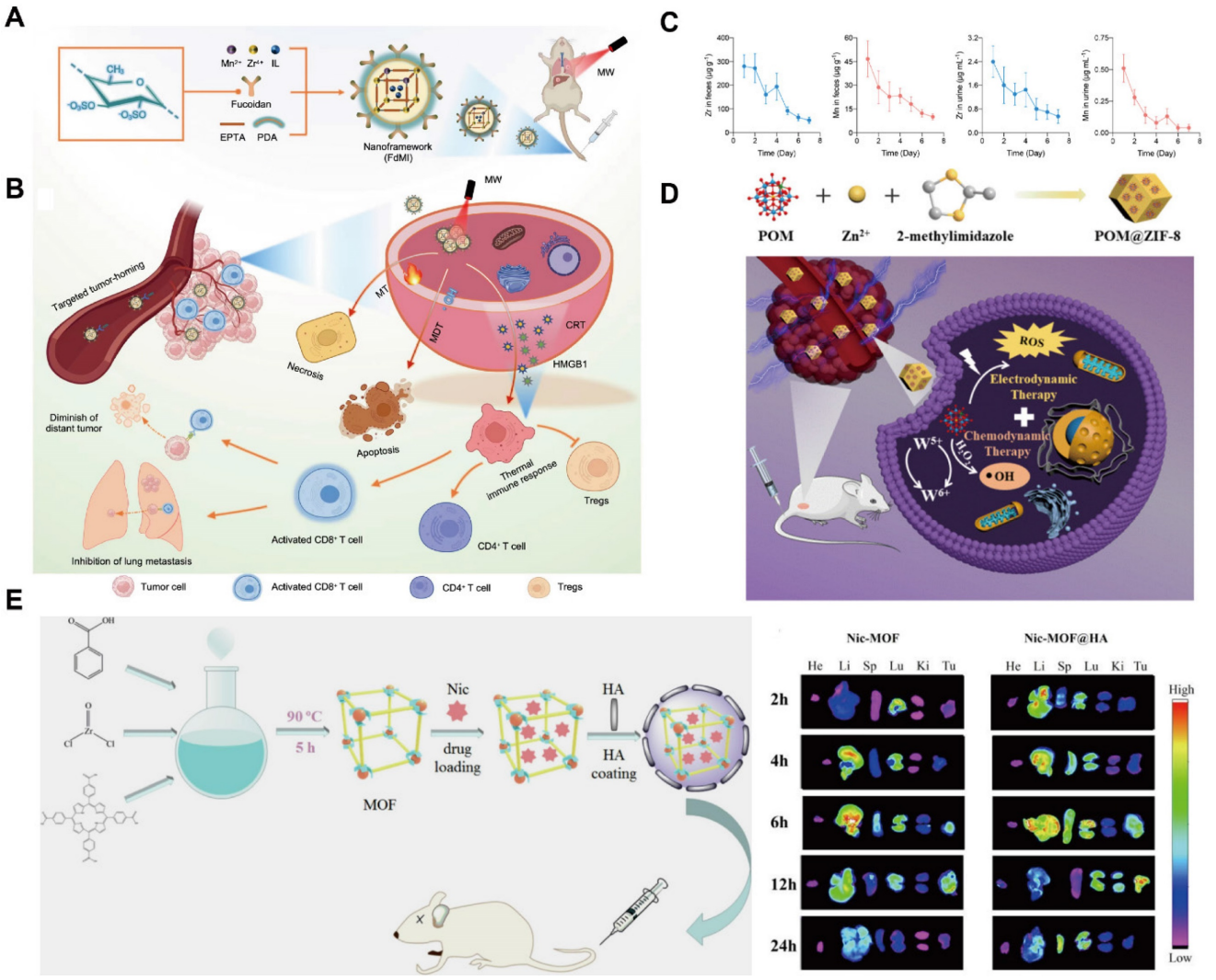

Figure 18. (A) Schematic synthesis of FdMI nanoframework; **(B)** Schematic diagram of the synergistic therapeutic mechanism of FdMI nanoframework; **(C)** Zr/Mn concentrations in feces/urine after *i.v.* injection of FdMI. Adapted with permission from [173], copyright 2024 American Chemical Society; **(D)** Schematic illustration of POM@ZIF-8 for EDT/CDT. Adapted with permission from [175], copyright 2022 American Chemical Society; **(E)** Synthesis of Nic-MOF@HA NPs and their biodistribution: representative ex vivo fluorescence images of major organs at different time points post-injection. (Tu: Tumor; He: Heart; Li: Liver; Sp: Spleen; Lu: Lung; Ki: Kidney). Adapted with permission from [176], copyright 2022 Elsevier.

Electrodynamic therapy (EDT) represents another emerging modality in which electrical stimulation catalyzes the in-situ generation of ROS, enabling uniform tumor ablation across the entire electric field rather than being confined to regions near the electrodes. This approach is characterized by reliable therapeutic efficacy and high reproducibility [174]. Beyond conventional electrocatalytic materials such as Fe_3O_4 and Pt, MOFs have attracted increasing attention as versatile nanoplatforms for EDT due to their structural tunability and multifunctionality. Moreover, the combination of EDT with CDT has demonstrated synergistic enhancement of ROS-mediated tumor ablation through complementary internal and external stimuli. Leveraging the pH-responsive properties of polyoxometalate-modified ZIF-8 (POM@ZIF-8) [175], POM can be released from the MOF matrix under acidic TME to function as an electrosensitizer. Within the applied electric field, POM generated ROS while simultaneously participating in Fenton-like reactions, thereby achieving potent and synergistic tumor eradication (Figure 18D).

Active targeting with MOFs is commonly achieved by functionalizing the surface of drug-loaded MOF nanoparticles with targeting ligands (such as antibodies, peptides, nucleic acid aptamers, polysaccharides, or hyaluronic acid) through physical or chemical means. This approach significantly enhances the precision of drug delivery to tumor cells, thereby improving therapeutic efficacy while minimizing off-target toxicity. For example, nicorandil (Nic) was encapsulated within MOFs, and HA was subsequently adsorbed on the MOF surface via electrostatic interactions (Figure 18E). Owing to the specific recognition of HA by the CD44 receptor

overexpressed on tumor cells, Nic-MOF@HA exhibited significantly enhanced tumor accumulation throughout the observation period with non-HA-modified MOFs, confirming the effectiveness of active targeting and therapy [176]. In addition to surface functionalization, the intrinsic properties of MOFs could also be exploited to achieve targeted treatment. In particular, MOFs enable stimulus-responsive drug release in response to tumor microenvironment–associated cues, allowing precise spatiotemporal control over drug delivery. Moreover, certain therapeutic agents exhibit activity only upon exposure to specific physical or chemical stimuli, for which MOFs serve as ideal carriers. This paradigm, referred to as stimulus-responsive targeting, including pH-responsive zinc- and iron-based MOFs, as well as ATP-responsive and GSH-responsive MOF-based drug delivery systems. These nanoplatforms primarily relied on endogenous TME responses, exogenous stimuli, such as magnetic field-responsive and thermosensitive MOFs have also been employed for targeted cancer therapy [177].

Enzyme therapy represents another promising non-invasive anticancer strategy, enabling the localized generation of cytotoxic species from non-toxic substrates without damaging normal tissues, thereby reducing the adverse effects associated with conventional therapies. For instance, enzyme-like catalytic activity can initiate cascade reactions that generates ROS, ultimately inducing tumor cell death [178]. Manganese, an essential trace element, serves as a key cofactor in numerous metalloenzymes and nanozymes, including manganese catalase (MnCAT), manganese superoxide dismutase (MnSOD), and peroxidase (POD), and plays a critical role in inducing Fenton-like reactions. Recently, a Mn-based single-atom catalyst (Mn-N/C) was constructed by encapsulating coordinatively unsaturated monatomic Mn nanocatalysts within a ZIF-8 [179]. Benefiting from the large specific surface area and tunable pore structure of ZIF-8, the Mn-N/C catalyst exhibits high enzymatic activity for ROS generation while simultaneously activating the STING signaling pathway, thereby achieving potent antitumor therapeutic efficacy.

Conclusion and perspectives

This review summarizes recent advances in MOF-based anticancer agents, highlighting their expanding applications across a broad spectrum of therapeutic modalities, including PDT, PTT, SDT, CDT, RT, gene therapy, immunotherapy, as well as multi-modal therapies over the past decade [180-183]. These developments are largely driven by the remarkable structural tunability and functional versatility of MOFs. Substantial progress has been achieved in exploiting MOFs as DDS, molecular imaging agents, and multifunctional therapeutic platforms. The tunable synthetic parameters and unique physicochemical properties enable efficient encapsulation of diverse therapeutic agents, thereby advancing their utility as drug carriers, imaging probes, and integrated nanotheranostic systems. Notably, the integration of therapeutic and diagnostic functionalities within a single MOF-based platform holds promise for further enhancing precision nanomedicine and therapeutic efficacy [184-186].

Despite the encouraging advances, significant challenges remain on the path toward clinical translation. MOFs designed for biomedical applications must prioritize low toxicity and controlled degradability. While nanoscale dimensions (typically < 200 nm) improve circulation and tumor accumulation, they may also increase nanotoxicity risks, including inflammation and cell death. Importantly, MOF toxicity is highly composition-dependent. Ca-, Bi-, or Eu-MOFs generally exhibit minimal toxicity, whereas Ti-, Fe-, Co-, Al-, or Cr-MOFs display low to moderate, and Zr-, Mg-, Gd-, Ni-, Zn-MOFs demonstrate moderate toxicity. Among reported systems, Fe-MOFs are the most extensively studied, reflecting their biomedical relevance. Toxicity mechanisms include reactive species generation by redox-active metals (*e.g.*, Ag, Cu, Fe, Cd), ion-homeostasis disruption (*e.g.*, Ga, Fe, Zn, Cd), and insoluble-protein accumulation (*e.g.*, Pb, Mn, Ag, Co). Organic linker toxicity is primarily associated with membrane permeability, with carboxylate-based linkers generally exhibiting lower toxicity than azolate ligands. Surface charge further influences toxicity, as positively charged surfaces enhance cellular uptake but also increase cytotoxic risk [187]. Additionally, residual solvents and additives from MOF synthesis may pose safety concerns, underscoring the need for green synthesis.

Degradability in biological environments is another critical design factor for biomedical MOFs. While nanosizing enhances therapeutic performance, it often compromises structural stability, as increased surface area accelerates interactions with biological media and promotes degradation. MOF stability could be partially predicted using the Hard and Soft Acids and Bases (HSAB) principle: stable MOFs generally comprise carboxylate ligands (hard Lewis bases) coordinated with high-valent metal ions (hard Lewis acids). Alternatively, strong coordination can also arise from azolate-based ligands paired with low-valent transition metals. Additional factors influencing stability include metal cluster nuclearity, ligand coordination strength, chelating group number

and type, defect density, open metal sites, and the hydrophilic–hydrophobic balance of the framework.

Hydrophilic surfaces generally reduce aggregation and improve dispersion, whereas hydrophobic MOFs exhibit stronger serum protein adsorption, leading to accelerated clearance and reduced stability. Moreover, MOF physicochemical properties, particularly surface charge and chemistry, further govern colloidal and chemical stability in biological fluids. A careful balance between toxicity and degradability is therefore essential. Rapid degradation may increase the release of metal ions and organic ligands, elevating toxicity risks. Consequently, MOF nanoparticles should ideally be constructed from low-toxicity components. MOF degradation does not always yield the original building blocks; instead, materials may undergo recrystallization, amorphization, or transformation into metal oxides or insoluble phosphates, which may not induce immediate toxicity [188]. Appropriate dosing must be rigorously optimized, and long-term safety validated through extended *in vivo* studies. Establishing robust quality control standards is also critical to ensure batch-to-batch reproducibility and scalability. Moreover, key translational challenges-such as controlled release in clinical settings, metal ion excretion pathways, and long-term biosafety-require systematic investigation. Encouragingly, several MOF-based systems, including ZIF-8 and PCN-222, have advanced to preclinical studies [189]. However, concerns remain regarding the stability of ZIF-8 under physiological pH, particularly the risk of premature drug leakage and potential neurotoxicity resulting from sustained zinc ion release. Notably, the MOF-based radiosensitizers RiMO-301 (NCT0583-8729, NCT03444714) and RiMO-401 (NCT06182579) have progressed to Phase II and Phase I clinical trials, respectively, for the treatment of head and neck cancer and advanced solid tumors [190]. Their well-defined mechanisms of action and small-molecule-based manufacturing processes facilitate translational development. In particular, the clinical progress of RiMO-301 is expected to significantly influence confidence and investment across the broader MOF research landscape.

Overall, the requirements for MOFs in biomedical applications are substantially more stringent than those for industrial uses. Prior to clinical implementation, systematic and advanced investigations are essential to elucidate the relationships among their toxicity, biodistribution, and intrinsic material properties, including composition, particle size, stability, morphology, surface chemistry, and administration routes. Integrating comprehensive *in vitro* and *in vivo* evaluations with advanced modeling approaches will enable a more holistic understanding of MOF–biological interactions.

At present, the clinical translation of MOF-based therapeutics remains at an early stage, with several unresolved challenges: 1. Complexity of multifunctional design and potential toxicity. While multifunctional MOF nanoplatforms enable targeted imaging and therapy, their structural complexity and reliance on heavy metals hinder scalability and raise safety concerns. Simplified designs and scalable synthesis strategies are therefore required to bridge laboratory research and clinical application [191-193]. Surface modification with ligands, antibodies, or peptides improves targeting specificity but remains difficult to reproduce with consistent biocompatibility [194,195]. 2. Biosafety and biocompatibility concerns. Most existing studies focus on short-term toxicity [196], whereas long-term toxicity, immune compatibility, and bioaccumulation remain insufficiently explored. Strategies incorporating endogenous or low-toxicity metal ions and biomolecule-derived ligands may improve safety profiles. 3. Biological metabolism and clearance. Comprehensive understanding of MOF degradation, metabolism, and excretion pathways is critical to prevent chronic accumulation and adverse outcomes [197].

Given these challenges, future research should prioritize the development of simpler, environmentally sustainable, and multifunctional MOF platforms that maintain high porosity and tunable architecture while enhancing stability, circulation time, and biosafety. Understanding how degradation behavior influences drug release, tumor accumulation, and systemic tolerance will be central to rational MOF design. In addition, the subchronic and chronic toxicity of degradation products-both metal ions and organic linkers-requires detailed molecular-level investigation. To accelerate clinical progress, several strategic priorities should be addressed. First, the development of advanced *in vivo* tools to monitor MOF biodistribution and pharmacokinetics, along with standardized frameworks for evaluating absorption, distribution, metabolism, and excretion (ADME), is needed. Additionally, rigorous validation of safety and efficacy to bridge preclinical and clinical studies [198]. Finally, the application of design principles derived from clinically approved nanomedicines.

In conclusion, MOFs represent a transformative platform for next-generation antitumor therapeutics. Their unique ability to integrate drug delivery, imaging, and therapeutic functions within a single modular system positions them as powerful

candidates for precision oncology. Although substantial translational challenges remain, the rapid progress achieved to date highlights the immense potential of MOF-based nanoplatforms for future cancer diagnosis and therapy.

Abbreviations

MOFs: Metal-Organic Frameworks; **SBUs**: Secondary Building Units; **COFs**: Covalent Organic Frameworks; **IUPAC**: International Union of Pure and Applied Chemistry; **siRNA**: short interfering RNA; **FL**: Fluorescence Imaging; **MRI**: Magnetic Resonance Imaging; **CT**: Computed Tomography; **PET**: Positron Emission Tomography; **PAI**: Photoacoustic Imaging; **PS**: Photosensitizers; **PDT**: Photodynamic Therapy; **RT**: Radiotherapy; **TME**: Tumor Microenvironment; **EPR**: Enhanced Permeability and Retention effects; **LAG**: Liquid-assisted Grinding; **ILAG**: Ion- and Liquid-assisted Grinding; **SPCNs**: Spherical Porous Carbon Nanoparticles; **SACs**: Single-atom Catalysts; **AI**: Artificial Intelligence; **CSD**: Cambridge Structural Database; **LbL**: Layer-by-layer; **CTAB**: Cety-ltrimethylammonium Bromide; **FA**: Folic Acid; **HA**: Hyaluronic Acid; **PEG**: Polyethylene Glycol; **O_2**: Oxygen; **PDA**: Polydopamine; **Ce6**: Chlorin e6; **DDS**: drug delivery systems; **DOX**: Doxorubicin; **AIDS**: Acquired Immune Deficiency Syndrome; **PBS**: Phosphate-buffered Saline; **IBU**: Ibuprofen; **SBF**: Simulated Body Fluid; **5-FU**: 5-Fluorouracil; **CAA**: Cis-aconitic-anhydride; **GSH**: Glutathione; **pDNA**: Plasmid DNA; **RNAi**: RNA interfere; **mRNA**: Messenger RNA; **miRNA**: Micro RNA; **ICG**: Indocyanine Green; **IP**: Infrared-Photothermal; **FDA**: Food and Drug Administration; **DHA**: Dihydro-artemisinin; **aPD-1**: anti-Programmed Death-1; **SPIONs**: Superparamagnetic Iron Oxide Nanoparticles; **Py**: Pyrrole; **PPy**: Polypyrrole; **UCL**: Upconversion Luminescence; **GNRs**: Gold Nanorods; **LA**: Lactobionic Acid; **NIR**: Near-infrared; **PTT**: Photothermal Therapy; **OVA**: Ovalbumin; **CpG ODNs**: Cytosine-phosphate-guanine Oligodeoxy-nucleotides; **TLR7/8**: Toll-like Receptor 7/8; **CDT**: Chemodynamic Therapy; **SDT**: Sonodynamic Therapy; **STING**: Stimulator of Interferon Genes; **RDT**: Radiodynamic Therapy; **$^1O_2$**: Singlet Oxygen; **Hb**: hemoglobin; **MTX**: Methotrexate; **ROS**: Reactive Oxygen Species; **H_2O_2**: Hydrogen Peroxide; **TPZ**: Tirapazamine; **HAP**: Hypoxic-activated Precursor; **DC**: Dendritic Cell; **MDSCs**: Myeloid-derived Suppressor Cells; **VB**: Valence Band; **CB**: Conduction Band; **•OH**: Hydroxyl Radicals; **ABTS**: 2,2′-azino-bis(3-ethylbenzothiazoline-6-sulfonic acid); **PVP**: Polyvinylpyrrolidone; **GOx**: Glucose Oxidase; **CAR**: Chimeric Antigen Receptor; **TCR**: T-cell Receptor-engineered; **NK**: natural killer; **TAAs**: Tumor-associated Antigens; **ICD**: Immunogenic Cell Death; **DAMPs**: Damage Associated Molecular Patterns; **Mn-MO**F: Manganese-based MOF; **TLR9**: Toll-like Receptor 9; **ATVs**: Adoptive T cell Vectors; **$CaCO_3$**: calcium carbonate; **MHC**: Major Histocompatibility Complex; **RNP**: Ribonucleoprotein; **PEI**: Polyethyleneimine; **MTH1**: MutT Homolog 1; MT: Microwave Thermotherapy; **MDT**: Microwave-dynamic Therapy; **EDT**: Electrotherapy; **POM**: polyoxometalate; **Nic**: Nicorandil; **MnCAT**: Manganese Catalase; **MnSOD**: Manganese Superoxide Dismutase; **POD**: Peroxidase; **HSAB**: Hard and Soft Acids and Bases.

Acknowledgments

This work was partially supported by the National Natural Science Foundation of China (32371446), the Sichuan Science and Technology Program (2026YFHZ0049, 2026NSFSCZY0081) and the 1.3.5 project for disciplines of excellence (ZYYC23019) of the West China Hospital, Sichuan University. We thank BioRender (biorender.com) for providing the templates and tools for creating the table of content of this review.

Author contributions

H.-L. Yu and P. Mi conceived the outline of this review. H.-L. Yu collected papers for writing, drafted the original manuscript, and performed the creation of figures/tables. H.-L. Yu, G. Lin and P. Mi helped revise the manuscript and discuss the content. P. Mi supervised this project and finalized this manuscript. All authors have read and approved the final manuscript.

Competing interests

The authors have declared that no competing interest exists.

References

1. Siegel RL, Miller KD, Wagle NS, Jemal A. Cancer statistics. 2023. CA Cancer J Clin. 2023; 73: 17-48.
2. Mi P. Stimuli-responsive nanocarriers for drug delivery, tumor imaging, therapy and theranostics. Theranostics. 2020; 10: 4557-88.
3. Liu J, Cabral H, Mi P. Nanocarriers address intracellular barriers for efficient drug delivery, overcoming drug resistance, subcellular targeting and controlled release. Adv Drug Deliver Rev. 2024; 207: 115239.
4. Lin G, Mi P, Chu C, Zhang J, Liu G. Inorganic nanocarriers overcoming multidrug resistance for cancer theranostics. Adv Sci. 2016; 3: 1600134.
5. van der Meel R, Sulheim E, Shi Y, Kiessling F, Mulder WJM, Lammers T. Smart cancer nanomedicine. Nat Nanotechnol. 2019; 14: 1007-17.
6. Hoskins BF, Robson R. Design and construction of a new class of scaffolding-like materials comprising infinite polymeric frameworks of 3D-linked molecular rods. A reappraisal of the zinc cyanide and cadmium cyanide structures and the synthesis and structure of the diamond-related frameworks $[N(CH_3)_4][Cu^{I}Zn^{II}(CN)_4]$ and Cu^{I}[4,4',4'',4'''-tetracyanotetraphenylmethane]$BF_4 \cdot xC_6H_5NO_2$. J Am Chem Soc. 1990; 112: 1546-54.
7. Bernard FH, Richard R. Infinite polymeric frameworks consisting of three dimensionally linked rod-like segments. J Am Chem Soc. 1989; 111: 5962-4.
8. Yaghi OM, Li G, Li H. Selective binding and removal of guests in a microporous metal-organic framework. Nature. 1995; 378: 703-6.

9. Xu W, Wu Y, Gu W, Du D, Lin Y, Zhu C. Atomic-level design of metalloenzyme-like active pockets in metal-organic frameworks for bioinspired catalysis. Chem Soc Rev. 2024; 53: 137-62.
10. Dou Y, Zhang W, Kaiser A. Electrospinning of metal-organic frameworks for energy and environmental applications. Adv Sci. 2020; 7: 1902590.
11. Shah RH, Ali S, Raziq F, Ali S, Ismail PM, Shah SY, et al. Exploration of metal organic frameworks and covalent organic frameworks for energy-related applications. Coord Chem Rev. 2023; 477: 214968.
12. De D, Sahoo P. The impact of MOFs in pH-dependent drug delivery systems: Progress in the last decade. Dalton Trans. 2022; 51: 9950-65.
13. Bieniek A, Terzyk AP, Wisniewski M, Roszek K, Kowalczyk P, Sarkisov L, et al. MOF materials as therapeutic agents, drug carriers, imaging agents and biosensors in cancer biomedicine: Recent advances and perspectives. Prog Mater Sci. 2021; 117: 100743.
14. Liang RX, Li FZ, Chen XJ, Tan FY, Lan T, Yang JJ, et al. Multimodal imaging-guided strategy for developing Lu-labeled metal-organic framework nanomedicine with potential in cancer therapy. ACS Appl Mater Interfaces. 2023; 15: 45713-24.
15. He YP, Li DF, Wu L, Yin XZ, Zhang XJ, Patterson LH, et al. Metal-organic frameworks for gene therapy and detection. Adv Funct Mater. 2023; 33: 2212277.
16. Ni WD, Wu JY, Fang HP, Feng YJ, Hu YY, Lin L, et al. Photothermal-chemotherapy enhancing tumor immunotherapy by multifunctional metal-organic framework-based drug delivery system. Nano Lett. 2021; 21: 7796-805.
17. Ni KY, Luo TK, Lan GX, Culbert A, Song Y, Wu T, et al. A nanoscale metal-organic framework to mediate photodynamic therapy and deliver CpG oligodeoxynucleotides to enhance antigen presentation and cancer immunotherapy. Angew Chem Int Ed. 2022; 61: 1108-12.
18. Bao W, Liu M, Meng J, Liu S, Wang S, Jia R, et al. MOFs-based nanoagent enables dual mitochondrial damage in synergistic antitumor therapy via oxidative stress and calcium overload. Nat Commun. 2021; 12: 6399.
19. Zhuang J, Kuo CH, Chou LY, Liu DY, Weerapana E, Tsung CK. Optimized metal-organic-framework nanospheres for drug delivery: Evaluation of small-molecule encapsulation. ACS Nano. 2014; 8: 2812-9.
20. Li B, Wang XY, Chen L, Zhou YL, Dang WT, Chang J, et al. Ultrathin Cu-TCPP MOF nanosheets: A new theragnostic nanoplatform with magnetic resonance/near-infrared thermal imaging for synergistic phototherapy of cancers. Theranostics. 2018; 8: 4086-96.
21. Wang YM, Liu W, Yin XB. Multifunctional mixed-metal nanoscale coordination polymers for triple-modality imaging-guided photodynamic therapy. Chem Sci. 2017; 8: 3891-7.
22. Demir Duman F, Forgan RS. Applications of nanoscale metal-organic frameworks as imaging agents in biology and medicine. J Mater Chem B. 2021; 9: 3423-49.
23. Chen XJ, Zhang MJ, Li SN, Li L, Zhang LY, Wang TT, et al. Facile synthesis of polypyrrole@metal-organic framework core-shell nanocomposites for dual-mode imaging and synergistic chemo-photothermal therapy of cancer cells. J Mater Chem B. 2017; 5: 1772-8.
24. Mallakpour S, Nikkhoo E, Hussain CM. Application of MOF materials as drug delivery systems for cancer therapy and dermal treatment. Coord Chem Rev. 2022; 451: 214262.
25. Ni KY, Xu ZW, Culbert A, Luo TK, Guo NI,Yang KT, et al. Synergistic checkpoint-blockade and radiotherapy-radiodynamic therapy via an immunomodulatory nanoscale metal-organic framework. Nat Biomed Eng. 2022; 6: 1449-50.
26. Shi Y, van der Meel R, Chen X, Lammers T. The EPR effect and beyond: Strategies to improve tumor targeting and cancer nanomedicine treatment efficacy. Theranostics. 2020; 10:7921-4.
27. Hussain Z, Rahim MA, Jan N, Shah H, Rawas-Qalaji M, Khan S, et al. Cell membrane cloaked nanomedicines for bio-imaging and immunotherapy of cancer: Improved pharmacokinetics, cell internalization and anticancer efficacy. J Control Release. 2021; 335: 130-57.
28. Abrahams BF, Hoskins BF, Michail DM, Robson R. Assembly of porphyrin building-blocks into network structures with large channels. Nature. 1994; 369: 727-9.
29. Li H, Eddaoudi M, O'Keeffe M, Yaghi OM. Design and synthesis of an exceptionally stable and highly porous metal-organic framework. Nature. 1999; 402: 276-9.
30. Férey G, Mellot-Draznieks C, Serre C, Millange F, Dutour J, Surblé S, et al. A chromium terephthalate-based solid with unusually large pore volumes and surface area. Science. 2005; 309: 2040-2.
31. Furukawa H, Cordova KE, O'Keeffe M, Yaghi OM. The chemistry and applications of metal-organic frameworks. Science. 2013; 341: 1230444.
32. Horcajada P, Chalati T, Serre C, Gillet B, Sebrie C, Baati T, et al. Porous metal-organic-framework nanoscale carriers as a potential platform for drug delivery and imaging. Nat Mater. 2010; 9: 172-8.
33. Hermes S, Witte T, Hikov T, Zacher D, Bahnmuller S, Langstein G, et al. Trapping metal-organic framework nanocrystals: An in-situ time-resolved light scattering study on the crystal growth of MOF-5 in solution. J Am Chem Soc. 2007; 129: 5324-5.
34. Yao JF, He M, Wang K, Chen RZ, Zhong ZX, Wang HT. High-yield synthesis of zeolitic imidazolate frameworks from stoichiometric metal and ligand precursor aqueous solutions at room temperature. CrystEngComm. 2013; 15: 3601-6.
35. Baig RBN, Varma RS. Alternative energy input: Mechanochemical, microwave and ultrasound-assisted organic synthesis. Chem Soc Rev. 2012; 41: 1559-84.
36. Jhung SH, Lee JH, Chang JS. Microwave synthesis of a nanoporous hybrid material, chromium trimesate. Bull Korean Chem Soc. 2005; 26: 880-1.
37. Vaitsis C, Sourkouni G, Argirusis C. Metal organic frameworks (MOFs) and ultrasound: A review. Ultrason Sonochem. 2019; 52: 106-19.
38. Haque E, Khan NA, Park JH, Jhung SH. Synthesis of a metal-organic framework material, iron terephthalate, by ultrasound, microwave, and conventional electric heating: A kinetic study. Chem Eur J. 2010; 16: 1046-52.
39. Neto OJD, Fros ACD, Barros BS, Monteiro AFD, Kulesza J. Rapid and efficient electrochemical synthesis of a zinc-based nano-MOF for Ibuprofen adsorption. New J Chem. 2019; 43: 5518-24.
40. Campagnol N, Van Assche T, Boudewijns T, Denayer J, Binnemans K, De Vos D, et al. High pressure, high temperature electrochemical synthesis of metal-organic frameworks: Films of MIL-100 (Fe) and HKUST-1 in different morphologies. J Mater Chem A. 2013; 1: 5827-30.
41. Klimakow M, Klobes P, Thunemann AF, Rademann K, Emmerling F. Mechanochemical synthesis of metal-organic frameworks: A fast and facile approach toward quantitative yields and high specific surface areas. Chem Mater. 2010; 22: 5216-21.
42. Chen BL, Eddaoudi M, Hyde ST, O'Keeffe M, Yaghi OM. Interwoven metal-organic framework on a periodic minimal surface with extra-large pores. Science. 2001; 291: 1021-3.
43. Taylor KML, Rieter WJ, Lin WB. Manganese-based nanoscale metal-organic frameworks for magnetic resonance imaging. J Am Chem Soc. 2008; 130: 14358-9.
44. Lu KD, He CB, Lin WB. Nanoscale metal-organic framework for highly effective photodynamic therapy of resistant head and neck cancer. J Am Chem Soc. 2014; 136: 16712-5.
45. Saeb MR, Rabiee N, Mozafari M, Verpoort F, Voskressensky LG, Luque R. Metal-organic frameworks (MOFs) for cancer therapy. Materials. 2021; 14: 7277.
46. Gao WY, Chrzanowski M, Ma SQ. Metal-metalloporphyrin frameworks: A resurging class of functional materials. Chem Soc Rev. 2014; 43: 5841-66.
47. Ding M, Liu W, Gref R. Nanoscale MOFs: From synthesis to drug delivery and theranostics applications. Adv Drug Deliver Rev. 2022; 190: 114496.
48. Zorainy MY, Alkalla MIG, Kaliaguine S, Boffito DCC. Revisiting the MIL-101 metal-organic framework: Design, synthesis, modifications, advances, and recent applications. J Mater Chem A. 2021; 9: 22159-217.
49. Talebi J, Halladj R, Askari S. Sonochemical synthesis of silver nanoparticles in Y-zeolite substrate. J Mater Sci. 2012; 45: 3318-24.
50. Qiu LG, Li ZQ, Wu Y, Wang W, Xu T, Jiang X. Facile synthesis of nanocrystals of a microporous metal-organic framework by an ultrasonic method and selective sensing of organoamines. Chem Commun. 2008; 31: 3642-4.
51. Yaghi OM, Li HL, Groy TL. Construction of porous solids from hydrogen-bonded metal complexes of 1,3,5-benzenetricarboxylic acid. J Am Chem Soc. 1996; 118: 9096-101.
52. Xiao X, Zou L, Pang H, Xu Q. Synthesis of micro/nanoscaled metal-organic frameworks and their direct electrochemical applications. Chem Soc Rev. 2020; 49: 301-31.
53. Ameloot R, Stappers L, Fransaer J, Alaerts L, Sels BF, De Vos DE. Patterned growth of metal-organic framework coatings by electrochemical synthesis. Chem Mater. 2009; 21: 2580-2.
54. Fernandez-Bertran JF, Hernandez MP, Reguera E, et al. Characterization of mechanochemically synthesized imidazolates of Ag^{+1}, Zn^{+2}, Cd^{+2}, and Hg^{+2}: Solid state reactivity of nd^{10} cations. J Phys Chem Solids. 2006; 67: 1612-7.
55. Tan D, García F. Main group mechanochemistry: From curiosity to established protocols. Chem Soc Rev. 2019; 48: 2274-92.
56. Taylor KML, Jin A, Lin WB. Surfactant-assisted synthesis of nanoscale gadolinium metal-organic frameworks for potential multimodal imaging. Angew Chem Int Ed. 2008; 47: 7722-5.
57. Sun WZ, Zhai XS, Zhao L. Synthesis of ZIF-8 and ZIF-67 nanocrystals with well-controllable size distribution through reverse microemulsions. Chem Eng J. 2016; 289: 59-64.
58. Faustini M, Kim J, Jeong GY, Kim JY, Moon HR, Ahn WS, et al. Microfluidic approach toward continuous and ultrafast synthesis of metal-organic framework crystals and hetero structures in confined microdroplets. J Am Chem Soc. 2013; 135: 14619-26.
59. Liu L, Wei HB, Zhang LY, Li JP, Dong JX. Ionothermal synthesis of the metal-organic framework compound $Cu_3(BTC)_2$. Stud Surf Sci Catal. 2008; 174: 459-62.
60. Wang CH, Kim J, Tang J, Kim M, Lim H, Malgras V, et al. New strategies for novel MOF-derived carbon materials based on nanoarchitectures. Chem. 2020; 6: 19-40.
61. Wu J, Zhu X, Li Q, Fu Q, Wang B, Li B, et al. Enhancing radiation-resistance and peroxidase-like activity of single-atom copper nanozyme via local coordination manipulation. Nat Commun. 2024; 15: 6174.
62. Wei S, Li A, Liu JC, Li Z, Chen W, Gong Y, et al. Direct observation of noble metal nanoparticles transforming to thermally stable single atoms. Nat. Nanotechnol. 2018; 13: 856-61.
63. Seetharaj R, Vandana PV, Arya P, Mathew S. Dependence of solvents, pH, molar ratio and temperature in tuning metal organic framework architecture. Arab J Chem. 2019; 12: 295-315.

64. Tran H, Gurnani R, Kim C, Pilania G, Kwon H-K, Lively RP, et al. Design of functional and sustainable polymers assisted by artificial intelligence. Nat Rev Mater. 2024; 9: 866-86.
65. Jumper J, Evans R, Pritzel A, Green T, Figurnov M, Ronneberger O, et al. Highly accurate protein structure prediction with AlphaFold. Nature. 2021; 596: 583-9.
66. Sarker IH. Machine learning: Algorithms, real-world applications and research directions. SN Comput Sci. 2021; 2: 160.
67. Moghadam PZ, Li A, Wiggin SB, Tao A, Maloney AGP, Wood PA, et al. Development of a Cambridge structural database subset: A collection of metal-organic frameworks for past, present, and future. Chem Mater. 2017; 29: 2618-25.
68. Zheng Z, Zhang O, Nguyen HL, Rampal N, Alawadhi AH, Rong Z, et al. ChatGPT research group for optimizing the crystallinity of MOFs and COFs. ACS Cent Sci. 2023; 9: 2161-70.
69. Cai G, Yan P, Zhang L, Zhou HC, Jiang HL. Metal-organic framework-based hierarchically porous materials: Synthesis and applications. Chem Rev. 2021; 121: 12278-326.
70. Tan W, Wei T, Huo J, Loubidi M, Liu T, Liang Y, Deng L. Electrostatic interaction-induced formation of enzyme-on-MOF as chemo-biocatalyst for cascade reaction with unexpectedly acid-stable catalytic performance. ACS Appl Mater Interfaces. 2019; 11: 36782-8.
71. Vaidya LB, Nadar SS, Rathod VK. Entrapment of surfactant modified lipase within zeolitic imidazolate framework (ZIF)-8. Int J Biol Macromol. 2020; 146: 678-86.
72. Avci C, Imaz I, Carné-Sánchez A, Pariente JA, Tasios N, Pérez-Carvajal J, et al. Self-assembly of polyhedral metal-organic framework particles into three-dimensional ordered superstructures. Nat Chem. 2017; 10: 78-84.
73. Li W, Zhang Y, Yu Z, Zhu T, Kang J, Liu K, et al. *In situ* growth of a stable metal-organic framework (MOF) on flexible fabric via a layer-by-layer strategy for versatile applications. ACS Nano. 2022; 16: 14779-91.
74. Segura JL, Royuela S, Mar Ramos M. Post-synthetic modification of covalent organic frameworks. Chem Soc Rev. 2019; 48: 3903-45.
75. Yang S, Peng L, Sun DT, Asgari M, Oveisi E, Trukhina O, et al. A new post-synthetic polymerization strategy makes metal-organic frameworks more stable. Chem Sci. 2019; 10: 4542-9.
76. Wan X, Zhang H, Xu L, Pan W, Zhang J, Song L, et al. Metabolic hijacking: An MOF-based nanoprogrammer overcomes drug resistance in glioblastoma. Nano Lett. 2025; 25: 12859-68.
77. Chen C, Shen M, Wan X, Sheng L, Hao N, Li M, et al. Decoy extracellular vesicles overcome triple-negative breast cancer heterogeneity via membrane-cytoplasm-mitochondria cascade targeting. Adv Sci. 2025; 12: e07975.
78. Christodoulou I, Lyu P, Soares CV, Patriarche G, Serre C, Maurin G, et al. Nanoscale iron-based metal-organic frameworks: Incorporation of functionalized drugs and degradation in biological media. Int J Mol Sci. 2023; 24.
79. Yang J, Chen XJ, Li YS, Zhuang QX, Liu PF, Gu JL. Zr-based MOFs shielded with phospholipid bilayers: Improved biostability and cell uptake for biological applications. Chem Mater. 2017; 29: 4580-9.
80. Shi Z, Chen X, Zhang L, Ding S, Wang X, Lei Q, Fang W. FA-PEG decorated MOF nanoparticles as a targeted drug delivery system for controlled release of an autophagy inhibitor. Biomater Sci. 2018; 6: 2582-90.
81. Wang YB, Wu WB, Mao D, Teh C, Wang B, Liu B. Metal-organic framework assisted and tumor microenvironment modulated synergistic image-guided photo-chemo therapy. Adv Funct Mater. 2020; 30: 2002431.
82. Liu Z, Gao Y, Shao W, Guo X, Zhao D, Yang R, et al. Multidimensional applications and challenges of metal-organic frameworks (MOFs) in biomedicine: From drug safety evaluation to drug delivery. J Biomedi Mater Res A. 2025; 113: e37952.
83. Chen J, Hu S, Sun M, Shi J, Zhang H, Yu H, et al. Recent advances and clinical translation of liposomal delivery systems in cancer therapy. Eur J Pharm Sci. 2024; 193: 106688.
84. Beach MA, Nayanathara U, Gao Y, Zhang C, Xiong Y, Wang Y, et al. Polymeric nanoparticles for drug delivery. Chem Rev. 2024; 124: 5505-616.
85. Rathi P, Chowdhury S, Siril PF. A decade-long journey in design strategies and structure-property relationships of covalent organic framework nanocarriers for anticancer drug delivery. Small. 2025; 21: e05835.
86. Park H, Otte A, Park K. Evolution of drug delivery systems: From 1950 to 2020 and beyond. J Control Release. 2022; 342: 53-65.
87. Thenmozhi R, Moorthy MS, Sivaguru J, Manivasagan P, Bharathiraja S, Oh YO, et al. Synthesis of silica-coated magnetic hydroxyapatite composites for drug delivery applications. J Nanosci Nanotechnol. 2019; 19: 1951-8.
88. Vázquez-González M, Willner I. DNA-responsive SiO_2 nanoparticles, metal-organic frameworks, and microcapsules for controlled drug release. Langmuir. 2018; 34: 14692-710.
89. Gao P, Chen YY, Pan W, Li N, Liu Z, Tang B. Antitumor agents based on metal-organic frameworks. Angew Chem Int Ed. 2021; 60: 16763-76.
90. Liang W, Wied P, Carraro F, Sumby CJ, Nidetzky B, Tsung CK, et al. Metal-organic framework-based enzyme biocomposites. Chem Rev. 2021; 121: 1077-129.
91. He CB, Lu KD, Liu DM, Lin WB. Nanoscale metal-organic frameworks for the co-delivery of cisplatin and pooled siRNAs to enhance therapeutic efficacy in drug-resistant ovarian cancer cells. J Am Chem Soc. 2014; 136: 5181-4.
92. Horcajada P, Serre C, Maurin G, Ramsahye NA, Balas F, Vallet-Regi M, et al. Flexible porous metal-organic frameworks for a controlled drug delivery. J Am Chem Soc. 2008; 130: 6774-80.
93. Cunha D, Ben Yahia M, Hall S, Miller SR, Chevreau H, Elkaim E. Rationale of drug encapsulation and release from biocompatible porous metal-organic frameworks. Chem Mater. 2013; 25: 2767-76.
94. Chalati T, Horcajada P, Couvreur P, Serre C, Ben Yahia M, Maurin G, et al. Porous metal organic framework nanoparticles to address the challenges related to busulfan encapsulation. Nanomedicine. 2011; 6: 1683-95.
95. Ferey G, Serre C, Mellot-Draznieks C, Millange F, Surble S, Dutour J, et al. A hybrid solid with giant pores prepared by a combination of targeted chemistry, simulation, and powder diffraction. Angew Chem Int Ed. 2004; 43: 6296-301.
96. Horcajada P, Serre C, Vallet-Regi M, Sebban M, Taulelle F, Ferey G. Metal-organic frameworks as efficient materials for drug delivery. Angew Chem Int Ed. 2006; 45: 5974-8.
97. Park KS, Ni Z, Cote AP, Choi JY, Huang RD, Uribe-Romo FJ, et al. Exceptional chemical and thermal stability of zeolitic imidazolate frameworks. Proc Natl Acad Sci U S A. 2006; 103: 10186-91.
98. Sun CY, Qin C, Wang XL, Yang GS, Shao KZ, Lan YQ, et al. Zeolitic imidazolate framework-8 as efficient pH-sensitive drug delivery vehicle. Dalton Trans. 2012; 41: 6906-9.
99. Vasconcelos IB, da Silva TG, Militao GCG, Soares TA, Rodrigues NM, Rodrigues MO, et al. Cytotoxicity and slow release of the anti-cancer drug doxorubicin from ZIF-8. RSC Adv. 2012; 2: 9437-42.
100. Li YT, Jin J, Wang DW, Lv JW, Hou K, Liu YL, et al. Coordination-responsive drug release inside gold nanorod@metal-organic framework core-shell nanostructures for near-infrared-induced synergistic chemo-photothermal therapy. Nano Res. 2018; 11: 3294-305.
101. Zhang H, Zhang Q, Liu C, Han B. Preparation of a one-dimensional nanorod/metal organic framework Janus nanoplatform via side-specific growth for synergistic cancer therapy. Biomater Sci. 2019; 7: 1696-704.
102. Yan JQ, Liu C, Wu QW, Zhou JN, Xu XY, Zhang LR, et al. Mineralization of pH-Sensitive doxorubicin prodrug in ZIF-8 to enable targeted delivery to solid tumors. Anal Chem. 2020; 92: 11453-61.
103. Xu MR, Hu Y, Ding WP, Li FF, Lin J, Wu M, et al. Rationally designed rapamycin-encapsulated ZIF-8 nanosystem for overcoming chemotherapy resistance. Biomaterials. 2020; 258: 120308.
104. Liu WW, Semcheddine F, Jiang H, Wang XM. Acid-responsive multifunctional zeolitic imidazolate framework-8 (ZIF-8) nanocomposites for tumor chemo-photothermal synergistic therapy. Bioconjugate Chem. 2022; 33: 1405-14.
105. Liedana N, Galve A, Rubio C, Tellez C, Coronas J. CAF@ZIF-8: One-step encapsulation of caffeine in MOF. ACS Appl Mater Interfaces. 2012; 4: 5016-21.
106. Zhao H, Zhao Y, Liu D. pH and H_2S dual-responsive magnetic metal-organic frameworks for controlling the release of 5-fluorouracil. ACS Appl Bio Mater. 2021; 4: 7103-10.
107. Jia QJ, Li ZZ, Guo CP, Huang XY, Kang MM, Song YP, et al. PEGMA-modified bimetallic NiCo Prussian blue analogue doped with Tb(III) ions: Efficiently pH-responsive and controlled release system for anticancer drug. Chem Eng J. 2020; 389: 124468.
108. Wang JQ, Mi P, Lin G, Wang YXJ, Liu G. Chen XY. Imaging-guided delivery of RNAi for anticancer treatment. Adv Drug Deliver Rev. 2016; 104: 44-60.
109. Morris W, Briley WE, Auyeung E, Cabezas MD, Mirkin CA. Nucleic acid-metal organic framework (MOF) nanoparticle conjugates. J Am Chem Soc. 2014; 136: 7261-4.
110. Li YT, Zhang K, Liu PR, Chen M, Zhong YL, Ye QS, et al. Encapsulation of plasmid DNA by nanoscale metal-organic frameworks for efficient gene transportation and expression, Adv Mater. 2019; 31: e1901570.
111. Lyu F, Zhang Y, Zare RN, Ge J, Liu Z. One-pot synthesis of protein-embedded metal-organic frameworks with enhanced biological activities. Nano Lett. 2014; 14: 5761-5.
112. Zhuang J, Gong H, Zhou JR, Zhang QZ, Gao WW, Fang RH, et al. Targeted gene silencing *in vivo* by platelet membrane-coated metal-organic framework nanoparticles. Sci Adv. 2020; 6: eaaz6108.
113. Zhao HX, Li TT, Yao C, Gu Z, Liu CX, Li JH, et al. Dual roles of Metal-organic frameworks as nanocarriers for miRNA delivery and adjuvants for chemodynamic therapy. ACS Appl Mater Interface. 2021; 13: 6034-42.
114. Farasati Far B, Naimi-Jamal MR, Daneshgar H, Rabiee N. Co-delivery of doxorubicin/sorafenib by DNA-decorated green ZIF-67-based nanocarriers for chemotherapy and hepatocellular carcinoma treatment. Environ Res. 2023; 225: 115589.
115. Li Y, Zhang F, Liu W, Shao M, Hao Z, Zhang H, et al. Endogenous glutathione-activated DNA nanoprobes for spatially controllable imaging of microRNA in living cells. Chem Comm. 2023; 59: 5431-4.
116. Sun P, Li Z, Wang J, Gao H, Yang X, Wu S, et al. Transcellular delivery of messenger RNA payloads by a cationic supramolecular MOF platform. Chem Comm. 2018; 54: 11304-7.
117. Mi P, Wang F, Nishiyama N, Cabral H. Molecular cancer imaging with polymeric nanoassemblies: From tumor detection to theranostics. Macromol Biosci. 2017; 17: 1600305.
118. Liu J, Cabral H, Song B, Aoki I, Chen ZY, Nishiyama N, et al. Nanoprobe-based magnetic resonance imaging of hypoxia predicts responses to radiotherapy, immunotherapy, and sensitizing treatments in pancreatic tumors. ACS Nano. 2021; 15: 13526-38.

119. Cai W, Gao HY, Chu CC, Wang XY, Wang JQ, Zhang PF, et al. Engineering phototheranostic nanoscale metal-organic frameworks for multimodal imaging-guided cancer therapy. ACS Appl Mater Interfaces. 2017; 9: 2040-51.
120. Wan XY, Zhong H, Pan W, Li YH, Chen YY, Li N, et al. Programmed release of dihydroartemisinin for synergistic cancer therapy using $CaCO_3$ mineralized metal-organic framework. Angew Chem Int Ed Engl. 2019; 58: 14134-9.
121. Mi P, Kokuryo D, Cabral H, Wu HL, Terada Y, Saga T, et al. A pH-activatable nanoparticle with signal-amplification capabilities for non-invasive imaging of tumour malignancy. Nat Nanotechnol. 2016; 11: 724-30.
122. Cui H, Zhao YY, Wu Q, You Y, Lan Z, Zou KL, et al. Microwave-responsive gadolinium metal-organic frameworks nanosystem for MRI-guided cancer thermotherapy and synergistic immunotherapy. Bioact Mater. 2024; 33: 532-44.
123. Meng ZH, Huang HB, Huang D, Zhang F, Mi P. Functional metal-organic framework-based nanocarriers for accurate magnetic resonance imaging and effective eradication of breast tumor and lung metastasis. J Colloid Interface Sci. 2021; 581: 31-43.
124. Wan SS, Cheng Q, Zeng X, Zhang XZ. A Mn(III)-sealed metal-organic framework nanosystem for redox-unlocked tumor theranostics. ACS Nano. 2019; 13: 6561-71.
125. Min H, Wang J, Qi Y, Zhang Y, Han X, Xu Y, et al. Biomimetic metal-organic framework nanoparticles for cooperative combination of antiangiogenesis and photodynamic therapy for enhanced efficacy. Adv Mater. 2019; 31: e1808200.
126. Zhou H, Qi M, Shao J, Wang FS, Li XL, Zhou ZG, et al. Manganese oxide/metal-organic frameworks-based nanocomposites for tumor micro-environment sensitive $^{1}H/^{19}F$ dual-mode magnetic resonance imaging *in vivo*. J Organomet Chem. 2021; 933: 121652.
127. Wu MX, Gao J, Wang F, Yang J, Song N, Jin XY, et al. Multistimuli Responsive core-shell nanoplatform constructed from Fe_3O_4@MOF equipped with pillar[6]arene nanovalves. Small. 2018; 14: 1704440.
128. Huang JN, Li N, Zhang CM, Meng ZW. Metal-organic framework as a microreactor for *in situ* fabrication of multifunctional nanocomposites for photothermal-chemotherapy of tumors *in vivo*. ACS Appl Mater Interfaces. 2018; 10: 38729-38.
129. Wang DD, Zhou JJ, Chen RH, Ship RH, Wang CL, Lu J, et al. Core-shell metal-organic frameworks as Fe^{2+} suppliers for Fe^{2+}-mediated cancer therapy under multimodality imaging. Chem Mater. 2017; 29: 3477-89.
130. Li YT, Tang JL, He LC, Liu Y, Liu YL, Chen CY, et al. Core-shell upconversion nanoparticle@metal-organic framework nanoprobes for luminescent/magnetic dual-mode targeted imaging. Adv Mater. 2015; 27: 4075-80.
131. Dekrafft KE, Xie ZG, Cao GH, Tran S, Ma LQ, Zhou OZ, et al. Iodinated nanoscale coordination polymers as potential contrast agents for computed tomography. Angew Chem Int Ed. 2009; 48: 9901-4.
132. Zhang T, Wang L, Ma C, Wang WQ, Ding J, Liu S, et al. BODIPY-containing nanoscale metal-organic frameworks as contrast agents for computed tomography. J Mater Chem B. 2017; 5: 2330-6.
133. Guo HB, Yi S, Feng K, Xia YQ, Qu XW, Wan F, et al. *In situ* formation of metal organic framework onto gold nanorods/mesoporous silica with functional integration for targeted theranostics. Chem Eng J. 2021; 403: 126432.
134. Deng X, Rong J, Wang L, Vasdev N, Zhang L, Josephson L, et al. Chemistry for positron emission tomography: Recent advances in ^{11}C-, ^{18}F-, ^{13}N-, and ^{15}O-labeling reactions. Angew Chem Int Ed. 2019; 58: 2580-605.
135. He ZM, Huang XL, Wang C, Li XL, Liu YJ, Zhou ZJ, et al. A catalase-like metal-organic framework nanohybrid for O_2-evolving synergistic chemoradiotherapy. Angew Chem Int Ed. 2019; 58: 8752-6.
136. Chen DQ, Yang DZ, Dougherty CA, Lu WF, Wu HW, He XR, et al. *In vivo* targeting and positron emission tomography imaging of tumor with intrinsically radioactive metal-organic frameworks nanomaterials. ACS Nano. 2017; 11: 4315-27.
137. Liu Y, Gong CS, Dai Y, Yang Z, Yu G, Liu Y, et al. *In situ* polymerization on nanoscale metal-organic frameworks for enhanced physiological stability and stimulus-responsive intracellular drug delivery. Biomaterials. 2019; 218: 119365.
138. Zhao Z, Swartchick CB, Chan J. Targeted contrast agents and activatable probes for photoacoustic imaging of cancer. Chem Soc Rev. 2022; 51: 829-68.
139. An L, Cao M, Zhang X, Lin J, Tian Q, Yang S. pH and glutathione synergistically triggered release and self-assembly of Au nanospheres for tumor theranostics. ACS Appl Mater Interfaces. 2020; 12: 8050-61.
140. Shang WT, Zeng CT, Du Y, Hui H, Liang X, Chi CW, et al. Core-shell gold nanorod@metal-organic framework nanoprobes for multimodality diagnosis of glioma. Adv Mater. 2017; 29: 1604381.
141. Deng XR, Liang S, Cai XC, Huang SS, Cheng ZY, Shi YS, et al. Yolk-shell structured Au nanostar@metal-organic framework for synergistic chemo-photothermal therapy in the second near-infrared window. Nano Lett. 2019; 19: 6772-80.
142. Zhang Y, Wang FM, Ju EG, Liu Z, Chen ZW, Ren JS, et al. Metal-organic-framework-based vaccine platforms for enhanced systemic immune and memory response. Adv Funct Mater. 2016; 26: 6454-61.
143. Feng Z, Chen G, Zhong M, Lin L, Mai Z, Tang Y, et al. An acid-responsive MOF nanomedicine for augmented anti-tumor immunotherapy via a metal ion interference-mediated pyroptotic pathway. Biomaterials. 2023; 302: 122333.
144. Hu HL, Dai ZC, Zhang FF, Xin CL, An Q, Meng XY, et al. Metal organic frameworks based intelligent nanoadjuvants for boosting tumor immunotherapy through enhanced ICD and lactic acid regulation. Chem Eng J. 2024; 479: 147464.
145. Wang HM, Chen YQ, Wang H, Liu XQ, Zhou X, Wang F. DNAzyme-loaded metal-organic frameworks (MOFs) for self-sufficient gene therapy. Angew Chem Int Ed. 2019; 58: 7380-4.
146. Ni K, Xu Z, Culbert A, Luo T, Guo N, Yang K, et al. Synergistic checkpoint-blockade and radiotherapy-radiodynamic therapy via an immunomodulatory nanoscale metal-organic framework. Nat Biomed Eng. 2022; 6: 144-56.
147. Wang C, Li J, Jiang X, Ma X, Zhen W, Tillman L, et al. Bifunctional metal-organic framework synergistically enhances radiotherapy and activates STING for potent cancer radio-immunotherapy. Angew Chem Int Ed. 2025; 64: e202417027.
148. Zhao Y, Liang C, Mei Z, Yang H, Wang B, Xie C, et al. Oxygen-enriched MOF-hemoglobin X-ray nanosensitizer for enhanced cancer radio-radiodynamic therapy. ACS Mater. Lett. 2023; 5: 3237-47.
149. Wang T, Li S, Zou Z, Hai L, Yang X, Jia X, et al. A zeolitic imidazolate framework-8-based indocyanine green theranostic agent for infrared fluorescence imaging and photothermal therapy. J Mater Chem B. 2018; 6: 3914-21.
150. Yin X, Ran S, Cheng H, Zhang M, Sun W, Wan Y, et al. Polydopamine-modified ZIF-8 nanoparticles as a drug carrier for combined chemo-photothermal osteosarcoma therapy. Colloids Surf B. 2022; 216: 112507.
151. Yang RH, Hou MM, Gao Y, Zhang L, Xu ZG, Kang YJ, et al. Indocyanine green-modified hollow mesoporous Prussian blue nanoparticles loading doxorubicin for fluorescence-guided tri-modal combination therapy of cancer. Nanoscale. 2019; 11: 5717-31.
152. Hu F, Mao D, Kenry Y, Wang W, Wu D, Zhao DK, et al. Metal-organic framework as a simple and general inert nanocarrier for photosensitizers to implement activatable photodynamic therapy. Adv Funct Mater. 2018; 28: 1707519.
153. Zheng Q, Liu X, Zheng Y, Yeung KWK, Cui Z, Liang Y, et al. The recent progress on metal-organic frameworks for phototherapy. Chem Soc Rev. 2021; 50: 5086-125.
154. Kim K, Lee S, Jin E, Palanikumar L, Lee JH, Kim JC, et al. MOF × biopolymer: Collaborative combination of metal organic framework and biopolymer for advanced anticancer therapy. ACS Appl Mater Interfaces. 2019; 11: 27512-20.
155. Zhu W, Zhang L, Yang Z, Liu P, Wang J, Cao J, et al. An efficient tumor-inducible nanotheranostics for magnetic resonance imaging and enhanced photodynamic therapy. Chem Eng J. 2019; 358: 969-79.
156. Zhang D, Ye ZJ, Wei L, Luo HB, Xiao LH. Cell membrane-coated porphyrin metal-organic frameworks for cancer cell targeting and O_2-evolving photodynamic therapy. ACS Appl Mater Interfaces. 2019; 11: 39594-602.
157. Yin SY, Song GS, Yang Y, Zhao Y, Wang P, Zhu LM, et al. Persistent regulation of tumor microenvironment via circulating catalysis of $MnFe_2O_4$@metal-organic frameworks for enhanced photodynamic therapy. Adv Funct Mater. 2019; 29: 1901417.
158. Yu HL, Li YC, Zhang ZY, Ren JJ, Zhang L, Xu ZG, et al. Silk fibroin-capped metal-organic framework for tumor-specific redox dyshomeostasis treatment synergized by deoxygenation-driven chemotherapy. Acta Biomater. 2022; 138: 545-60.
159. Son S, Kim JH, Wang XW, Zhang CL, Yoon SA, Shin J, et al. Multifunctional sonosensitizers in sonodynamic cancer therapy. Chem Soc Rev. 2020; 49: 3244-61.
160. Xu QB, Zhan GT, Zhang ZL, Yong TY, Yang XL, Gan L. Manganese porphyrin-based metal-organic framework for synergistic sonodynamic therapy and ferroptosis in hypoxic tumors. Theranostics. 2021; 11: 1937-52.
161. Liang S, Xiao X, Bai LX, Liu B, Yuan M, Ma PA, et al. Conferring Ti-based MOFs with defects for enhanced sonodynamic cancer therapy. Adv Mater. 2021; 33: 2100333.
162. Wang W, Pan X, Yang H, Wang H, Wu Q, Zheng L, et al. Bioactive metal-organic frameworks with specific metal-nitrogen (M-N) active sites for efficient sonodynamic tumor therapy. ACS Nano. 2021; 15: 20003-12.
163. Wang X, Zhong X, Liu Z, Cheng L. Recent progress of chemodynamic therapy-induced combination cancer therapy. Nano Today. 2020; 35: 100946.
164. Liu F, Lin L, Zhang Y, Wang YB, Sheng S, Xu CN, et al. A tumor-microenvironment-activated nanozyme-mediated theranostic nanoreactor for imaging-guided combined tumor therapy. Adv Mater. 2019; 31: 1902885.
165. Zhao L, Li Z, Wei J, Xiao Y, She Y, Su Q, et al. Juglone-loaded metal-organic frameworks for H_2O_2 self-modulating enhancing chemodynamic therapy against prostate cancer. Chem Eng J. 2022; 430: 143729.
166. Fang C, Deng Z, Cao GD, Chu Q, Wu YL, Li X, et al. Co-ferrocene MOF/glucose oxidase as cascade nanozyme for effective tumor therapy. Adv Funct Mater. 2020; 30: 1910085.
167. Yan SQ, Luo ZC, Li ZL, Wang Y, Tao J, Gong CY, et al. Improving cancer immunotherapy outcomes using biomaterials. Angew Chem Int Ed. 2020; 59: 17332-43.
168. Zhang XL, Lu Y, Jia D, Qiu W, Ma XB, Zhang XL, et al. Acidic microenvironment responsive polymeric MOF-based nanoparticles induce immunogenic cell death for combined cancer therapy. J Nanobiotechnology. 2021; 19: 1-17.
169. Zhan GT, Xu QB, Zhang ZL, Wei ZH, Yong TY, Bie NN, et al. Biomimetic sonodynamic therapy-nanovaccine integration platform potentiates Anti-PD-1 therapy in hypoxic tumors. Nano Today. 2021; 38: 101195.

170. Zhao Q, Gong ZJ, Li ZH, Wang JY, Zhang JL, Zhao ZF, et al. Target reprogramming lysosomes of CD8+ T cells by a mineralized metal-organic framework for cancer immunotherapy. Adv Mater. 2021; 33: 2100616.
171. Xu X, Liu C, Wang Y, Koivisto O, Zhou J, Shu Y, et al. Nanotechnology-based delivery of CRISPR/Cas9 for cancer treatment. Adv Drug Deliv Rev. 2021; 176: 113891.
172. Pu YY, Yin HH, Dong CH, Xiang HJ, Wu WC, Zhou BG, et al. Sono-controllable and ROS-sensitive CRISPR-Cas9 genome editing for augmented/synergistic ultrasound tumor nanotherapy. Adv Mater. 2021; 33: 2104641.
173. Cheng X, He C, Huang J, Li J, Hu Z, Wang L, et al. A tumor-homing nanoframework for synergistic microwave tumor ablation and provoking strong anticancer immunity against metastasis. ACS Nano. 2024; 18: 29121-39.
174. Wang G, Li J, Wang L, Yang Y, Wu J, Tang W, et al. Manganese-doped potassium chloride nanoelectrodes to potentiate electrochemical immunotherapy. ACS Nano. 2024; 18: 10885-901.
175. Song Y, Sun Y, Tang M, Yue Z, Ni J, Zhao J, et al. Polyoxometalate modified by zeolite imidazole framework for the pH-responsive electrodynamic/chemodynamic therapy. ACS Appl Mater Interfaces. 2022; 14: 4914-20.
176. Xia MT, Yan Y, Pu HY, Du XN, Liang JY, Sun YN, et al. Glutathione responsive nitric oxide release for enhanced photodynamic therapy by a porphyrinic MOF nanosystem. Chem Eng J. 2022; 442:136295.
177. Yao C, Zhang R, Xie Z, Wu Y, Wu X. A magnetically actuated MOF-based nanozyme for intensified induction of ferroptosis and immunogenic cell death via autophagy blockade. Small. 2025; 21: e2409026.
178. Wang D, Wu H, Wang C, Gu L, Chen H, Jana D, et al. Self-assembled single-site nanozyme for tumor-specific amplified cascade enzymatic therapy. Angew Chem Int Ed. 2021; 60: 3001-7.
179. Qiao W, Chen J, Zhou H, Hu C, Dalangood S, Li H, et al. A single-atom manganese nanozyme Mn-N/C promotes anti-tumor immune response via eliciting type I interferon signaling. Adv Sci. 2024; 11: e2305979.
180. Lin G, Tillman L, Luo T, Jiang X, Fan Y, Liu G, et al. Nanoscale metal-organic layer reprograms cellular metabolism to enhance photodynamic therapy and antitumor immunity. Angew Chem Int Ed. 2024; 63: e202410241.
181. Wang T, Yang J, Ding J, Yuan Y, Wu Y, Zhang J, et al. A metal-organic framework-based immune-regulating nanocarrier depot for enhanced combination cancer immunotherapy. ACS Nano. 2025; 19: 23629-46.
182. Ye Y, Wang H, Jiang J, Cao X, Sun J, Jiang Y, et al. Biomimetic self-guiding nanomotors boost active immunotherapy. ACS Nano. 2025; 19: 37954-71.
183. Xu P, He J, Xu T, Wang W, Wu B, Chen R, et al. Synergistic integration of extracellular vesicles and metal-organic frameworks: unlocking new opportunities in disease diagnosis and therapy. Theranostics. 2025; 15: 8609-38.
184. Huang G, Zhang L, Feng J, Wu D, Wu L, Pan W, et al. Hypoxia-responsive covalent organic framework nanoplatform for breast-cancer-targeted cocktail immunotherapy via triple therapeutic switch mechanisms. Small. 2025; 21: e2407553.
185. Zhao H, Jin S, Liu Y, Wang Q, Tan BSN, Wang S, et al. A second near-infrared window-responsive metal-organic-framework-based photosensitizer for tumor immunotherapy via synergistic ferroptosis and STING activation. J Am Chem Soc. 2025; 147: 4871-85.
186. Min Y, Li Q, Zhao Z, Wen Q, Xu W, Adeli M, et al. Metallosalphen-covalent organic framework-based semiconducting artificial enzymes with radio-activable antitumor immunity for suppressing tumor metastasis and recurrence. ACS Nano. 2025; 19: 37373-97.
187. Ettlinger R, Lächelt U, Gref R, Horcajada P, Lammers T, Serre C, et al. Toxicity of metal-organic framework nanoparticles: from essential analyses to potential applications. Chem. Soc. Rev. 2022; 51: 464-84.
188. Velásquez-Hernández MD, Linares-Moreau M, Astria E, Carraro F, Alyami MZ, Khashab NM, et al. Towards applications of bioentities@MOFs in biomedicine. Coord Chem Rev. 2021; 429:213651.
189. Peplow M. Chemistry nobel materials in the clinic drug delivery. Nat Biotechnol. 2025; 43: 1751-.
190. Cui Y, Liu J, Cui L, Wei C, Xu M, Wu Z, et al. Tumor-targeting and activatable biomimetic nanococktails synergistically regulate immune responses for spatiotemporal immunotherapy of low immunogenic solid tumors. Nano Today. 2024; 57: 102380.
191. Cheng X, Xu J, Cui Y, Liu J, Chen Y, He C, et al. Nanovesicles for lipid metabolism reprogram-enhanced ferroptosis and magnetotherapy of refractory tumors and inhibiting metastasis with activated innate immunity. ACS Nano. 2025; 19: 7213-30.
192. Liu J, Cui Y, Cabral H, Tong A, Yue Q, Zhao L, et al. Glucosylated nanovaccines for dendritic cell-targeted antigen delivery and amplified cancer immunotherapy. ACS Nano. 2024; 18: 25826-40.
193. Liu J, Lin F, Hu G, Zhang R, Gong C, Sun X, et al. Dendritic cell-targeted tumor antigen delivery by glucosylated lipid nanoparticles for precision tumor immunotherapy. J Control Release. 2026; 392: 114671.
194. Liu F, Li S, Huang C, Bi Z, Xiang X, Zhang S, et al. Self-assembled nanoplatform-mediated co-delivery of brusatol to sensitize sorafenib for hepatocellular carcinoma treatment. RSC Adv. 2025; 15: 11675-87.
195. Li SM, Tan LF, Meng XW. Nanoscale metal-organic frameworks: Synthesis, biocompatibility, imaging applications, and thermal and dynamic therapy of tumors. Adv Funct Mater. 2020; 30: 1908924.
196. Fu DY, Liu X, Zheng X, Zhou M, Wang W, Su G, et al. Polymer-metal-organic framework hybrids for bioimaging and cancer therapy. Coord Chem Rev. 2022; 456: 214393.
197. Cabral H, Li J, Miyata K, Kataoka K. Controlling the biodistribution and clearance of nanomedicines. Nat Rev Bioeng. 2024; 2: 214-32.
198. Mi P, Miyata K, Kataoka K, Cabral H. Clinical translation of self-assembled cancer nanomedicines. Adv Therapeutics. 2021; 4: 2000159.